COLD SHUT FORMATION IN CASTINGS

by

Luiz Augusto Siqueira Bittencourt

A Thesis Submitted to the
Faculty of Graduate Studies and Research
in Partial Fulfillment of the Requirements for
the Degree of Master of Engineering.

Department of Mining and Metallurgical Engineering
McGill University
Montreal, Canada

September 1979

To my parents

Augusto and Lady,

to my wife Eliane,

and to my sons

Claudio and Eduardo.

ABSTRACT

An experimental investigation into cold shut formation in castings has been carried out. Results indicate that cold shuts are formed when liquid metal, overflowing solid metal, does not completely remelt the solid. As the occurrence of the defect depends upon the thermal energy of the liquid, effective superheat (superheat at which the liquid meets the solid metal) is the most important variable affecting the cold shut formation. This superheat is controlled by both the pouring rate and the superheat at pouring.

A mathematical model was developed to predict the remelting phenomena (involved in the formation of the defect) of an idealised system. Critical conditions for cold shut formation have been calculated in terms of melt superheat, temperature of solid metal and distance from the point of pouring.

The collision of two liquid metal streams also causes the formation of cold shuts due to splashes which quickly solidify on the mold wall.

The alloy composition was found to affect the appearance of the defect due to the mode of solidification. While pure Pb and the Pb-Sn eutectic produced very marked defects, a Pb-19% Sn alloy with a wide freezing range formed cold shuts which were neither as visible nor as continuous as those formed in congruent melting alloys.

Results have shown that the head of metal has a strong influence on the occurrence of misruns.

It was found that water is an adequate fluid for simulating the collision of two streams of liquid metal inside a channel.

RESUME

Une recherche expérimentale sur la formation de "reprise" lors d'une coulée a été faite. Les resultats indiquent que cette "reprise" est formée, lorsque le métal liquide qui recouvre le métal solide ne fait pas comlètement fondre le métal solide. La formation de cette imperfection dépends de l'énergie thermique du liquid, mais la température du liquide (température qui est supérieure au point de fusion) lorsque le métal liquide entre en contact avec le métal solide, est la facteur le plus important, quant à cette formation de ce "reprise". Cette température est contrôlée à la fois par le temps de la coulée et par la temperature de la coulée.

Un modèle mathématique a été développé afin de prévoir ce phénomène de refonte (impliqué dans la formation de cet imperfection), dans un système idèal.

Les conditions critiques pour la formation de cette "reprise" ont été calculées en fonction de la température de fusion, de la température du métal solide et de la distance à partir du point de coulée.

La collision de deux courrants de métal liquide causes aussi la formation de "reprise" dû aux éclaboussures qui se solidifient très rapidement sur les parois du moule.

La composition de l'alliage joue aussi un rôle dans la formation d'imperfections, dû au mode de solidification. Par exemple, le Pb pure et le Pb-Sn eutectique produisent des imperfections très marquées. Par contre un alliage de Pb-19% Sn, avec un large échelle de congélation, produit des "reprise" qui ne si sont ni visibles, ni continus, tels ceux formés par des alliages qui ont un même point de fusion.

Les résultats montrent que la pression de chute (tête de chute) a une forte influence sur la formation d'imperfections.

Il a été trouvé que l'eau est un fluide adéquat pour simuler la collision de deux courrants de métal liquide à l'intérieur d'un canal.

ACKNOWLEDGEMENTS

The author wishes to express his profound gratitude to those who have, in various ways, contributed to this work. He is particularly indebted to:

Dr. J.E. Gruzleski and Dr. R.I.L. Guthrie, directors of this study, for their constant interest, understanding and encouragement during the course of this work.

Messrs. S. Argyropoulos, F. Mucciardi, M. Tanaka, R. Harris and R. Barnhurst, graduate students of this department, for giving invaluable assistance in several phases of this study.

Mr. M. Knoepfel, for his help in constructing the apparatus, Mr. J. Quaroni, for correcting the English language of this thesis and Mrs. H. Rousseau for typing this manuscript.

The National Science and Engineering Research Council of Canada, the Canadian International Development Agency, Secretaria de Tecnologia Industrial and Companhia Siderurgica Nacional for their financial support.

TABLE OF CONTENTS

LIST OF FIGURES

LIST OF TABLES

CHAPTER 1. INTRODUCTION

1.1 A General View on Casting Defects

The art of metal casting is one of the oldest and most durable examples of the production of metal objects and will probably continue to be the best way to produce complicated shapes. The casting process, involving the flow of molten metal and the flow of heat, is the central part of the foundry industry. Basically, for a sound metal casting, the liquid metal should both fill the mold cavity as quickly as possible and solidify, by losing heat, from the remotest regions inward toward the source of molten metal. Only if the metal and heat flow sequence is properly coordinated, can the final product be expected to be free from defects. Otherwise, there will be a high probability of the occurrence of imperfections.

Many times, the appearance of a simple defect, well known to the foundryman, becomes a complex problem because the causes of casting defects are widespread throughout the foundry process. Table 1.1, showing the influence of 11 processes in the foundry on 10 common defects, illustrates where these defects can occur. It can be seen that metal composition, melting and patterns are, generally, less frequent, but not less important, causes of defect formation in castings.

At this point, a general explanation on those defects shown on Table 1.1 is useful.

Gas Defects (Blowholes, Pinholes, Blisters and Body Scars) are cavities (Fig. 1.1) caused by localized gas pressure that exceeds the metal pressure.[1]

Shrinkage Cavities are ragged cavities lined with dendrites[1] (Fig. 1.2). This defect can be easily confused with some of the gas defects. A helpful simple difference is that gas defects are smooth

TABLE 1.1

Causes of Casting Defects

Defects	Design	Patterns	Flasks & Rigging	Gates & Risers	Molding Sand	Core Practice	Molding Practice	Melting	Pouring	Metal Composition	Miscellaneous	Number of Operating Factors
1 Gas Defects	x		x	x	x	x	x	x	x	x	x	10
2 Shrinks	x	x	x	x				x	x	x		8
3 Inclusions	x			x	x	x	x	x	x		x	8
4 Expansion Defects	x		x	x	x	x	x		x			7
5 Hot Tears	x	x	x	x	x	x	x	x	x	x	x	11
6 Misruns & Cold Shuts	x	x	x	x	x	x	x	x	x	x	x	11
7 Runouts & Bleeders		x	x	x	x	x	x		x		x	8
8 Shifts	x	x	x			x	x		x			6
9 Cuts & Washes	x		x	x	x	x	x		x		x	8
10 Erosion Scabs	x	x	x	x	x	x	x		x			8
Number of Defects Caused by Each Factor	9	6	9	9	9	9	9	5	10	4	6	

Sources: References 1 and 2.

FIGURE 1.1 Typical gas evolution cavity on a cope surface.[1]

FIGURE 1.2 Typical shrinkage defect occurring in a thick section which could not be fed.[1]

and shrinkage cavities are dendritic, but the diagnosis must be as careful as possible. This defect is caused by lack of sufficient feed metal.

Inclusions (non-metallic) are particles of foreign material embedded in the metal[1] (Fig. 1.3) and may be due to the presence of slag or oxide particles in the molten metal.

Expansion Defects (Expansion Scabs, Buckle, Rat-tail, Blackening Scab and Pull Down) are indentations in the surface or rough layers of metal on the surface of the casting[1] (Fig. 1.4). These defects arise from faults in mold construction or from poor-quality sand.

Hot Tears are cracks (Fig. 1.5) developed during solidification and are caused by a restriction from contracting in certain areas which become under tension.

Misruns and Cold Shuts will be analyzed in Section 1.2.

Runouts and Bleeders are incomplete castings[1] (Fig. 1.6) and are due to, for instance, a weak mold or premature removal of clamp.

Shift is a mismatch of the casting at the parting line[1] (Fig. 1.7) and is probably caused by pattern equipment, flask equipment or molding practice.

Cuts and Washes are rough spots and areas of excess metal[1] (Fig. 1.8) caused by erosion of the mold.

Erosion Scab is an expansion defect in which the loosened sand has been eroded away by the motion of metal[1] (Fig. 1.9).

On the appearance of any type of defect, a very careful analysis must be made in order to avoid incorrect diagnosis which can

FIGURE 1.3 Typical surface defect defined as inclusions.[1]

FIGURE 1.4 Expansion scab caused by slow pouring which permitted excessive heating of the cope surface before metal contact.[1]

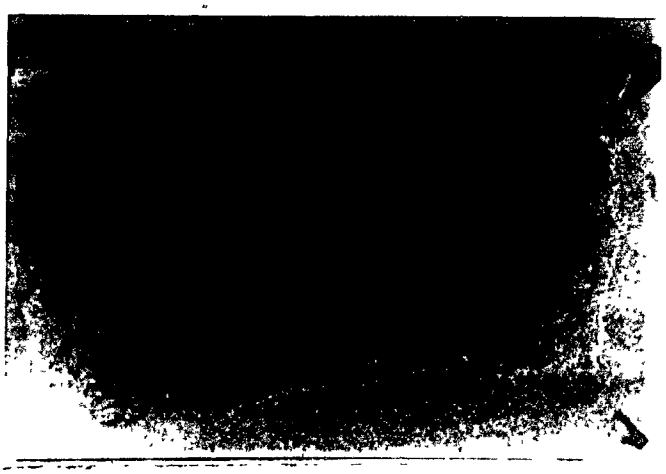

FIGURE 1.5 A hot tear in a steel casting.[4]

FIGURE 1.6 Typical parting line runout occurred as a result of the core holding the cope out.[1]

FIGURE 1.7 A typical mold shift is shown where a cope and drag did not match.[1]

FIGURE 1.8 Typical wash or cut in the gate area.[1]

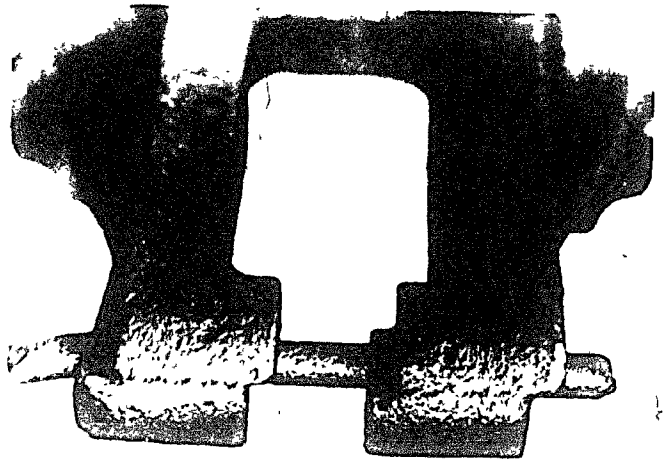

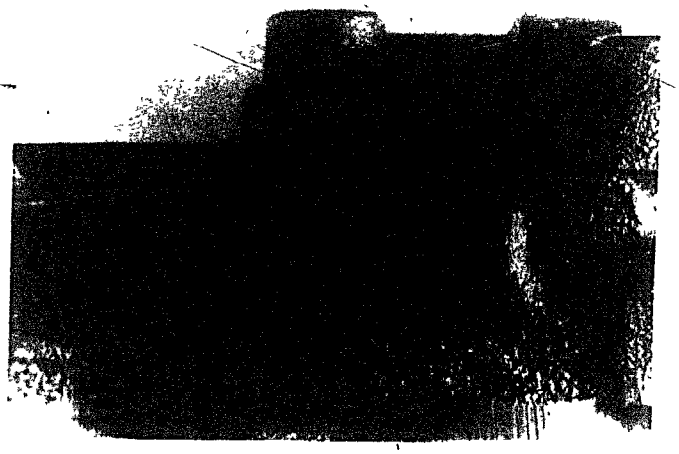

FIGURE 1.9 Typical erosion scab on the core surface.[1]

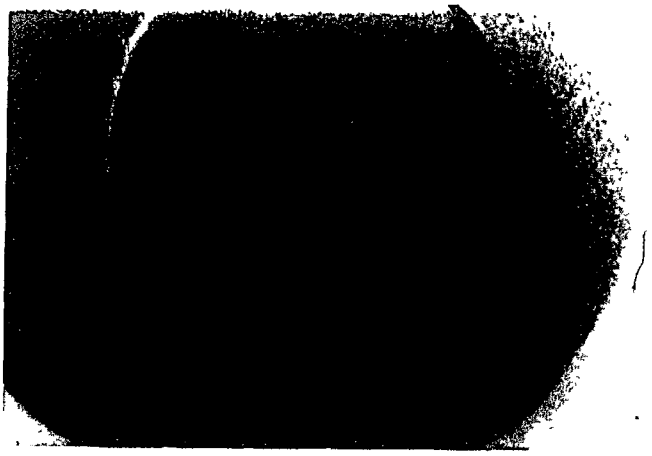

be expensive. Many times the cures for the actual defect are the opposite of those for the defect the analyst has in mind.

Economically, the occurrence of any imperfection is always detrimental to the foundry industry. This is particularly true if the defect is not detected before delivery of the casting to the customer. If the defect is discovered in the foundry, some extra process will become necessary, for instance grinding, in order to avoid scrapping the entire casting. In either case, there is a waste of both manpower and energy.

A common defect which increases the cost of any casting is cold shut. Various aspects of the formation of this defect will now be reviewed.

1.2 Cold Shuts: A Literature Review

Although the appearance of any casting defect is becoming economically more and more important, due to quality and energy consideration, the mechanism of formation of many imperfections remains unknown because few attempts have been made to treat these common defects in a scientific manner. Cold shuts, for instance, are a quite common surface defect being, in many cases, the number one source of unsalable castings. Despite this, the exact conditions governing their formation have not yet been identified.

A cold shut can be described as a definite discontinuity on the casting surface with the appearance of a crack with rounded edges (Fig. 1.10). A literature review has shown that it has generally been assumed to be caused by the meeting of two streams of metal.[1,3-7]

FIGURE 1.10 a) Lion's Head - the whole casting.
Material: commercial pure lead
Magnification: 0.3x

FIGURE 1.10 b) Detail of cold shut.
Material: commercial pure lead
Magnification: 0.5x

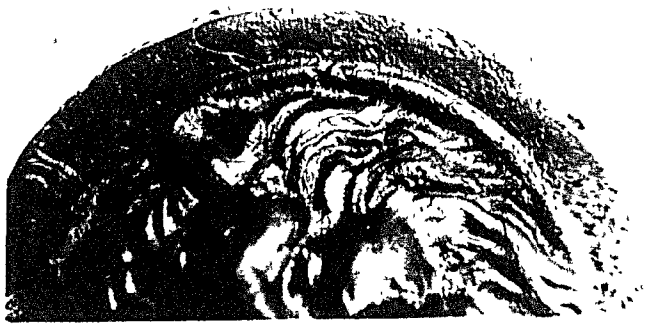

Although few researchers have worked on this defect, some interesting conclusions can be drawn from their work which is dealt with in the remainder of this chapter.

1.2.1 Cold Shuts in Sand Castings

Gorbachev and Zhukov[8], studying the formation of soft structures in the white iron, poured wedge samples in sand molds with a steel plate as a chill in the small end. These samples were poured in an intermittent stream of variable pause and compared with wedges poured without intermission. They found that the soft structure in the chilled layer had a much lower hardness than the fully chilled structure and they concluded that the local loss of hardness in the white iron layer is due to the eddy formation in the chill areas. In this case, the cold shut formation depends on whether the eddy is completely or partially solidified. In the first case, a cold shut is formed. In the second case, cold shut is avoided.

Kvasha et al.[9] have developed a special mold (Fig. 1.11) to study the lap formation on the surface of iron castings. They have found that the carbon, formed by pyrolisis of the hydrocarbons contained on the metal/mold interface, is adsorbed on the surface of the metal. If, subsequently, the accumulations of carbon are not absorbed by the metal, laps are formed on the surface of the castings. Thus, the material in the laps and visible on the surfaces is amorphous carbon. They have also found that:

- For a given sand, the number of laps formed is proportional to the degree of compaction.

FIGURE 1.11 Mold developed to study the mechanism of lap formation.[9]

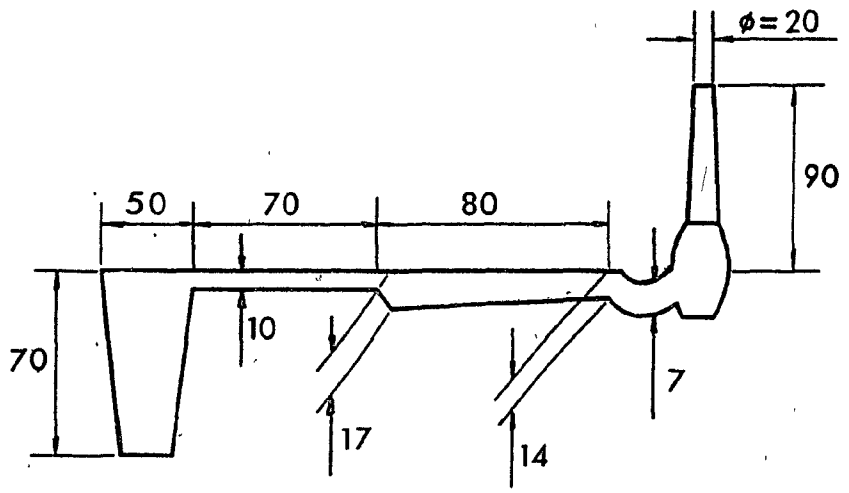

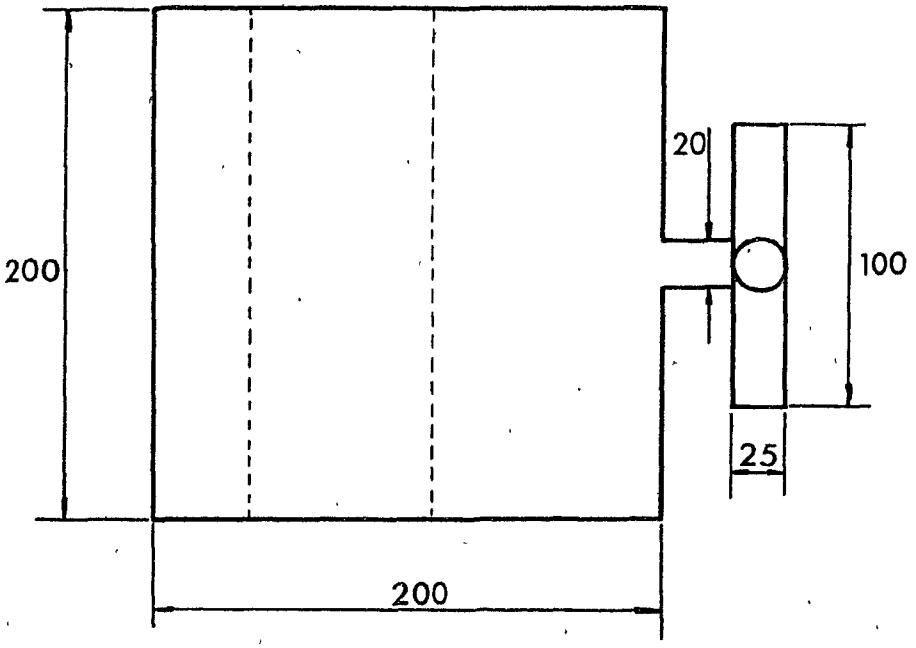

UNIT = Not given in reference 9.
Likely to be cm.

- All other parameters being constant, between 3.5% and 7.0%, water content has a low effect on lap formation.
- The metal composition is not important but the pouring temperature exerts a strong influence on the defect formation.
- There is not any significant change in structure of the metal at the points where most of the laps are found.

Lillieqvist[10], working on the influence of temperature on the surface appearance of steel castings has found that the cold shut formation is inversely proportional to the tapping temperature of a basic open hearth furnace (Fig. 1.12).

1.2.2 Fluidity: An Important Factor

A superficial analysis of Table 1.1 shows that the cold shut is one of the few casting defects whose causes can be found in almost every process in the foundry, the cleaning operation being the only exception. Although metal composition is not a very common cause of most of the defects, it is of utmost importance to the cold shut formation and it is generally blamed, together with pouring practice, for the major percentages of cold shuts. This is because the composition exerts a strong influence on the fluidity which is accepted to be among the most usual causes of cold shuts.[4,11] Here, it should be pointed out that the term "fluidity", in the foundry sense, means the ability of the metal to fill the mold cavity and it is the value of an empirical measure of the distance the molten metal can reach in a standard mold (spiral channel[3] or vacuum fluidity test[12]) before being stopped by solidification.

FIGURE 1.12 Influence of tapping temperature on cold shut formation.[10]

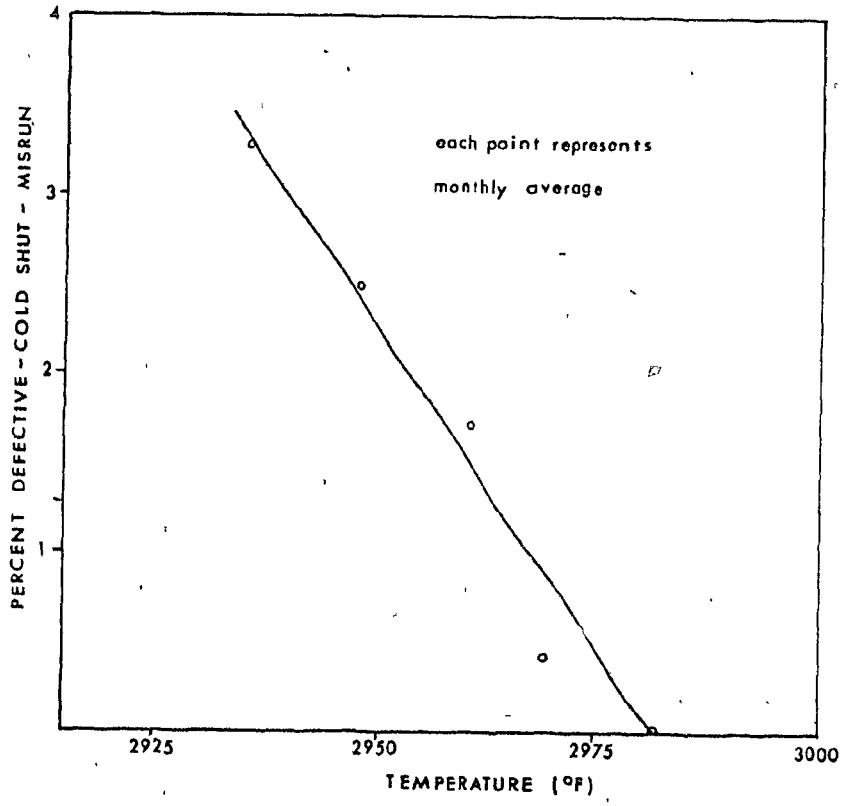
PERCENT DEFECTIVE - COLD SHUT - MISRUN
4
3
2
1
each point represents
monthly average
2925
2950
2975
3000
TEMPERATURE (°F)

The relationship between metal composition and fluidity has been studied by some workers and it is explained on the basis of the mode of solidification. Ragone et al.[12], working on Pb-Sn alloys and using the vacuum fluidity test (which has better accuracy than the spiral test because it avoids the human factor in pouring and because the pressure head is instantaneously applied) show that fluidity is inversely proportional to the freezing range (liquidus temperature - solidus temperature) and proportional to the superheat. This is shown in Figures 1.13 and 1.14 and it is due to the solidification behavior which is well explained by Niesse et al.[13]

Pure metal with no superheat, entering the mold cavity, begins solidification immediately with a smooth liquid-solid interface (Fig. 1.15a). Metal continuing to flow continues solidification along the mold wall (Fig. 1.15b) but flow is eventually choked-off at the entrance (Fig. 1.15c). The only effect of superheat on this mechanism is that the point where flow stoppage occurs is moved downstream with increasing superheat as can be seen in Fig. 1.16.

Adding a small amount of alloying element, sufficient to bring about dendritic growth during solidification, causes the liquid-solid interface to become corrugated. Solidification and flow stoppage are similar to that for pure metals (Fig. 1.17) but for dilute alloys the friction is much greater than in the case of pure metals because of the dendrites. If the alloy contains a high percentage of alloying element, dendrites can grow deep into the stream so that the friction becomes so high that choking-off occurs when only a small amount of solidification has taken place.

FIGURE 1.13 Relationship between fluidity and alloy composition in Pb-Sn system.[12]

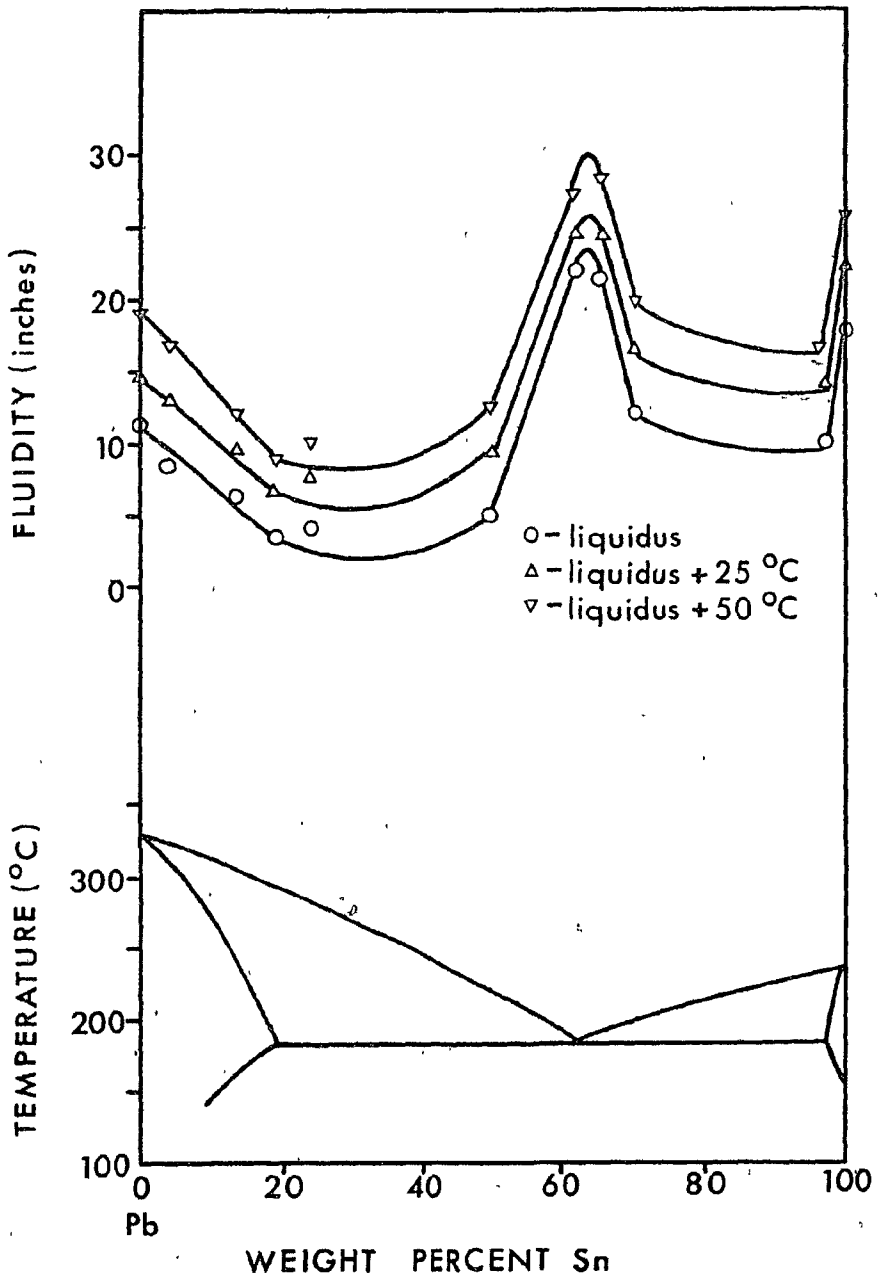
FLUIDITY (inches)
30
20
10
0
○ – liquidus
△ – liquidus + 25 °C
▽ – liquidus + 50 °C
TEMPERATURE (°C)
300
200
100
0
20
40
60
80
100
Pb
WEIGHT PERCENT Sn

FIGURE 1.14 Relationship between fluidity and superheat for Pb-65.25% Sn alloy.[12]

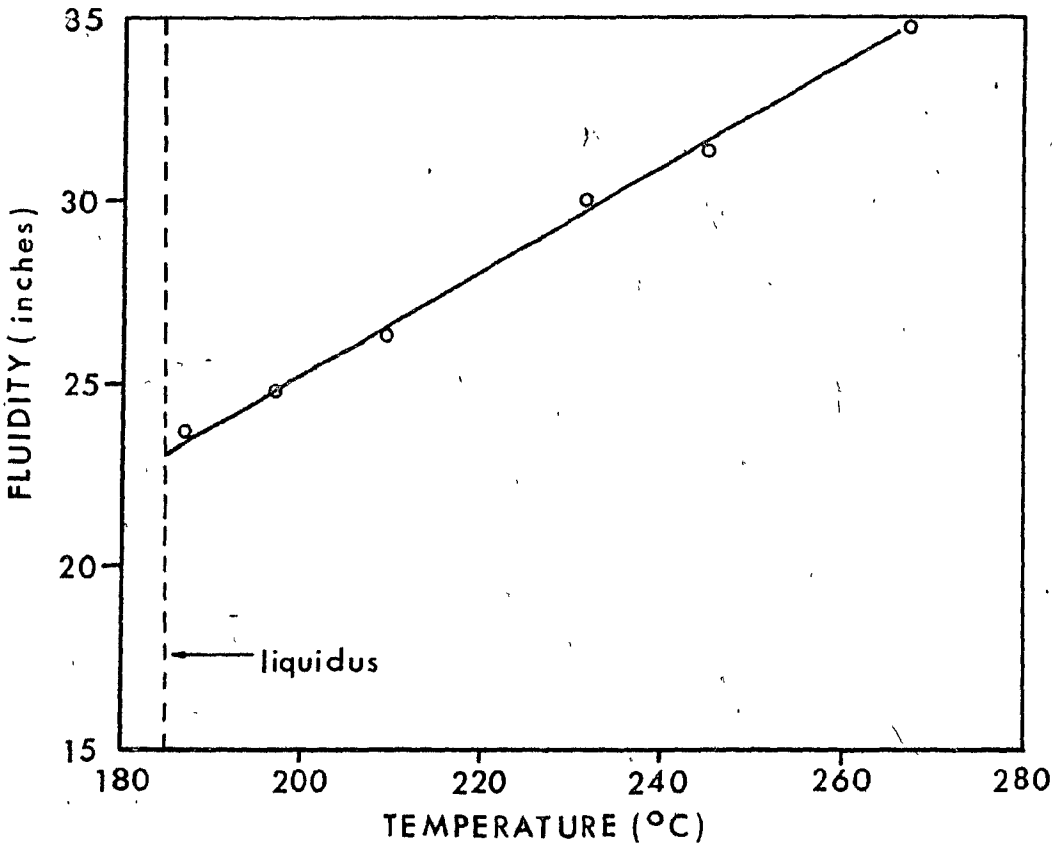
35
30
25
20
15
FLUIDITY (inches)
liquidus
180
200
220
240
260
280
TEMPERATURE (°C)

FIGURE 1.15 Schematic diagram of flow and solidification of a pure metal in a fluidity channel (no superheat).[13]

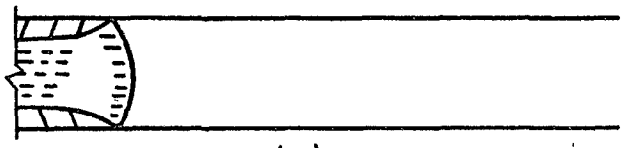

(a)

(b)

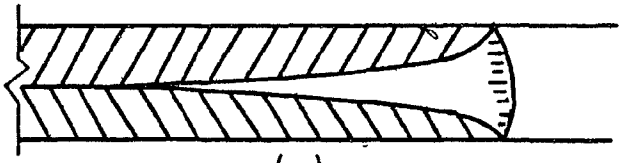

(c)

FIGURE 1.16 Schematic diagram of flow and solidification of a pure metal in a fluidity channel (with superheat).[13]

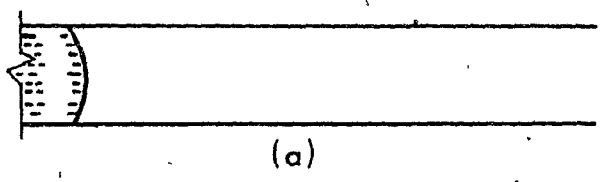

(a)

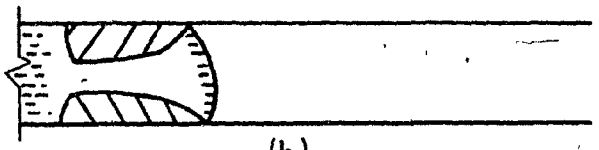

(b)

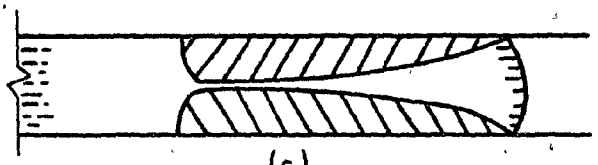

(c)

FIGURE 1.17 Schematic diagram of flow and solidification of a dilute alloy in a fluidity channel (no superheat).[13]

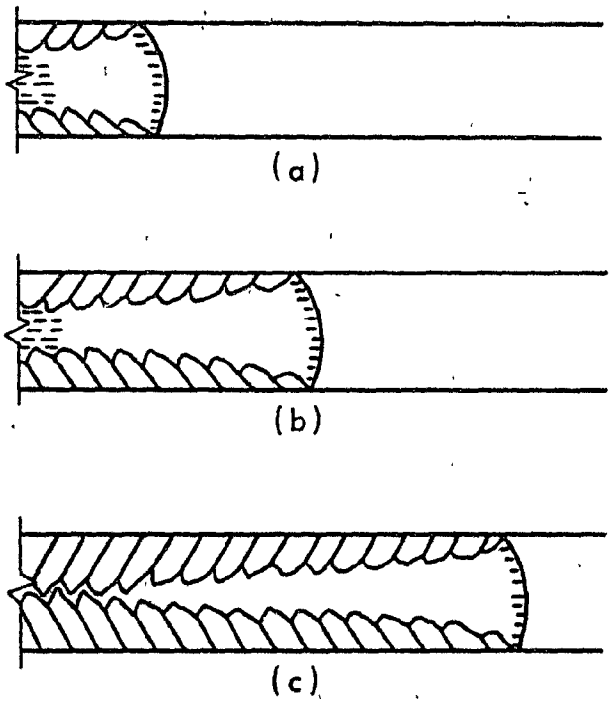
(a)
(b)
(c)

Another type of solidification can occur in alloys with a high percentage of solute and in which nucleation is not a problem. These alloys solidify with equiaxed dendrites. When the solid is growing, fine grains form at the front of the stream. Figure 1.18 shows that flow can be choked off at this front part of the metal stream when friction becomes sufficiently high. Thus, it can be concluded that pure metals and eutectics which freeze with smooth liquid-solid interfaces have a high fluidity. On the other hand, alloys with a freezing range solidify dendritically, and these dendrites prevent passage of further liquid, thereby causing a low fluidity.

Flemings et al., working on Mg alloys[14] and on Al alloys[15], and using the vacuum fluidity test as well, have obtained the same results as those for the Pb-Sn system.

1.2.3 Cold Shuts in Electron Beam Welds

The cold shut is not confined to sand castings alone, and it can be found in electron beam welds as well as in die castings. Its causes are thought to be much the same in all of these processes.

Wood and Mara[16], studying the elimination of cold shuts in deep, single-pass electron beam welds in uranium, have developed a technique for avoiding such a defect. This technique consists of using shims of a proper alloying metal. During the weld process, the shim is melted and mixed into the weld metal, enhancing the effective superheat by lowering the melting point on cooling.

Arata et al.[17], working on Al and iron-based alloys, and studying the characteristics of weld defects, have concluded that:

FIGURE 1.18 Schematic diagram of flow and solidification of an alloy which readily nucleates fine grains (no superheat).[13]

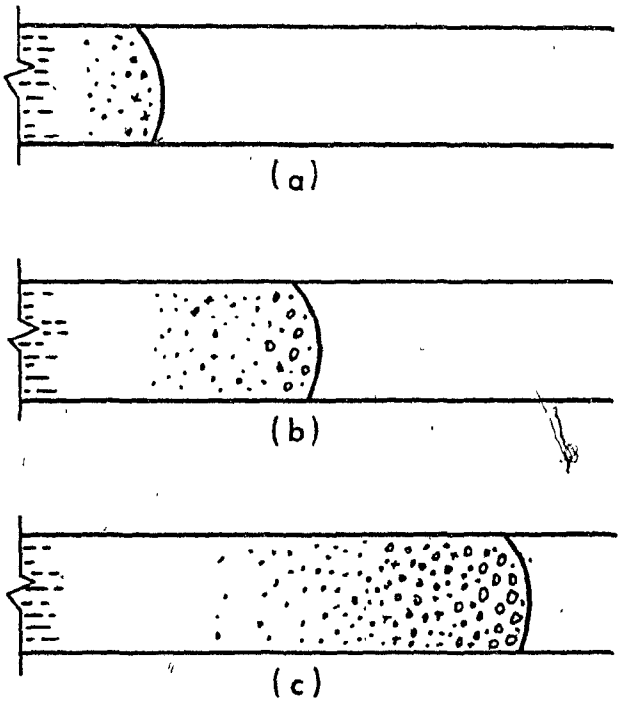
(a)
(b)
(c)

- The aluminum alloys had a higher number of cold shuts than the iron based alloys.
- Many of the cold shuts in aluminum alloy welds took place at the adjacent zone of maximum penetration weld. This did not occur with the iron-based alloys.
- Cold shuts tend to lower the fatigue strength, but it is not possible to state an exact relation between the number of cold shuts and their influence on fatigue (Fig. 1.19).

1.2.4 Cold Shuts in Die Casting

Surface defects also require attention in die casting. In this process, where molten metal is forced under pressure into metal molds (dies), the principal causes of cold shut[18] (Table 1.2) are the same as in sand casting (Table 1.1). Die casting has two types of surface defects[18]: low die temperature defect and high die temperature defect. Cold shut is an example of the first kind of defect. High die temperature defects include blisters, craters or pits, shadows or images, shrinkage areas and the defects resulting from die soldering.

In order to avoid cold shut formation, the die temperature can be raised. The defect elimination becomes complex when this overheating causes the appearance of some of the high temperature defect before the cold shut is totally eliminated. This complexity would be avoided if heat transfer, principally in thin sections, could be retarded.[19] This can be successfully achieved by applying proper coating materials, such as nickel-phosphorus alloy[20], which decrease the thermal conductivity of the die, extend the solidification time significantly, and therefore prevent the formation of cold shuts.

FIGURE 1.19 Influence of cold shut on fatigue of 5083 aluminum alloy.[17]

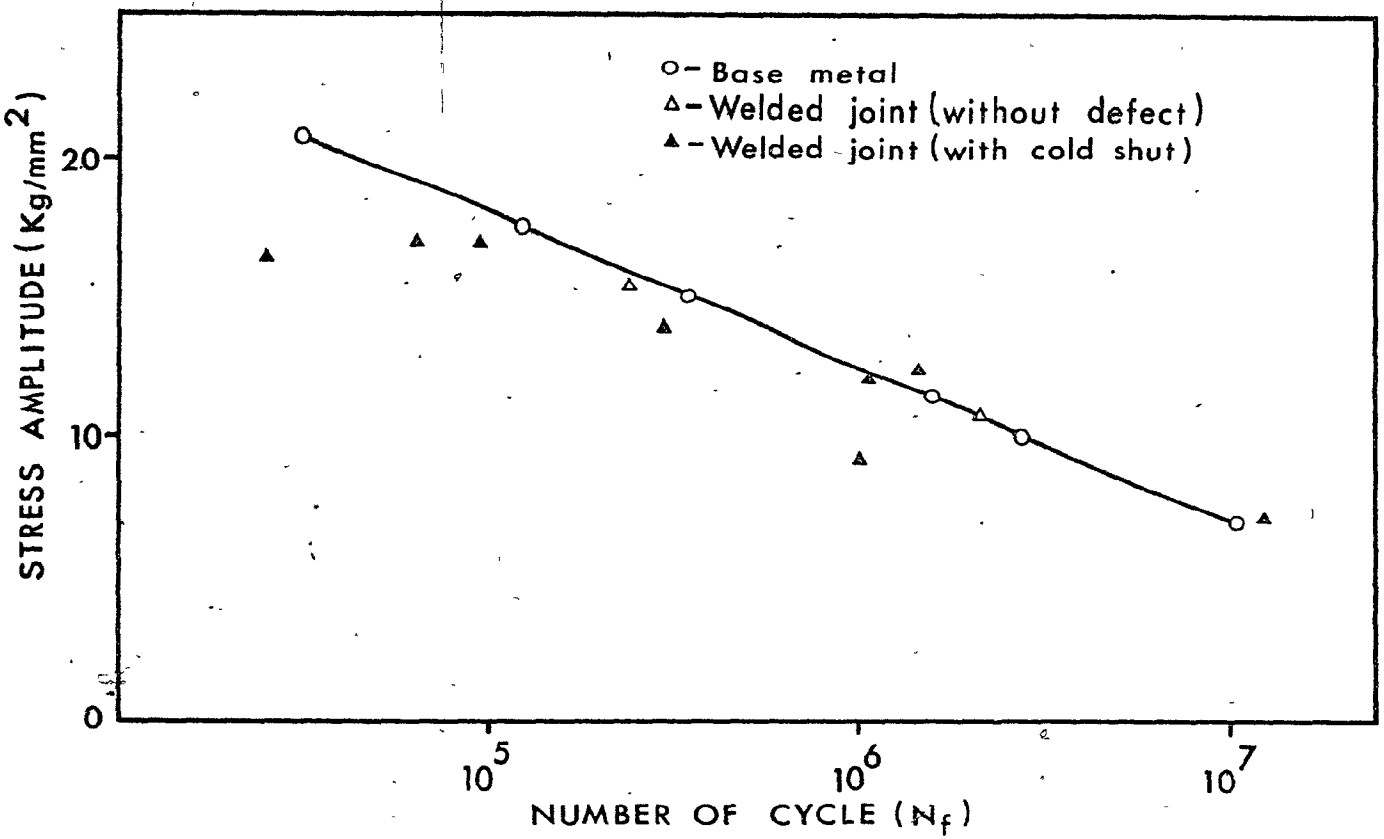
o– Base metal
Δ– Welded joint (without defect)
▲– Welded joint (with cold shut)
STRESS AMPLITUDE (Kg/mm2)
20
10
0
10^5
10^6
10^7
NUMBER OF CYCLE (Nf)

TABLE 1.2

Principal Causes of Cold Shut in Die Casting

1. Low injection pressure.
2. Cold dies.
3. Low metal temperature.
4. Oxide in the molten metal.
5. Improper die design.

1.3 Aims of the Present Work

As was pointed out, few attempts have been made to understand the mechanism of cold shut formation in castings. The works found in the literature are concerned with trying to avoid the defect formation without an extensive research as to its principal causes.

The present work involves an attempt to determine the exact conditions governing cold shut formation by the use of model systems combined with a study of the solidification of Pb and Pb-Sn alloys cast in a sand mold of simple geometry.

This work intends to answer the following questions:

1. What exactly is cold shut?
2. Under which conditions does it form?

CHAPTER 2. MODEL EXPERIMENTS WITH WATER AND MERCURY

With the most common and accepted definition of a cold shut in mind, that being "a surface defect formed by the meeting of two streams of metal", experiments were designed to produce this surface discontinuity by promoting the collision of two liquid streams. As the liquid behaviour promoting this particular phenomenon was not known, some simple experiments using water and mercury were scheduled before working on Pb and Pb-Sn alloys.

2.1 Similarity Criteria

For one system to be similar to another, conditions known as similarity criteria need to be satisfied. These criteria, being ratios of magnitudes, are expressed as dimensionless numbers and are of utmost importance in the design of models or pilot plants. Generally, in order to simulate all aspects of a process, it is necessary to achieve the four major states of similarity[21]: geometric, mechanical (static, kinematic and dynamic), thermal and chemical. In modelling a flow system, two of these criteria would have to be satisfied, these being: dynamic similarity (which automatically imposes kinematic similarity[21]) and geometric similarity (for which the dimensionless initial and boundary conditions are the same[22]).

For geometric similarity, the physical dimensions of the model were chosen to be the same as the casting unit used, as will be seen later.

For dynamic similarity, the relevant dimensional groupings pertaining to the flow of fluid through a channel following release from a raised reservoir are given in Table 2.1. The nomenclature used in this table is presented below:

TABLE 2.1

Dimensionless Groups Pertaining to Fluid Flow

Group	Formula	Equation	Quantities Represented
Froude	$\frac{u^2}{gL}$	2.1	$\frac{\text{inertial forces}}{\text{potential forces}}$
Reynolds	$\frac{\rho u D}{\mu}$	2.2	$\frac{\text{inertial forces}}{\text{viscous forces}}$
Weber	$\frac{\rho u^2 D}{\sigma}$	2.3	$\frac{\text{inertial forces}}{\text{surface tension forces}}$
Fanning Friction Factor, f	$\frac{\Delta P_f D}{\rho u^2 l}$	2.4	$\frac{\text{shear stress}}{\text{velocity head}}$

u = fluid velocity at channel entrance

g = acceleration due to gravity

L = characteristic length dimension of system

ρ = fluid density

μ = fluid viscosity

σ = surface tension

$\frac{\Delta P_f}{\rho}$ = friction head

l = length of pipe

D = hydraulic diameter of conduit

To obtain dynamic similarity, one, two, three or all four dimensionless numbers must be close for the fluids involved. Keeping these numbers almost constant, provides the desired similarity between the systems.

2.2 Apparatus

A transparent plastic mold of simple geometry (see Figs. 2.1 and 2.2) was constructed to allow for visual observation of flow phenomena involving two convergent streams. The mold dimensions and flow channels are shown in Figure 2.3. Three plastic plates 0.635 cm thick were also shaped in such a way that the height of the runner or channels could be reduced by placing plates over the base of the channel. Thus, experiments could be carried out with four different heights of runner: 0.635 cm, 1.27 cm, 1.905 cm and 2.54 cm.

The tank over the mold (Figs. 2.1 and 2.4) was constructed of the same material as the mold and was stoppered by a tapered circular section plug (made of soft rubber), to ensure reproducible pouring conditions and rates as far as possible.

As can be seen in Figure 2.1, the mold had a cover in which there were seven rectangular holes. Silk treated with a water repellent agent was glued onto the cover over these holes so that, by preventing the flow of water and by permitting the flow of air, the cloth would simulate the permeability of sand molds.

2.3 Experimental Procedures

A sufficient quantity of water to completely fill the mold was poured into the sealed mold. The plug was then pulled out, allowing

FIGURE 2.1 Plastic mold for water and mercury.

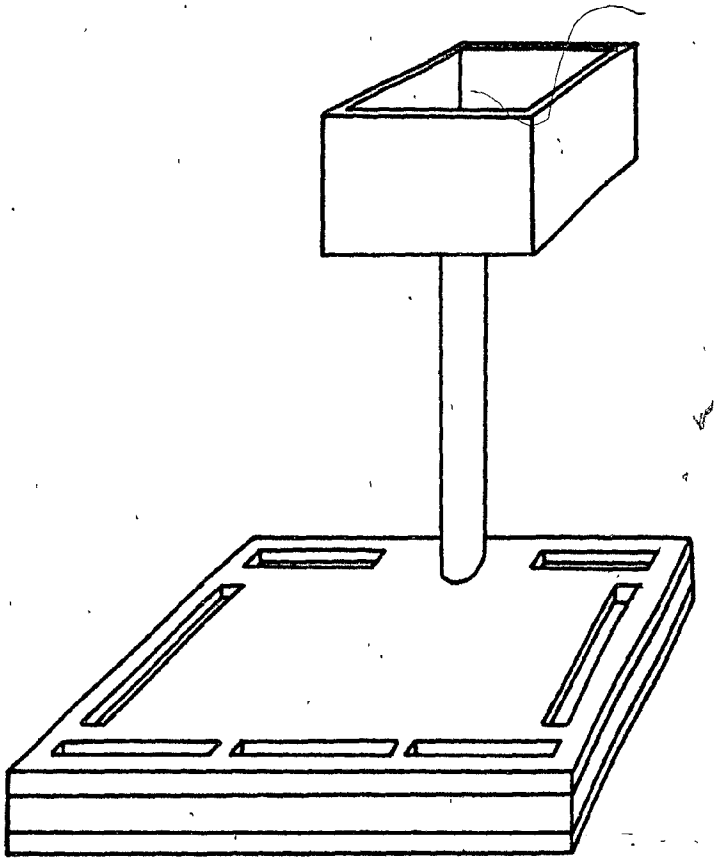

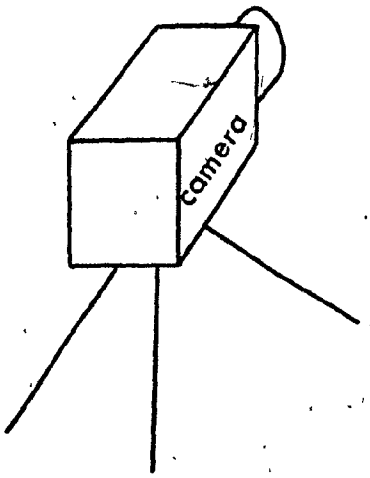
camera

FIGURE 2.2 Plastic mold without cover showing the runner.

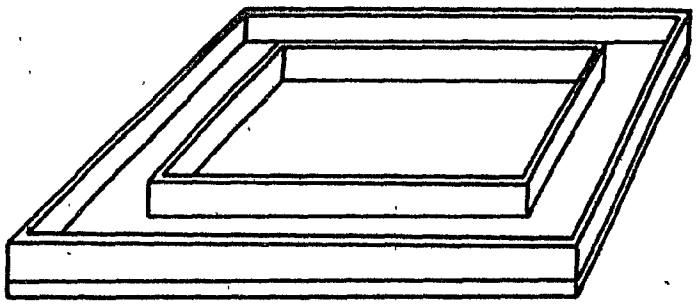

FIGURE 2.3 Dimensions of the plastic mold and direction of flow inside the channel.

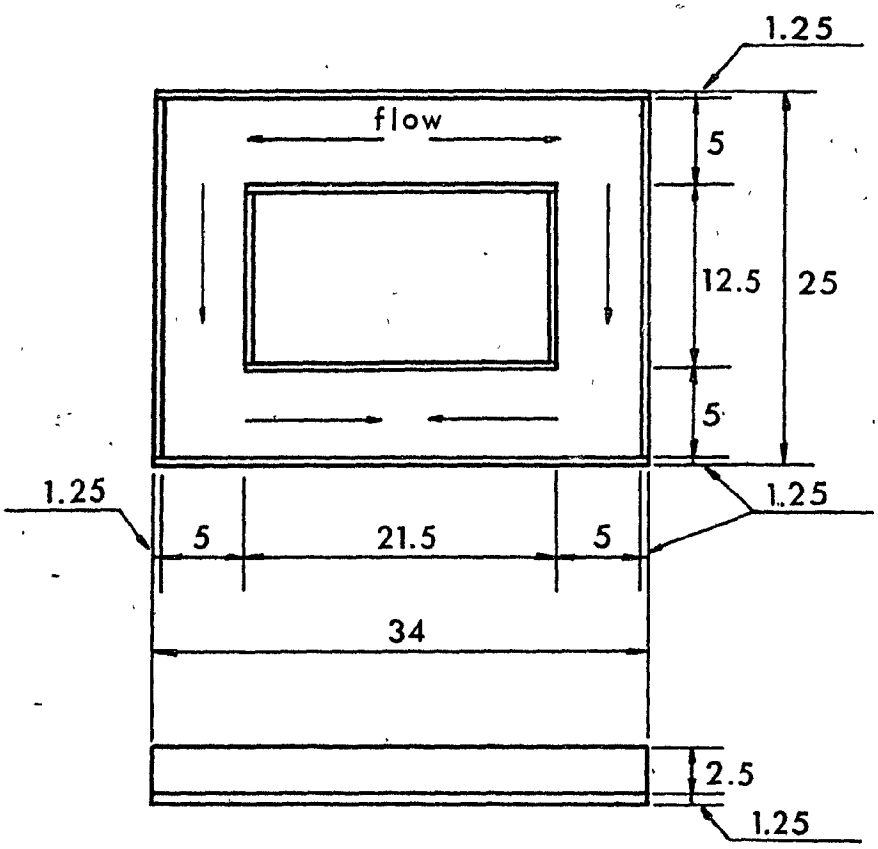

UNIT = cm

FIGURE 2.4 Tank used for reproducible pouring rates.

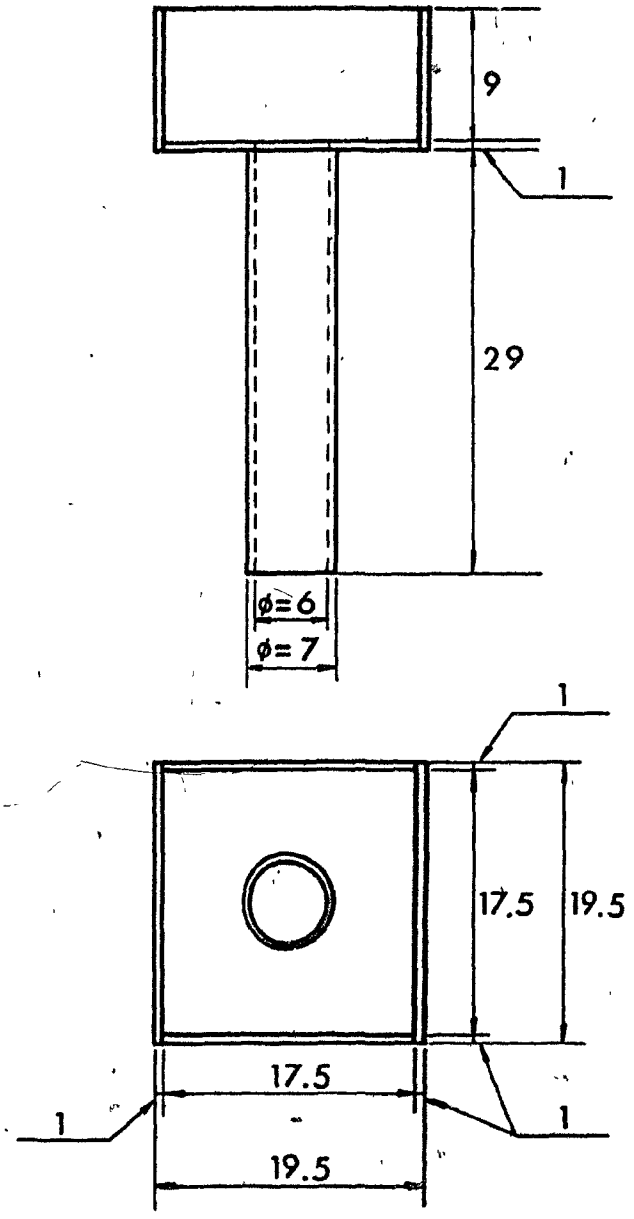

UNIT = cm

FIGURE 2.5 Friction factor as a function of Reynolds number.[21]

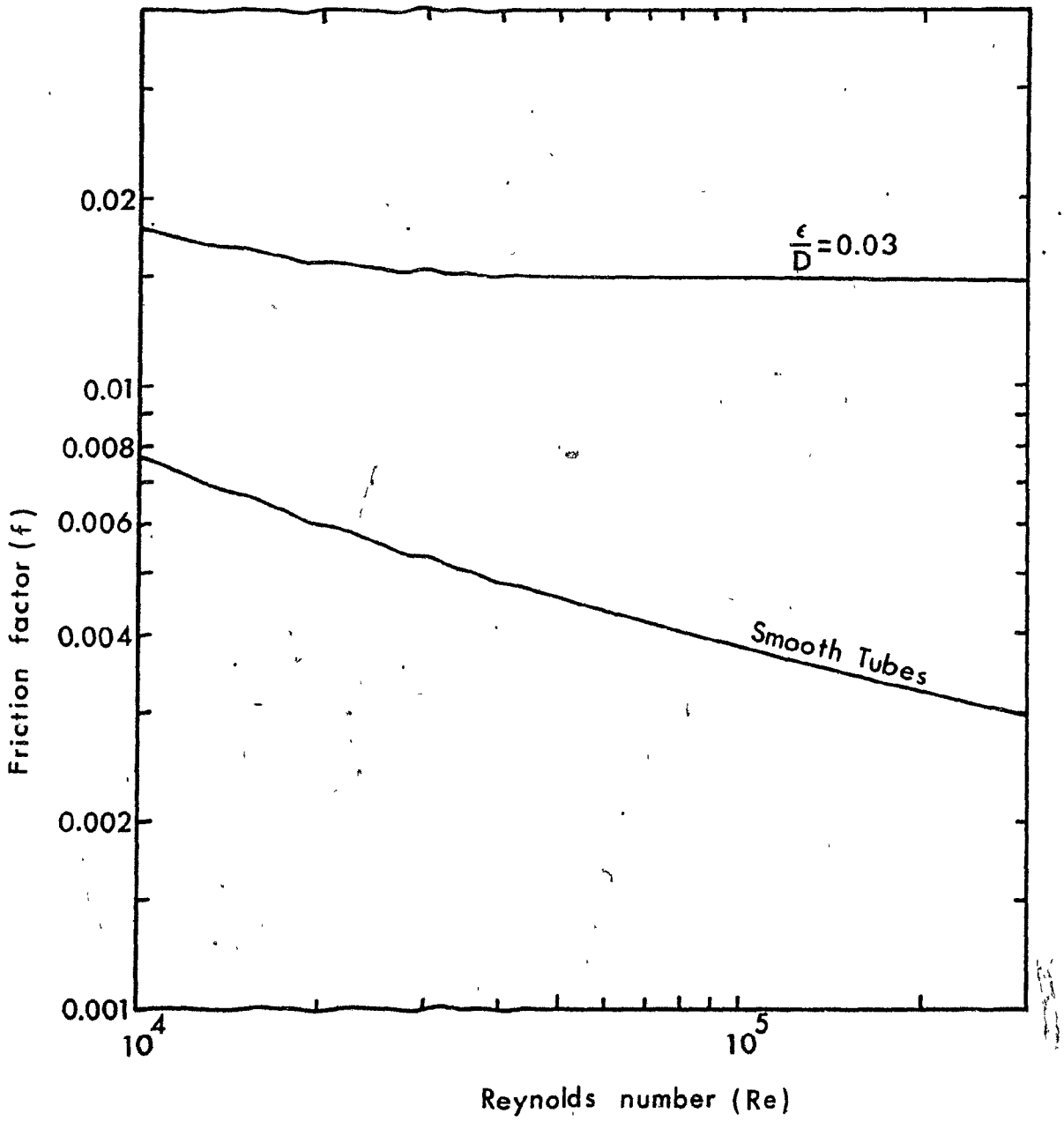
0.02
0.01
0.008
0.006
0.004
0.002
0.001
$\frac{\epsilon}{D}$=0.03
Smooth Tubes
Friction factor (f)
10^4
10^5
Reynolds number (Re)

FIGURE 2.6 Schematic representation of two streams of liquid meeting inside a channel. Time increases (from a) to e).

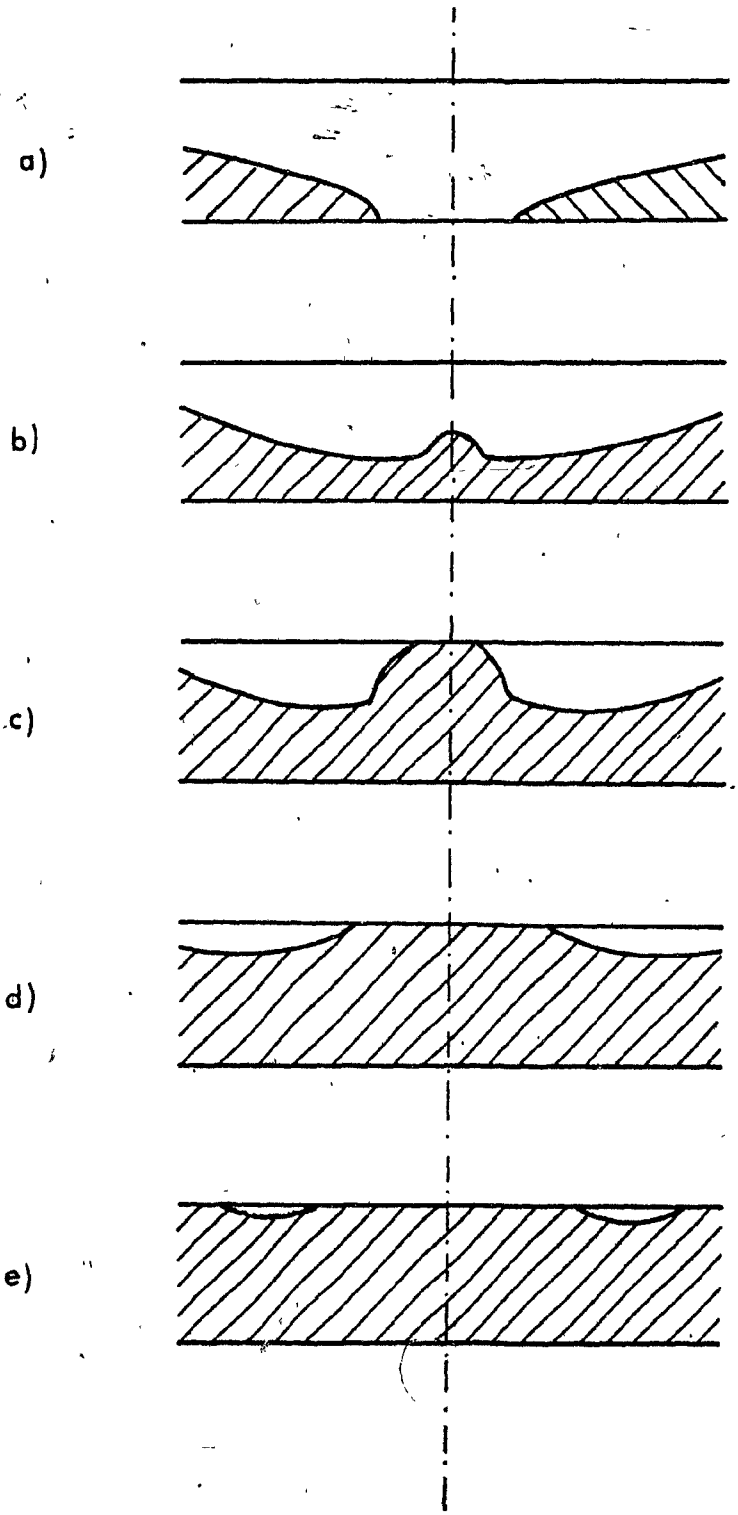
a)
b)
c)
d)
e)

FIGURE 2.7 Flow visualization for a channel 1.27 cm high.
Material: water
Film speed: 150 frames/sec
Time interval between prints: 1/150 sec
Time increases from a) to j)
Magnification: 0.4x

a

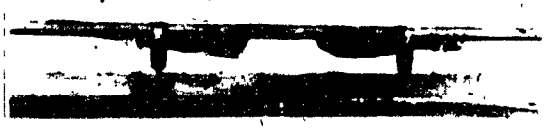

f

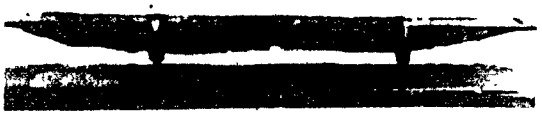

b

g

c

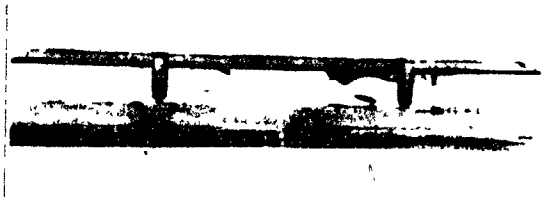

h

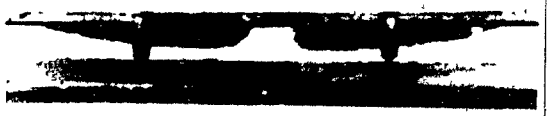

d

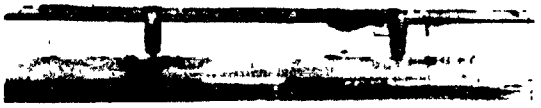

i

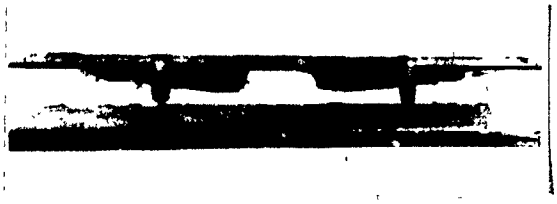

e

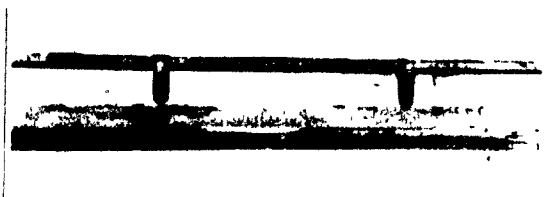

j

FIGURE 2.8 Flow visualization for a channel 1.27 cm high.
Material: mercury
Film speed: 150 frames/sec
Time interval between prints: 1/150 sec
Time increases from a) to h)
Magnification: 0.3x

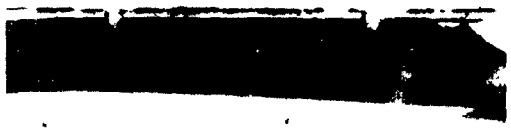

a

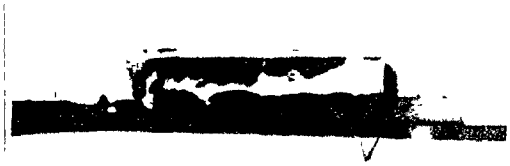

e

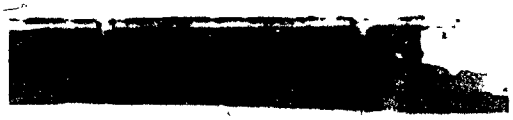

b

f

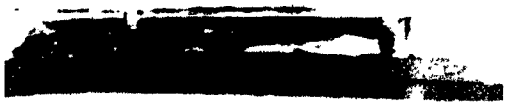

c

g

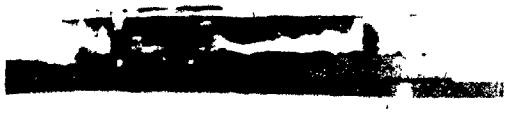

d

h

FIGURE 2.9 Flow visualization for a channel 0.635 cm high.
Material: water
Film speed: 150 frames/sec
Time interval between prints: 1/150 sec
Time increases from a) to j)
Magnification: 0.3x

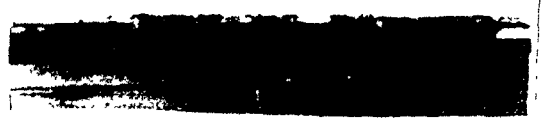

a

f

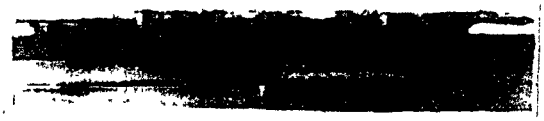

b

g

c

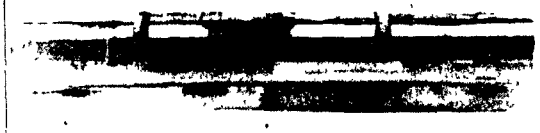

h

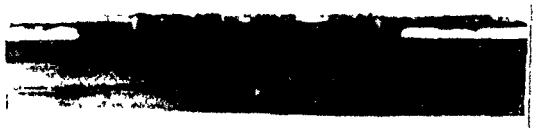

d

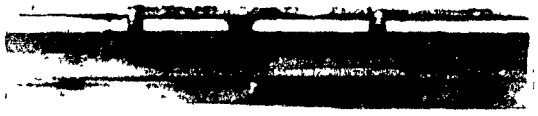

i

e

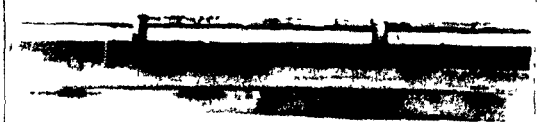

j

FIGURE 2.10 Flow visualization for a channel 0.635 cm high.
Material: mercury
Film speed: 150 frames/sec
Time interval between prints: 1/150 sec
Time increases from a) to h)
Magnification: 0.16x

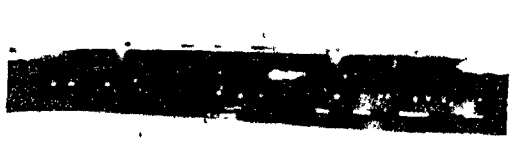

a

e

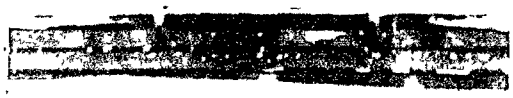

b

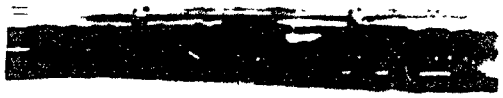

f

c

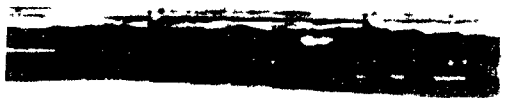

g

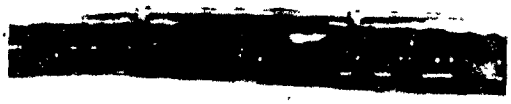

d

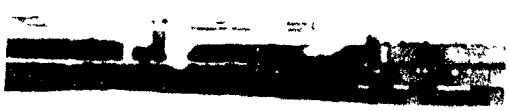

h

the water to flow into the mold. Mercury (technical grade) was also used so as to better reproduce liquid metal flow conditions in a real casting.

Each experiment was recorded using a video tape machine (model Sony AV3600) at a speed of 60 frames per second. The camera was located, for each experiment, perpendicular to the mold wall, and was focused on the area where the collision of the liquid streams would probably occur (Fig. 2.1). The experiments were recorded photographically, and black ink was added to the water to improve the contrast.

The photographs shown in the next section were taken with a Locam camera at a speed of 150 frames per second. The water and the mercury appear in white in all of these photographs.

2.4 Results

The experiments have shown that, under the same conditions, water and mercury exhibit similar behavior on meeting inside a channel, i.e. the two streams of liquid, on meeting, produce a wave and then start backfilling the mold as presented schematically in Figure 2.6. This behavior was always exhibited by both water and mercury, since the channel was sufficiently high to allow for the wave formation, as seen in Figure 2.7 and in Figure 2.8. In these figures the channel is 1.27 cm high, permitting the formation of the wave.

When the channel is not sufficiently high, the collision of the two streams is as presented in Figure 2.9 (water) and Figure 2.10 (mercury), in which it can be seen that both fluids, water and mercury, are as high as the channel itself, both fluids exhibiting the same behaviour.

Before analyzing the dimensionless numbers calculated and presented in Tables 2.2 and 2.3, it should be pointed out that as the runner is of noncircular cross section, the hydraulic diameter (D) is defined as:

$$D = \frac{4x \text{ cross sectional area}}{\text{wetted perimeter}} \tag{2.5}$$

The viscosity (μ) of mercury used was 0.015 Poise as reported elsewhere[28] while the surface tension (σ) for the fluids are reported by Iita et al.[30]

The velocity (u) was taken as the velocity at the channel entrance and was measured based on video recordings. The characteristic length dimension of the system (L) was taken as the height of the channel.

The friction factor (f) was estimated using experimental Reynolds numbers together with the data[21] given in Figure 2.5 which correlates the friction factor with both the relative roughness of the pipe (ε) and the Reynolds number (Re). As water and mercury were tested in a plastic mold, the curve taken was that for smooth tubes.

The behavior of the fluids was similar because the dimensionless numbers presented in Tables 2.2 and 2.3 are in the same region. The Froude numbers are equal for both fluids, while the Reynolds numbers show that water and mercury are flowing in a turbulent manner (Re > 3,000). The high Weber numbers show that, for both fluids, the inertial forces are far more important than the surface tension forces.

TABLE 2.2

Experimental Variables for the Flow of Water and Mercury in a Runner 1.27 cm High

Group	Formula	Fluid	u (cm/sec)	L (cm)	ρ (g/cm^3)	D (cm)	μ (Poise)	σ (dyne/cm)	Result
Froude	$\frac{u^2}{gL}$	water	65	1.27	-	-	-		Fr = 3.39
		mercury	65	1.27	-	-	-		Fr = 3.39
Reynolds	$\frac{\rho uD}{\mu}$	water	65	-	1	2.03	0.01		$Re = 1.3 \times 10^4$
		mercury	65	-	13.57	2.03	0.015		$Re = 1.2 \times 10^5$
Weber	$\frac{\rho u^2 D}{\sigma}$	water	65	-	1	2.03	-	74	We = 116
		mercury	65	-	13.57	2.03	-	487	We = 239
Friction Factor, f (Fig.2.5)	$\frac{\Delta P_f D}{\rho u^2 l}$	water							f = 0.0070
		mercury							f = 0.0036

TABLE 2.3

Experimental Variables for the Flow of Water and Mercury in a Runner 0.635 cm High

Group	Formula	Fluid	u (cm/sec)	L (cm)	ρ (g/cm^3)	D (cm)	μ (Poise)	σ (dyne/cm)	Result
Froude	$\frac{u^2}{gL}$	water	60	0.635	-	-	-	-	Fr = 5.78
		mercury	60	0.635	-	-	-	-	Fr = 5.78
Reynolds	$\frac{\rho uD}{\mu}$	water	60	-	1	1.13	0.01	-	$Re = 6.8 \times 10^3$
		mercury	60	-	13.57	1.13	0.015	-	$Re = 6.1 \times 10^4$
Weber	$\frac{\rho u^2 D}{\sigma}$	water	60	-	1	1.13	-	74	We = 55
		mercury	60	-	13.57	1.13	-	487	We = 113
Friction Factor, f (Fig.2.5)	$\frac{\Delta P_f D}{\rho u^2 l}$	water							f = 0.0085
		mercury							f = 0.0044

Using the equation for the friction factor (f) and its value obtained from the chart (Fig. 2.5), the equation for pressure drop (ΔP_f) can be derived, which leads to:

$$\Delta P_f = f \frac{\rho u^2 l}{D} \tag{2.6}$$

The calculation for the pressure drop has shown that, for a channel 1.27 cm high, it is equal to 6,000 dyne/cm^2 in the case of mercury, while for water it is equal to 860 dyne/cm^2. For a channel 0.635 cm high, the pressure drop for the mercury was calculated to be equal to 11,223 dyne/cm^2 while in the case of water it was equal to 1,598 dyne/cm^2. For both heights of the channel, the frictional energy losses for the mercury were calculated to be seven times greater than those for the water. Naturally, the greater kinetic energy associated with the flow of the denser mercury more than compensated for these higher absolute losses.

CHAPTER 3. EXPERIMENTS WITH LEAD AND LEAD-TIN ALLOYS

Knowing the kind of behavior which could be expected when there is a collision of two liquid streams inside a channel and knowing the dimensionless number which would describe the phenomenon, experiments with Pb and Pb-Sn alloys were designed in order to produce cold shuts on the surface of real castings. Lead and lead-tin alloys were selected because their low melting temperatures make them suitable for experimental work.

3.1 Molding Procedures

In order to obtain the meeting of two streams of molten metal, a pattern made of birch and yielding a mold (Figs. 3.1 and 3.2) with the same simple shape as the plastic mold (Fig. 2.3) was constructed. A flask was fabricated of oak with a cope 8.0 cm high and a drag 10.5 cm high. These two pieces of foundry equipment were designed in such a way as to allow visual observation (through a quartz glass window) of the meeting of the streams. The glass used was 2.5 cm wide, 0.5 cm thick and 15.0 cm long and was supplied by Lasalle Glass Blowing Co. Ltd. All the relevant properties of the quartz glass (as obtained from the manufacturer) are presented in Table 3.1.

In the experiments using both cope and drag, the pouring rate was controlled at the sprue, so that the flow speed was varied by changing the sprue diameter. The sprues used were tapered (nearly 10^{o}), 8.0 cm high, and their minimum diameters (where the pouring speed was regulated) were of six different dimensions, yielding the pouring rates presented in the Tables 3.3 and 3.4 of this chapter.

The molds were made of silica sand, AFS grain fineness number 140, bonded with 4 per cent by weight of each of western and southern

FIGURE 3.1 Dimensions of the sand mold and directions of flow inside the channel.

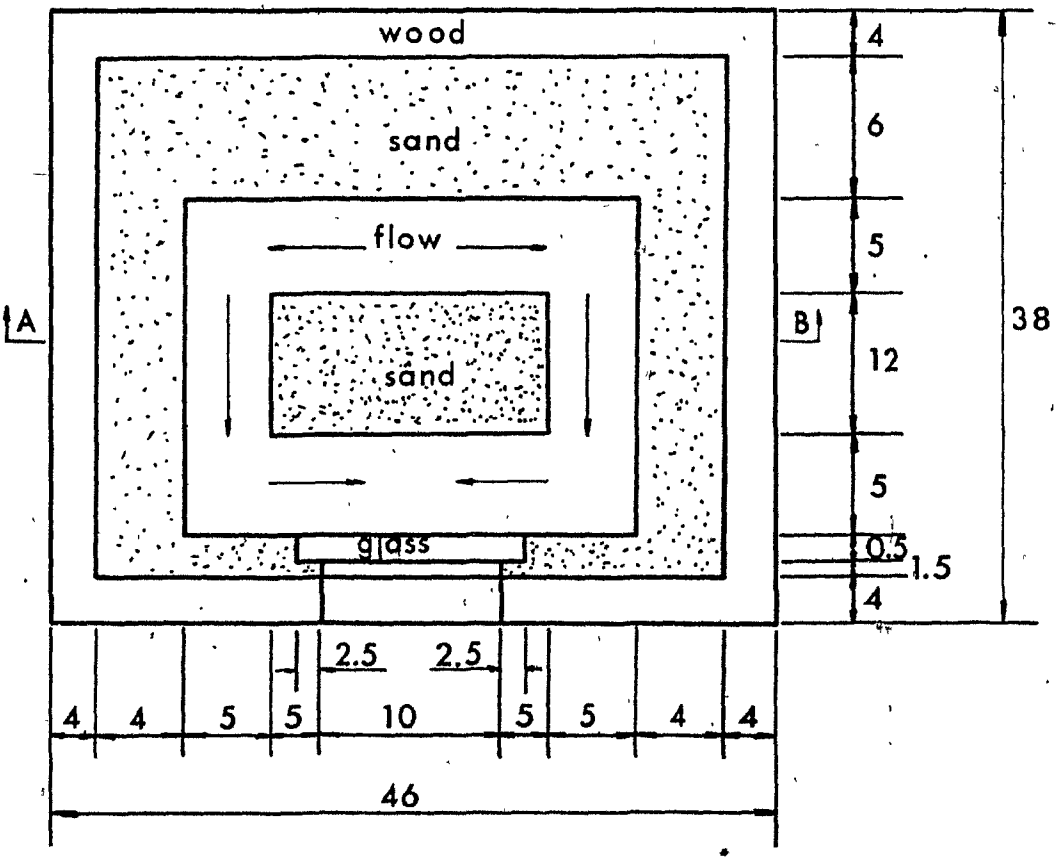
wood
sand
flow
sand
glass
A
B
4
6
5
12
5
0.5
1.5
4
38
2.5
2.5
4
4
5
5
10
5
5
4
4
46

UNIT= cm

FIGURE 3.2 Section AB of the sand mold.

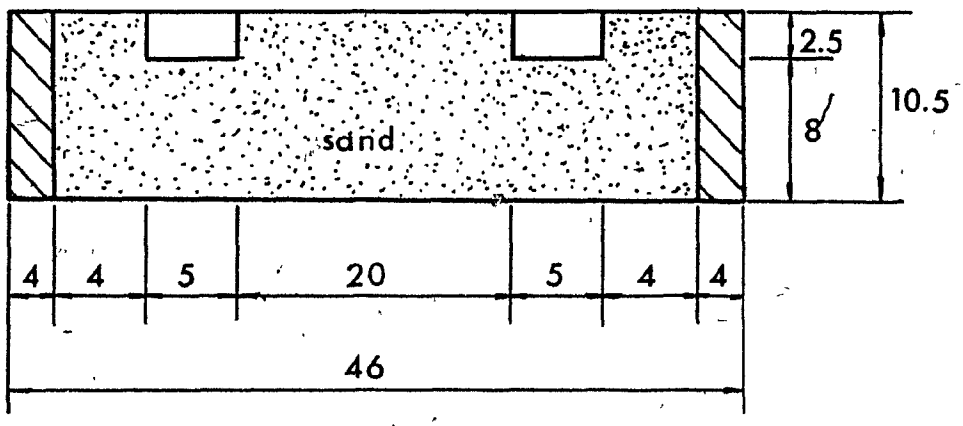

UNIT = cm

TABLE 3.1

Physical Properties of Quartz Glass

Properties	Unit	Value
density	g/cm^3	2.203
coefficient of linear expansion (0 to 1000°C)	/°C	5.4×10^{-7}
heat capacity (at 20°C)	cal/°C	0.166
heat conduction (at 20°C)	cal/cm-°C-sec	0.003
annealing point	°C	1210°C (1483 K)
softening point	°C	1650°C (1923 K)

bentonites and 4 per cent by weight of water. This fine-grained sand was chosen to produce a smooth finish on the surface of the casting, since the experiments were with small castings and the goal was to obtain a surface defect. The water content was controlled with a "Speedy" Moisture Tester (Thomas Ashworth & Co. Ltd., Burnley, England), and all sand mixes were mulled for about 15 minutes after the water was added.

Since molten metal coming into contact with sand causes a thin layer of clay adjacent to it to be baked, the sand mix was recycled after every 10 castings by adding 1 per cent by weight of each of western and southern bentonites.

All experiments were performed using green sand at the ambient temperature, and as for each run the sand was mixed and compacted (using

FIGURE 3.3 Flask.

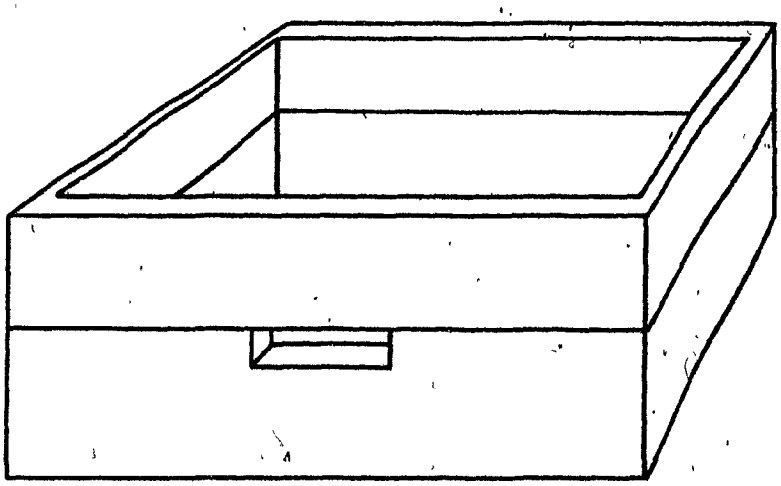

FIGURE 3.4 a) Graphite ladle.

FIGURE 3.4 b) Graphite plug.

a)

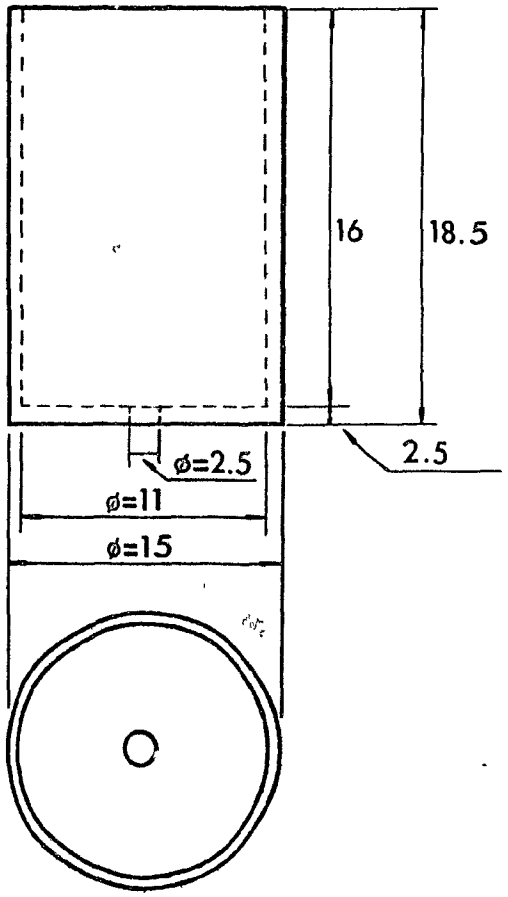

b)

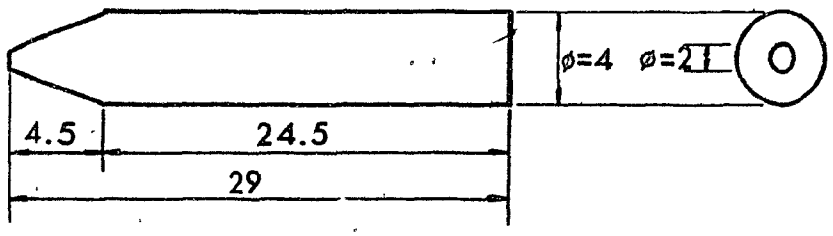

UNIT = cm

a manual bench hammer) in the same way, all the molds were assumed to have approximately the same physical properties.

3.2 Melting Procedures

In all experiments, including those with Pb-Sn alloys, the metal was melted in a conventional manner, using a gas-fired crucible furnace, and was superheated sufficiently to permit handling. Clay-graphite crucibles were used and the lead employed in all experiments was of commercial purity.

3.3 Pouring Procedures

In order to obtain reproducible pouring rates, a graphite ladle (Fig. 3.4a), with a 2.5 cm diameter hole at the center of the bottom, was used. The bottom hole was sealed by a graphite cylinder tapered at one end (Fig. 3.4b). In experiments with no cope, as described later, the pouring rate was controlled at this orifice.

The graphite ladle served as a tundish, and in order to avoid undesirable premature solidification, it was preheated before each experiment to 50^{o}C above the pouring temperature. This procedure was used in all experiments, including those with Pb-Sn alloys.

3.4 Experiments

Experiments were performed in an attempt to produce a special kind of cold shut suitable for scientific analysis. For this, the defect would have to be perpendicular to the flow velocity (i.e., vertical) and it should occur in a reproducible specified position to allow for

temperature measurements. This type of defect was found to be very difficult to produce and so the approach had to be changed several times. The various types of experiments are described below in chronological order.

3.4.1 Simple Experiments without Ladle

The first kind of experiment tried was to pour molten lead manually into the mold shown in Figure 3.1. The parameters involved in such castings are presented in Table 3.2. As will be seen in Section 3.5, the cold shuts were formed by layers because the pouring rates were insufficient (due to inadequacies in the pouring practice). Even when the superheats were varied, the defect continued to be formed in the same way.

3.4.2 Simple Experiments using Ladle

These experiments were similar to the first ones, the only difference being the use of the ladle. Its use as a tundish improved the pouring rates considerably, as well as making these rates reproducible. From this point on, the ladle was used in every experiment, except for the experiments outlined in Section 3.4.7. Although being reproducible, the pouring rates were still found to be inadequate for the production of the desired cold shut.

The experiments were carried out using lead and Table 3.3 shows the relevant values involved.

TABLE 3.2

Experimental Variables for Experiments without Ladle

Experiment Number	Superheat (°C)	Pouring Temperature (°C)	Sprue Diameter (cm)	Height of Runner (cm)
A1	100	427	2.5	2.54
A2	40	367	2.5	2.54
A3	20	347	2.5	2.54
A4	50	377	1.5	1.27
A5	50	377	1.0	1.27

3.4.3 Experiments Using Obstacles

As the experiments performed previously were not useful in the sense of temperature measurements because they did not produce a vertical cold shut, two experiments were carried out using obstacles, which both slowed the flow and caused splashing of the liquid metal. The obstacles were steel plates 1.2 cm wide, 5.0 cm long and 0.05 cm thick. They were embedded 0.6 cm in the sand, so that the actual obstacle height was 0.6 cm, and they were placed 9.5 cm apart, symmetrically to the center of the glass window (Fig. 3.1). As the first experiment resulted in cold shuts formed in layers as before, it was decided to place a copper plate between the two obstacles to accelerate the solidification in the area where the two streams of the liquid metal would meet. This approach also resulted in cold shuts formed as horizontal layers.

TABLE 3.3

Experimental Variables for Experiments using Ladle

Experiment Number	Superheat (°C)	Pouring Temperature (°C)	Sprue Diameter (cm)	Height of Runner (cm)	Pouring Rate (g/sec)
B1	35	362	1.5	1.27	230
B2	5	332	2.0	1.27	276
B3	3	330	2.0	1.27	no meeting
B4	4	331	2.0	1.27	288
B5	70	397	2.0	1.27	290
B6	5	332	0.5	1.27	no meeting
B7	10	337	0.5	1.27	no meeting
B8	15	342	0.5	1.27	no meeting
B9	100	427	0.5	1.27	58
B10	20	347	0.75	1.27	115

These experiments were performed using lead, and Table 3.4 shows the values involved.

TABLE 3.4

Experimental Variables for Experiments using Obstacles

Experiment Number	Superheat (°C)	Pouring Temperature (°C)	Sprue Diameter (cm)	Height of Runner (cm)	Pouring Rate (g/sec)
C1	15	342	1.5	1.27	216
C2	15	342	1.5	1.27	193

3.4.4 Experiments without Cope

These experiments were designed to reduce the flow momentum (by reducing the head of metal) in an attempt to produce a vertical cold shut. As the cope was not used, the sprue was eliminated and the pouring rate was controlled by the diameter of the bottom hole of the graphite ladle and by the metal head. Thus, the pouring rate was varied by changing the quantity of Pb inside the ladle. The variables involved in these experiments are shown in Table 3.5.

3.4.5 Experiments with a Chill Bottom in Half Mold

This kind of experiment was performed to try to solidify one stream of metal before the other could meet with it. In order to achieve this, a copper plate 5.0 cm wide and 0.3 cm thick was placed in the path of one of the two streams on the surface of the channel.

TABLE 3.5

Experimental Variables for Experiments without Cope

Experiment Number	Superheat (°C)	Pouring Temperature (°C)	Height of Runner (cm)	Metal Weight (g)	Pouring Rate (g/sec)
D1	70	397	1.27	4167	220
D2	20	347	1.27	2155	no meeting
D3	30	357	1.27	2126	-
D4	20	347	1.27	1531	no meeting
D5	20	347	1.27	2070	no meeting
D6	10	337	1.27	2778	-

This plate extended from the point of pouring to a point halfway around the entire channel. The copper, acting as a chilling agent, would solidify the metal quickly on its side, so that the liquid stream meeting the already solid metal would form the desired vertical defect. As the cope was not used, the pouring rate, as before, was changed by varying the quantity of lead inside the graphite ladle. The relevant values involved in such experiments are presented in Table 3.6, and the absence of pouring rates is explained in Section 3.5.5.

3.4.6 Experiments using Solid Inserts

These experiments were designed to allow temperature measurement during cold shut formation by placing a solid in the metal stream.

TABLE 3.6

Experimental Variables for Experiments with a Chill Bottom in Half Mold

Experiment Number	Superheat (°C)	Pouring Temperature (°C)	Height of Runner (cm)	Metal Weight (g)	Pouring Rate (g/sec)
E1	20	347	1.27	2268	-
E2	10	337	1.27	2041	no meeting
E3	15	342	1.27	2098	no meeting
E4	15	342	1.27	2495	-

A new geometrical simple pattern was developed so that the mold would have the shape shown in Figure 3.5. Inside the runner, three special samples of solid metal (Fig. 3.6), located in proper places (as shown in Fig. 3.5), were embedded in the sand with steel pins. The solid sample had the same composition as the liquid which would be poured over it and was made by rolling the metal until the desired thickness was reached. The 3.0 cm long plate was then bent to obtain the final shape (Fig. 3.6).

Since a cold shut would be formed if the solid sample did not remelt, it is clear that the surface condition of the sample - which does influence remelting - should have an effect on cold shut formation. Two kinds of surfaces were tested. Surface B (Table 3.7) is an oxidized surface. To obtain this, the Pb sample was heated to 250°C (150°C for Pb-Sn alloys), kept at this temperature for 20 minutes

FIGURE 3.5 Sand mold for experiments using solid inserts.

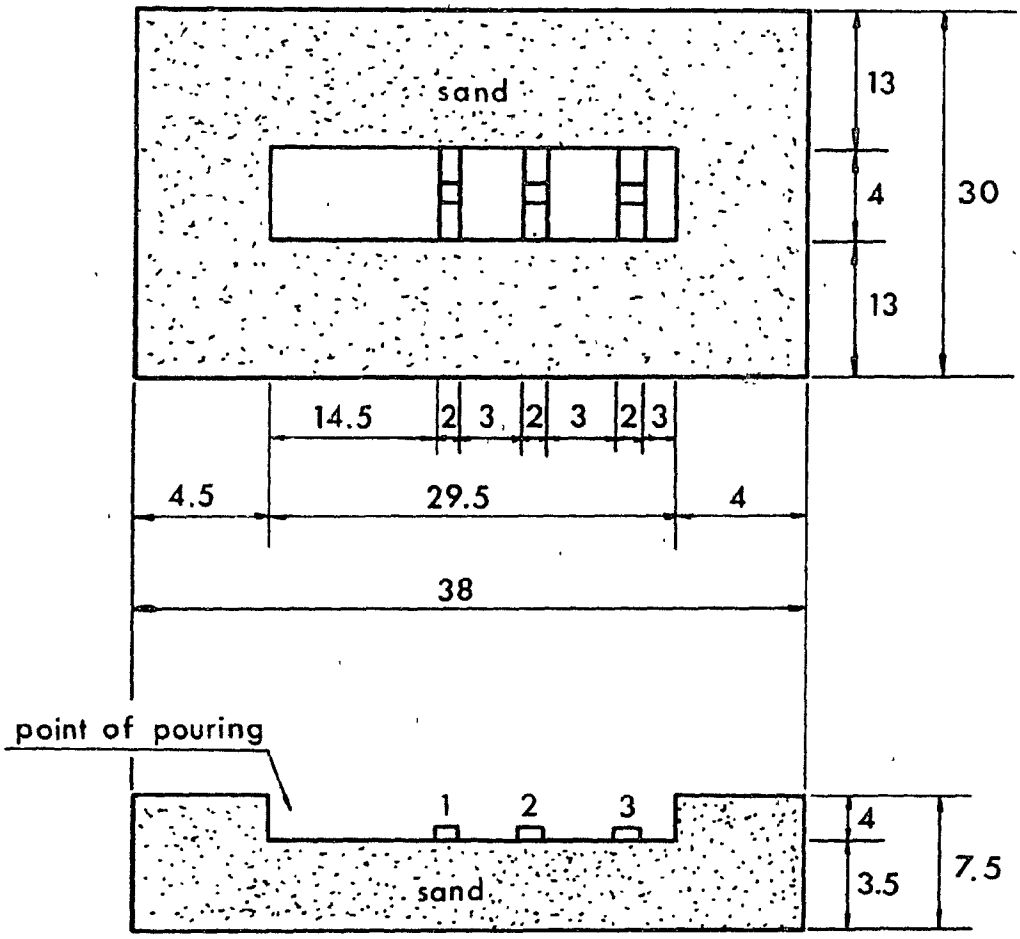
sand
13
4
30
13
14.5
2
3
2
3
2
3
4.5
29.5
4
38
point of pouring
1
2
3
4
3.5
7.5
sand

UNIT = cm

FIGURE 3.6 Two solid samples as placed on the channel.

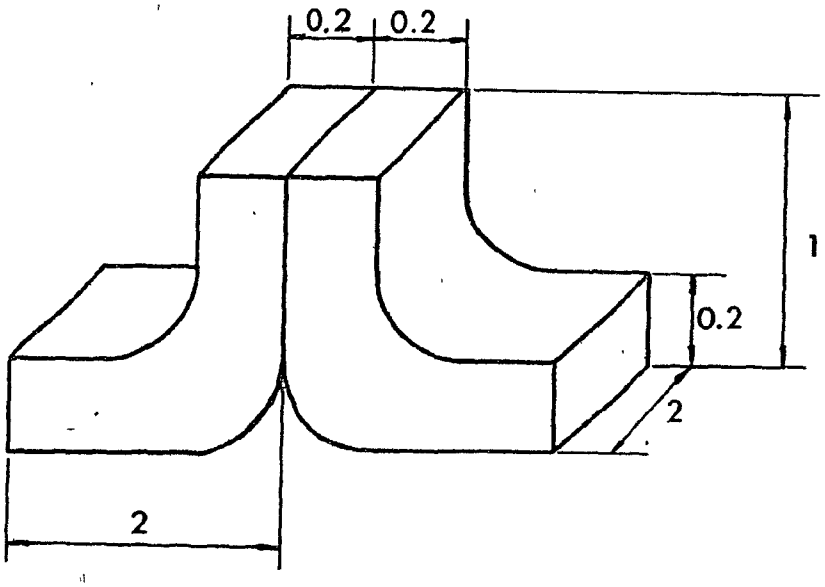

UNIT = cm

TABLE 3.7

Experimental Variables for Experiments using Solid Inserts

Experiment Number	Metal Composition	Superheat (°C)	Pouring Temperature (°C)	Metal Weight (g)	Sample Thickness (cm)	Surface Condition
F1	Pb	100	427	3650	0.2	C
F2	Pb	100	427	3650	0.2	B
F3	Pb	20	347	3650	0.2	B
F4	Pb	20	347	3650	0.2	C
F5	Pb	60	387	3650	0.2	C
F6	Pb	60	387	3650	0.2	B
F7	Pb-19% Sn	60	340	3400	0.2	C
F8	Pb-19% Sn	60	340	3900	0.2	B
F9	Pb	60	387	3750	0.2	C
F10	Pb	60	387	3650	0.2	B
F11	Pb-19% Sn	60	340	3500	0.2	C
F12	Pb-19% Sn	60	340	3650	0.2	B
F13	Pb	100	427	3900	0.2	B
F14	Pb	100	427	3500	0.2	B
F15	Pb-19% Sn	100	380	3000	0.2	B
F16	Pb-61.9% Sn	100	283	2600	0.2	B
F17	Pb-61.9% Sn	75	258	2500	0.2	B
F18	Pb-61.9% Sn	50	233	2600	0.2	B

and then cooled in air. Surface C (Table 3.7) was obtained by polishing the sample with a 600 silicon carbide paper.

A Pb-19% Sn alloy was used in this kind of experiment because it has the largest freezing range of the Pb-Sn system (Fig. 3.7) and the mode of solidification should play an important role. Experiments were also performed using an alloy of eutectic composition.

3.4.7 Experiments using a Stepped Mold

These experiments were designed to determine the effect of the splashing of the liquid metal on the cold shut formation. A new pattern was built to produce the mold shown in Figure 3.8. The graphite ladle was not used in these experiments which were performed with lead and in which the metal was poured into the mold at its shallow side.

Table 3.8 gives the experimental variables.

TABLE 3.8

Experimental Variables using a Stepped Mold

Experiment Number	Superheat (^{o}C)	Pouring Temperature (^{o}C)
G1	75	402
G2	150	477
G3	25	352

FIGURE 3.7 Pb-Sn Phase Diagram.

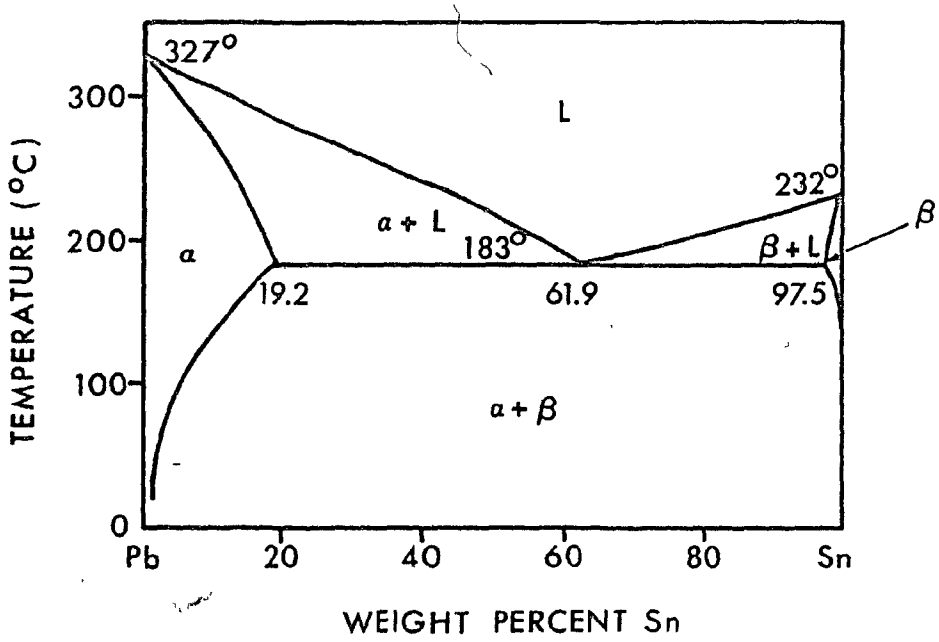
327°
L
232°
β
α + L
183°
β + L
α
19.2
61.9
97.5
α + β
300
200
100
0
TEMPERATURE (°C)
Pb
20
40
60
80
Sn
WEIGHT PERCENT Sn

FIGURE 3.8 The stepped mold.

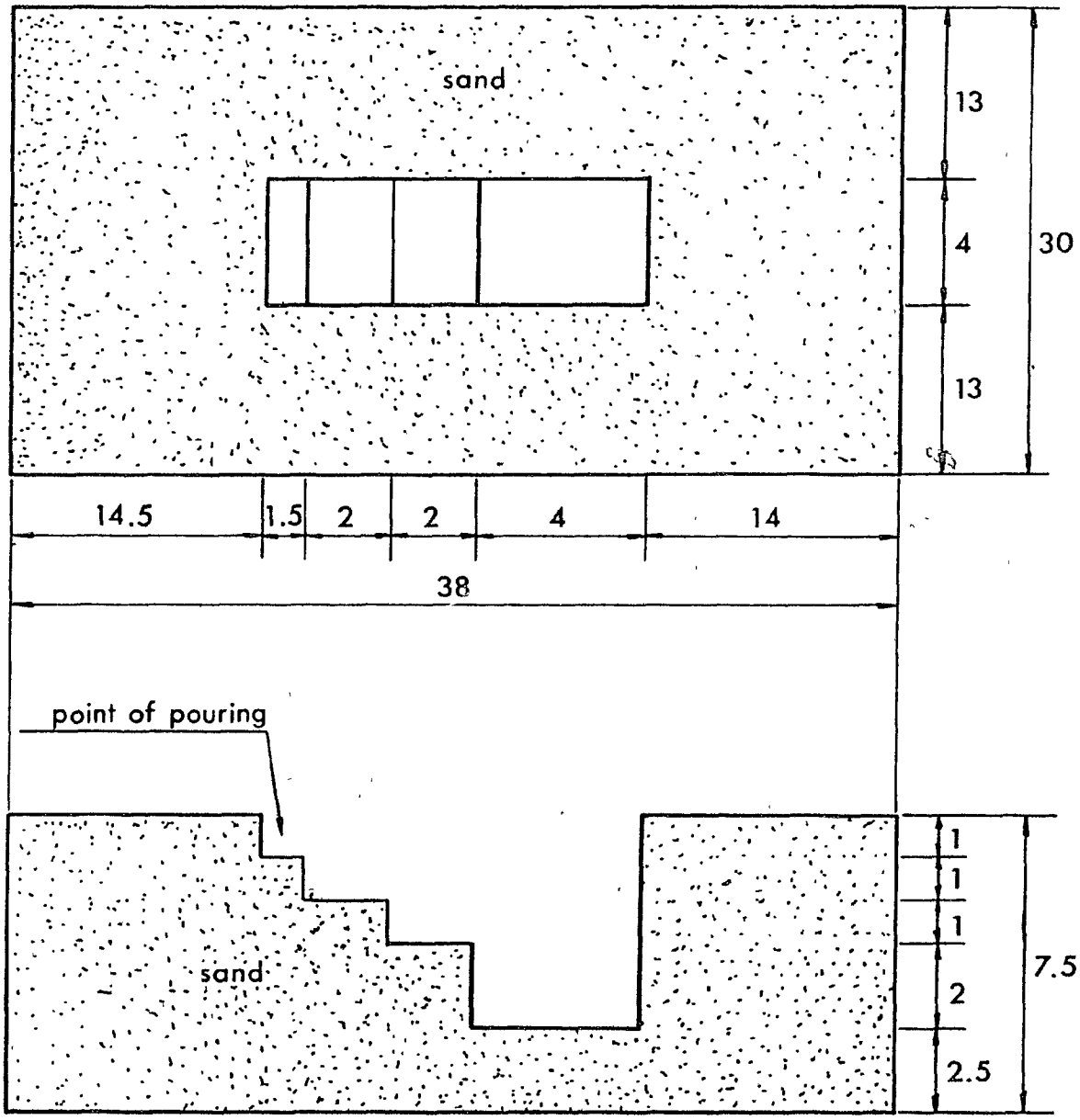

UNIT = cm

3.5 Results

As previously mentioned, the type of experiment was changed when the results were found to be unsuitable for this study. Results will be presented separately by type of experiment.

3.5.1 Simple Experiments without Ladle

These experiments, when the molten metal was poured manually into the mold, resulted in discontinuous pouring rates as well as pouring rates which varied from run to run. As no vertical defects were formed, the runner height, for the last two experiments, was reduced to half; however, suitable cold shuts were still not produced. In all experiments the cold shuts were formed as horizontal layers by liquid metal flowing over the already frozen metal in contact with the glass window. The typical defect formed is shown in Figure 3.9, which is a result of experiment number A5 (Table 3.2). The photograph shows the location where the two liquid streams met. The collision produced a wave which froze on the wall, forming a cold shut which outlined the flow pattern (indicated by the arrows in Figure 3.9). The cause of the formation of this layered defect could be the inconsistency of the pouring due to the human factor. Thus, the graphite ladle was used to make continuous pouring possible and also to increase the pouring rate. The pouring rates are not shown in Table 3.2, because they were discontinuous.

3.5.2 Simple Experiments using Ladle

The use of the ladle did, in fact, standardize the pouring rate but it still was not useful in promoting the desired vertical type

FIGURE 3.9 Typical cold shuts formed in experiments without ladle (superheat: 50°C).
Magnification: 1.3x

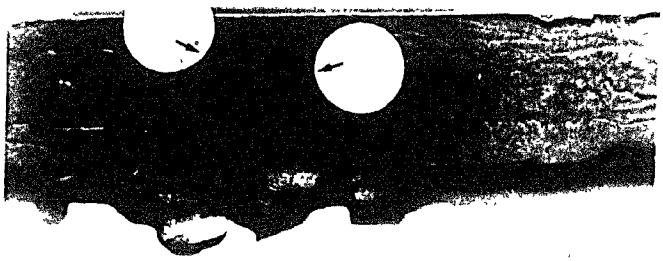

flow directions

of surface defect. Layered cold shuts continued to be formed exactly as before. Figure 3.10 (experiment number B2, Table 3.3) and Figure 3.11 (experiment number B5, Table 3.3) show that the cold shuts formed in experiments where the ladle was used had the same appearance as those formed when the ladle was not used. It is worth noting, by comparing Figure 3.10 with Figure 3.11, that the superheat did not make any noticeable difference in the appearance of the cold shuts. The same cannot be said about the pouring rate. Low pouring rates (58 g/sec), even at high superheats (100^{o}C), produced deeper defects (Figure 3.12, experiment B9, Table 3.3).

These experiments were also recorded (through the quartz glass) by using the video tape machine. In this way the pouring rates could be calculated and the flow behaviour could be analyzed more carefully. The behavior of the liquid metal was similar to that of the water and mercury presented in Chapter II. The two streams of liquid Pb collided and produced the same kind of wave (Fig. 3.13). Figures 3.13a and 3.13b show the solidified stream (dark, indicated by arrows) in contact with the glass window, the white line being due to light reflection. There was a small amount of leakage between the glass and the sand (visible at the right end of the window), but this did not affect the results obtained. Figures 3.13c to 3.13e show, beyond the solid metal (dark), that the molten metal produced the same wave (white, indicated by arrows) as the water and mercury on meeting inside a channel. Photographs 3.13f to 3.13o show that, once the liquid metal has touched the glass (mold wall), it solidifies instantaneously, the metal freezing from the point of contact progressively outwards in all directions in the plane of the window. These experiments have shown

FIGURE 3.10 Typical cold shuts formed in experiments using ladle (superheat: 5°C).
Magnification: 1.3x

FIGURE 3.11 Typical cold shuts formed in experiments using ladle (superheat: 70°C).
Magnification: 1.3x

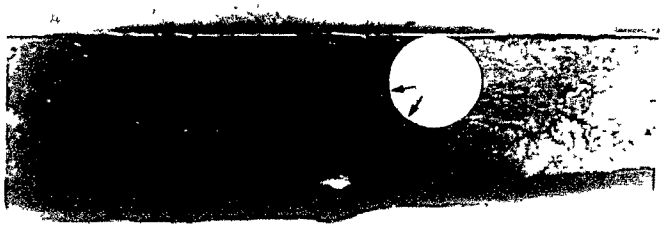

flow

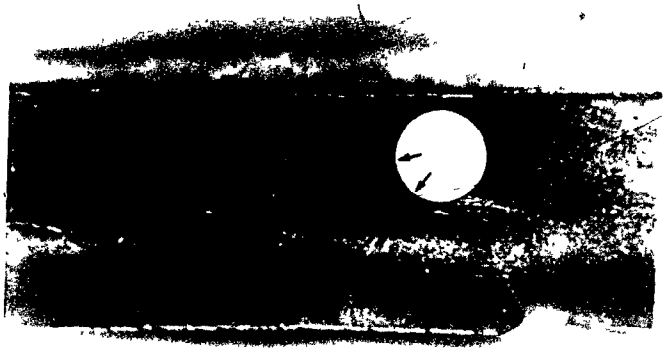

flow

FIGURE 3.12 Typical cold shuts formed in experiments using low pouring rate (superheat: 100°C).
Magnification: 1.2x

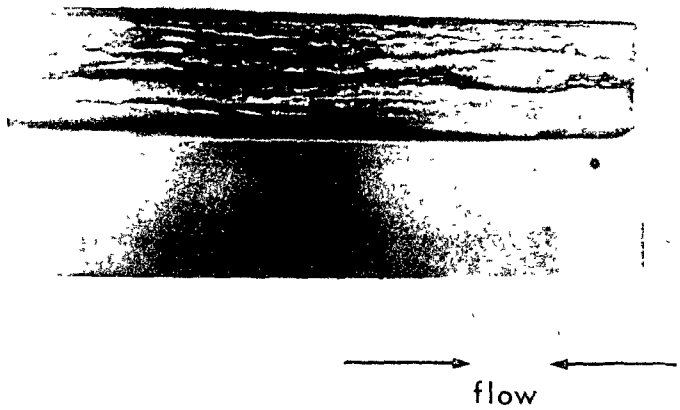
flow

FIGURE 3.13 Flow visualization for a channel 1.27 cm high.
Material: Pb (commercial purity)
Film speed: 150 frames/sec
Time increases from a) to 0)
Magnification: 0.6x

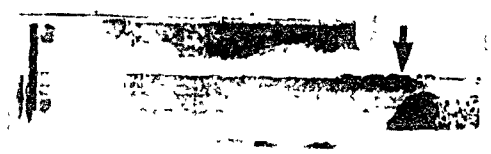

a

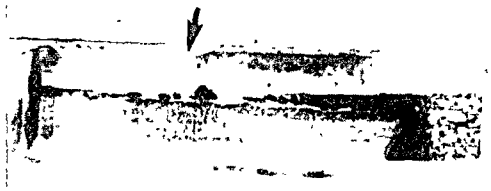

e

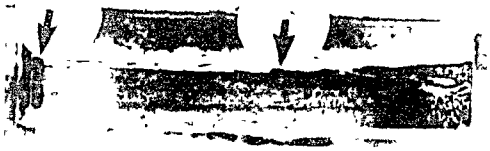

b

f

c

g

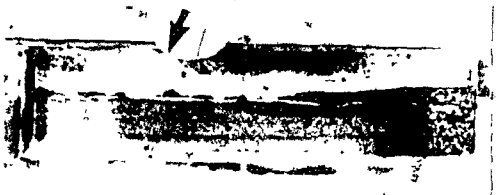

d

h

FIGURE 3.13 Continuation.

i

l

j

m

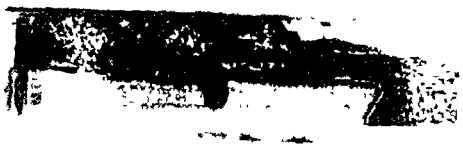

k

n

o

that the water system and the liquid metal system are similar when two streams of the same fluid (either water or lead) meet inside a channel. The similarity was achieved because the dimensionless numbers for both systems were kept close or in the same region as shown in Table 3.9. The hydraulic diameter (D) for the lead system was calculated using equation (2.5) as was done for the water and mercury systems. The velocity (u) was estimated using the following formula:

$$u = F_c\sqrt{2gL} \tag{3.1}$$

where F_c is a correction factor taken as 0.26. This value was obtained by comparing theoretical calculations with experimental results for water and mercury. This had to be done because the opaqueness of both the sand and the graphite ladle did not allow for video tape recording.

The viscosity of lead used was 0.025 Poise as reported elsewhere[12], while its surface tension was reported by Iida et al.[30]

The friction factor (f) was estimated using the chart[21] shown in Figure 2.5. For its use, it was assumed that the absolute roughness (ε) of the sand was in the same range of that of the concrete reported by Geiger and Poirer[28] ($\varepsilon = 0.02$ in). As the value of D is 2.03 cm which is equal to 0.8 in, the relative roughness (ε/D) of sand was taken as 0.03. For this curve, with $Re = 3.8\times10^4$, the value of f obtained was $f = 0.015$ (Table 3.9).

Table 3.9 shows that the Froude number for lead is not much different from that for water and mercury. The Reynolds number for the three fluids shows that all of them are flowing in a turbulent manner

TABLE 3.9

Experimental Variables for the Flow of Water, Mercury and Lead in a Runner 1.27 cm High

Group	Formula	Fluid	u (cm/sec)	L (cm)	ρ (g/cm^3)	D (cm)	μ (Poise)	σ (dyne/cm)	Result
Froude	$\frac{u^2}{gL}$	water	65	1.27	-	-	-	-	Fr = 3.39
		mercury	65	1.27	-	-	-	-	Fr = 3.39
		lead	42	1.27	-	-	-	-	Fr = 1.42
Reynolds	$\frac{\rho uD}{\mu}$	water	65	-	1	2.03	0.01	-	Re = 1.3×10^4
		mercury	65	-	13.57	2.03	0.015	-	Re = 1.2×10^5
		lead	42	-	11.3	2.03	0.025	-	Re = 3.8×10^4
Weber	$\frac{\rho u^2 D}{\sigma}$	water	65	-	1	2.03	-	74	We = 116
		mercury	65	-	13.57	2.03	-	487	We = 239
		lead	42	-	11.3	2.03	-	453	We = 89
Fanning Friction Factor, f	$\frac{\Delta P_f D}{\rho u^2 l}$	water							f = 0.0070
		mercury							f = 0.0036
		lead							f = 0.015

(Re > 3000). The Weber number shows that, for the three fluids studied, the inertial forces are much greater than the surface tension forces. Using equation (2.6) and the value of f obtained from Figure 2.5, it was found that the pressure drop (ΔP_f), in the case of lead, for a runner 1.27 cm high, is equal to 8,690 dyne/cm^2. This value is even greater than the pressure drop for mercury (Section 2.4) which means that, among the fluids used, molten lead loses more energy during flow.

Although losing much less energy than the other fluids, the water relative loss, $\frac{\Delta P_f}{\rho}$, is similar. As such, water is an adequate model for molten metal meeting inside a channel since the three dimensionless numbers calculated (Fr, Re and We) are also in the same region as those for lead and mercury.

Mercury has a steeper advancing wave profile than the other fluids (Figs. 2.7, 2.8 and 3.13) probably because of its non-wetting characteristic.

Another phenomenon observed was that, for castings using a sprue diameter equal to or greater than 1.0 cm, a surface defect always appeared at the bottom, exactly where the collision took place. This defect (Fig. 3.14, experiment number B2) seems to be an erosion scab (Section 1.1) which was formed due to turbulence in the flow.

Aluminum was also tested in this kind of experiment, but the quartz glass did not resist the high temperatures and cracked.

Four experiments did not produce cold shuts because both streams solidified before meeting. Experiment number B3 (Table 3.3), had too low a superheat and experiments number B6, B7 and B8 (Table 3.3), had too low pouring rates which caused solidification in the sprue.

FIGURE 3.14 Typical defect at the bottom of the samples when sprue diameter exceeded 1.0 cm.
Magnification: 1.0x

flow

Raising the superheat (experiment B9, Table 3.3) avoided this stoppage but did not prevent deep layered cold shuts (Fig. 3.12).

3.5.3 Experiments using Obstacles

Since the use of the ladle did not produce results which were amenable to temperature measurements, experiments were tried using obstacles to decrease the pouring speed as well as to cause splashing of the liquid metal. These two experiments produced the same wave formation, and again the cold shuts were formed in horizontal layers. It was thought that the flow momentum was too high, thus preventing the formation of a vertical cold shut. Therefore, the next step was to decrease the flow momentum by eliminating the cope (the upper part of the mold).

3.5.4 Experiments without Cope

The elimination of the cope did not contribute to the formation of vertical cold shuts. The defect was again formed in horizontal layers and the same wave as before was produced (Fig. 3.15, experiment D1, Table 3.5). Three experiments (D2, D4 and D5, Table 3.5) with a superheat of 20^{o}C did not allow the meeting of the two streams. Experiment D6 (Table 3.5) with lower superheat (10^{o}C) allowed the streams to collide due to the greater head of metal. The pouring rates for experiments number D3 and D6 do not appear in Table 3.5 because the streams were not adequately visible in the video tape.

3.5.5 Experiments with a Chill Bottom in Half Mold

This experimental approach proved to be more adequate than all others previously tried. The copper plate solidified one of the streams, so that when the liquid stream met the solid one, a cold shut was formed at the junction. This can be seen in Figure 3.16, which shows the bottom surface of the casting resulting from experiment number E4 (Table 3.6). The shape of the stream is clearly visible. Experiments number E2 and E3 did not produce the meeting of the streams due to the low head of metal while the pouring rates of experiments number E1 and E4 are not shown in Table 3.6 because the video tape for those experiments was inadequate.

Although this kind of experiment yielded better cold shuts, temperature measurement at the defect remained a problem due to the uncertainty in predicting the exact location of the cold shut. In the next series of experiments solid pieces of metal were placed in the liquid stream to produce cold shuts at a predictable location. This approach eliminated the problem of temperature measurement.

3.5.6 Experiments using Solid Inserts

This kind of experiment overcame the problem of the temperature measurement because it provided, in advance, the point where the liquid stream would meet the solid metal as well as allowing for variations in the surface conditions. Varying the superheat, the surface condition and the alloying element, several experiments were carried out, as shown in Table 3.7. After each experiment, the sample was sectioned at the three positions (1, 2 and 3), shown in Figure 3.5.

FIGURE 3.15 Typical cold shuts formed in experiments without cope (superheat: 70°C).
Magnification: 1.0x

FIGURE 3.16 Typical cold shuts formed on the bottom surface of the sample (superheat: 15°C).
Magnification: 1.0x

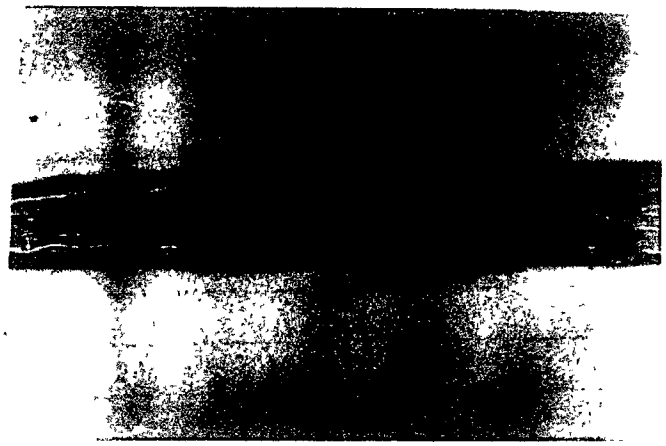

flow

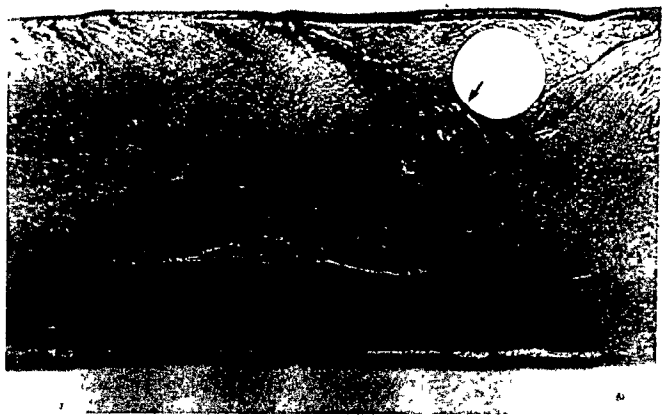

flow

The surfaces of each section were prepared metallographically by wet grinding on a silicon carbide belt (grit 80). Then, the specimens were ground on silicon carbide paper of successively finer grades (grits 220, 320, 400 and 600), and finally were polished on a polishing wheel using a metron cloth impregnated with an alumina suspension. Coarse polishing was done using 5 micron alumina, and 0.3 micron alumina was used for the final polish. The specimens, once polished, were etched, with the time of etching depending on the amount of the alloying element present. Pure lead was etched with a mixture of equal proportions of the following solutions:[23]

Solution A

15 g of ammonium molybdate

100 ml distilled water

Solution B

6 parts nitric acid (conc.)

4 parts distilled water

The Pb-Sn alloys were etched using the following solution:[23]

1 part nitric acid (conc.)

1 part distilled water

Comparing, for instance, the results for experiments number F5 and F6, it can be seen that, as is expected, for the same superheat

(60°C) the surface condition influenced the remelting of the sample, therefore affecting the cold shut formation. For low superheat (20°C), as illustrated by experiments number F4 and F3 (Table 3.10), the surface condition had only a small effect on the cold shut formation. Table 3.10 also shows that the liquid metal becomes cooler as it flows towards the farthest parts in the mold. Its capacity for remelting the solid is progressively lost downstream, and hence the farther the liquid metal is from the point of pouring, the higher is the probability for cold shut formation.

The effect of the superheat on the remelting phenomenon is also shown in Table 3.10. Comparing, for instance, experiments number F3, F6 and F2, it can be seen that, other conditions being constant, streams with higher superheats have a greater capacity for melting the solid pieces.

The influence of the alloying element, i.e. the solidification characteristic, on the remelting process is best shown in Tables 3.11 and 3.12, which separate the experiments according to surface condition. For the same superheat (experiments number F5 and F11, Table 3.11), the Pb-19% Sn alloy shows greater resistance to the remelting phenomenon than the unalloyed lead, and this is confirmed in Table 3.12 (experiments number F6 and F12). Table 3.11 also shows that, the superheat being constant (experiments number F5 and F11), the effect of the alloying element becomes greater as the liquid becomes cooler, which is also confirmed in Table 3.12 (experiments number F2 and F15). The eutectic alloy (Pb-61.9% Sn) has a lower resistance to remelting than the Pb-19% Sn alloy, as can be seen in Table 3.12 (experiments number

TABLE 3.10

Schematic Diagram of the Remelting Phenomenon

Experiment Number	Metal	Superheat (°C)	Position / Surface	1	2	3
F1	Pb	100	clean			
F2,F13,F14	Pb	100	oxidized			
F5,F9	Pb	60	clean			
F6,F10	Pb	60	oxidized			
F4	Pb	20	clean			
F3	Pb	20	oxidized			
F7,F11	Pb-19% Sn	60	clean			
F8,F12	Pb-19% Sn	60	oxidized			
F15	Pb-19% Sn	100	oxidized			
F16	Pb-61.9% Sn	100	oxidized			
F17	Pb-61.9% Sn	75	oxidized			
F18	Pb-61.9% Sn	50	oxidized			

LEGEND:  = complete remelting of top;  = partial remelting;  = no remelting

TABLE 3.11

Schematic Diagram of Remelting for Clean Samples

Experiment Number	Metal	Superheat (°C)	Position / Surface	1	2	3
F1	Pb	100	clean			
F5,F9	Pb	60	clean			
F7,F11	Pb-19% Sn	60	clean			
F4	Pb	20	clean			

LEGEND: as per Table 3.10

TABLE 3.12

Schematic Diagram of Remelting for Oxidized Samples

Experiment Number	Metal	Superheat (°C)	Position / Surface	1	2	3
F2,F13,F14	Pb	100	oxidized			
F15	Pb-19% Sn	100	oxidized			
F16	Pb-61.9% Sn	100	oxidized			
F6,F10	Pb	60	oxidized			
F8,F12	Pb-19% Sn	60	oxidized			
F17	Pb-61.9% Sn	75	oxidized			
F18	Pb-61.9% Sn	50	oxidized			
F3	Pb	20	oxidized			

LEGEND: as per Table 3.10

F15 and F16). The behavior of the eutectic alloy, in the sense of resistance to remelting, is similar to that of unalloyed lead, while the Pb-19% Sn alloy, due to its large freezing range (Fig. 3.7), presented a much greater resistance to the remelting process.

A sample which was not remelted is shown in Figure 3.17 (experiment number F9, Tables 3.7 and 3.10). The structural differences are clearly seen with the discontinuity being well defined (indicated by arrows) in this sample of lead. Figure 3.18 shows an almost entirely remelted sample of lead (experiment number F14, Tables 3.7 and 3.10). Although the cold shut here is formed in only a small part of the sample, the defect is still well defined, and is seen in the region indicated by the arrows. For the eutectic composition, the defect is again well defined, as can be seen in Figure 3.19 (experiment number F18, Tables 3.7 and 3.10). A closer view (Fig. 3.20) shows the structural difference between the two sides of the cold shut. The Pb-19% Sn alloy yielded a discontinuous cold shut. as seen in Figure 3.21 (experiment number F15, Tables 3.7 and 3.10) and in Figure 3.22, probably because of its large freezing range.

3.5.7 Experiments using a Stepped Mold

These last three experiments were designed to confirm that once splashing of liquid metal has occurred, a cold shut will probably be formed. Figure 3.23 (experiment number G3, Table 3.8) shows an example of a cold shut formed by metal splashing at the bottom surface of the last step of the sample. At higher superheat (75^{o}C), the cold shut is also formed as shown in Figure 3.24 (experiment number G1,

FIGURE 3.17 Typical structure obtained from experiments using inserts (not remelted).
Magnification: 3.4x

FIGURE 3.18 Typical structure obtained from experiments using inserts (almost totally remelted).
Magnification: 3.4x

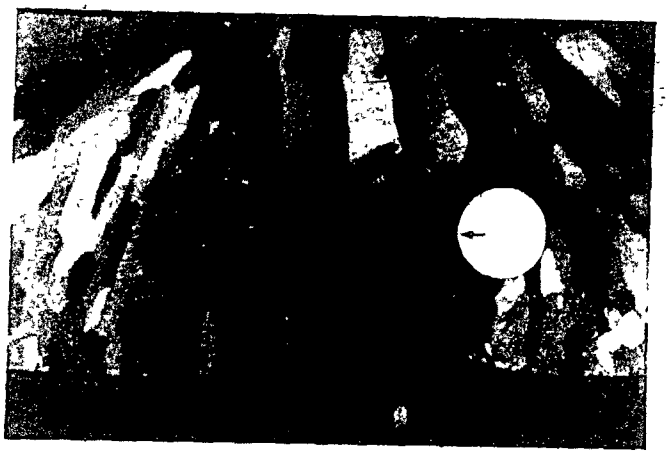

FIGURE 3.19 Typical cold shut formed in alloy of eutectic composition.
Magnification: 3.2x

FIGURE 3.20 Structural difference in both sides of cold shut for eutectic (not etched).
Magnification: 20x

FIGURE 3.21 Typical cold shut formed in Pb-19% Sn alloy.
Magnification: 1.5x

FIGURE 3.22 Structural difference in both sides of cold shut for Pb-19% Sn alloy (not etched).
Magnification: 20x

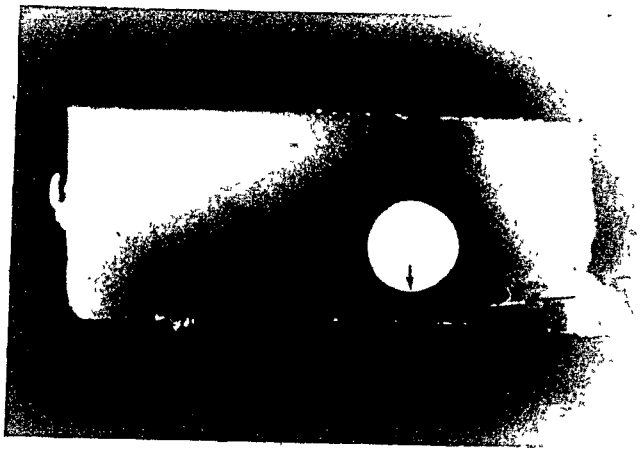

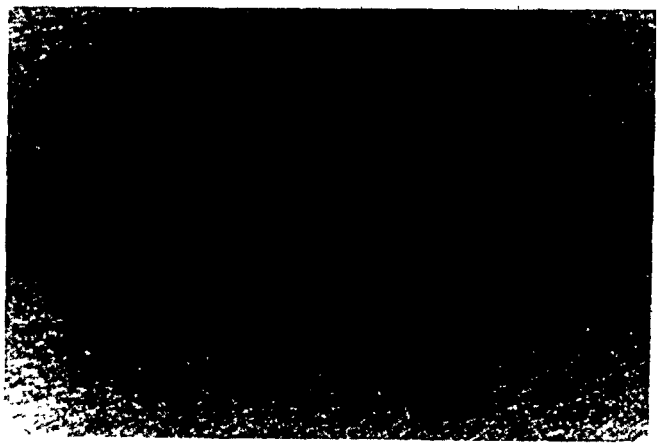

FIGURE 3.23 Bottom surface of sample from stepped mold.
Superheat: 25°C
Material: Pb
Magnification: 1.35x

FIGURE 3.24 Bottom surface of sample from stepped mold.
Superheat: 75°C
Material: Pb
Magnification: 1.35x

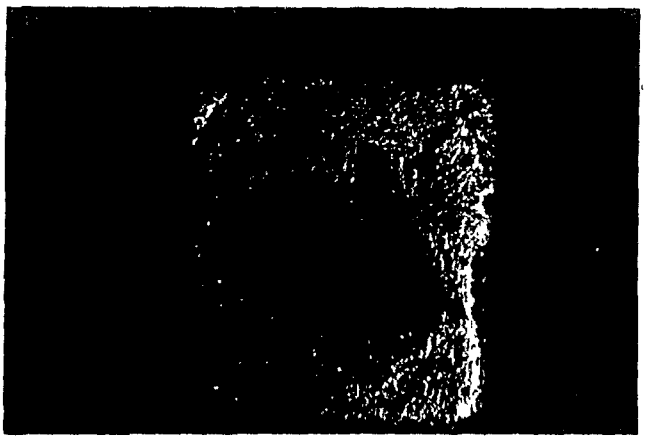

Table 3.8). At low superheats (25°C), in stepped molds, the formation of cold shuts by liquid metal flowing over solid metal is more likely to occur, and this is confirmed by Figure 3.25 (experiment number G3, Table 3.8) showing the side of the sample, where the layers of metal are clearly visible. At higher superheats (150°C), the defect still occurs but is less visible, as is seen in Figure 3.26 (experiment number G2, Table 3.8).

FIGURE 3.25 Cold shuts formed at the side of samples from stepped mold.
Superheat: 25°C
Material: Pb
Magnification: 1.25x

FIGURE 3.26 Cold shuts formed at the side of samples from stepped mold.
Superheat: 150°C
Material: Pb
Magnification: 1.4x

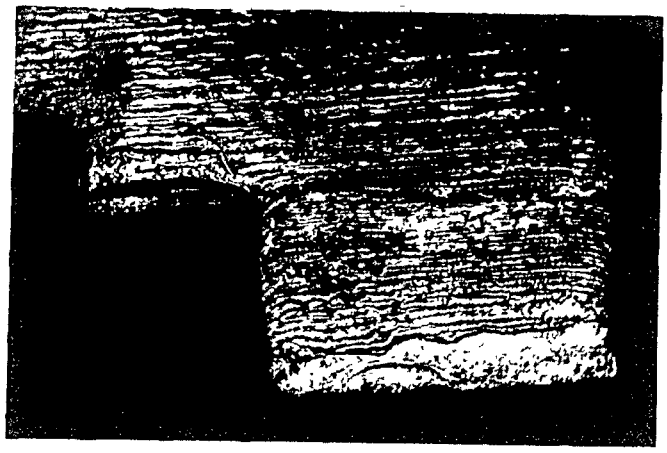

CHAPTER 4. HEAT TRANSFER MODEL

The mathematical model presented in this chapter was developed to investigate the phenomena which occur when two liquid metal streams collide. As presented in Chapter 3, it was determined that the necessary condition to promote significant cold shuts was to have a satellite fragment of the approaching stream freeze ahead of the main liquid flow, and this phenomenon was simulated by placing in the mold a solid piece of the same metal and allowing the parent liquid to overflow it. As such this represents an unsteady state heat transfer problem which can be solved, for the appropriate boundary and initial conditions, by various numerical algorithms. The method used in this study was chosen because of its mathematical simplicity and also because it can be programmed without much difficulty on a high speed digital computer. In this method, called the explicit finite-difference technique, once the initial temperature distribution is known, the calculation proceeds directly from one time increment to the next until the temperature distribution is calculated at the desired final state.

4.1 Definition of the Problem

The problem to be solved can be summarized in the following way: a solid metal in a sand mold is instantaneously heated by a liquid metal (both solid and liquid are of the same metal) which is brought in contact with it. Depending on certain variables influencing the heat transfer process, the solid piece may or may not be remelted. If the solid is entirely remelted, a cold shut is avoided. If not, a cold shut is formed.

4.2 General Equations

The unsteady state heat transfer problem stated in Section 4.1 can be solved by solving the general partial differential equation for heat condition given by:[21]

$$\alpha\{\frac{\partial^2 T}{\partial x^2} + \frac{\partial^2 T}{\partial y^2} + \frac{\partial^2 T}{\partial z^2}\} + \frac{\dot{q}(x,y,z)}{\rho . C_p} = \frac{\partial T}{\partial t} \qquad (4.1)$$

where $\alpha = \frac{k}{\rho C_p}$ = thermal diffusivity

T = temperature

x,y,z = spatial variables

$\dot{q}$ = heat generation per unit of volume

ρ = density

C_p = heat capacity

k = thermal conductivity

t = time

In the absence of heat conduction in the $y(\frac{\partial^2 T}{\partial y^2} = 0)$ and in the $z(\frac{\partial^2 T}{\partial z^2} = 0)$ directions, and in the absence of heat generation ($\dot{q} = 0$), equation (4.1) simplifies to:

$$\alpha \frac{\partial^2 T}{\partial x^2} = \frac{\partial T}{\partial t} \qquad (4.2)$$

The situation representing the contact of the liquid metal with the solid metal, at time $t = 0$, is outlined in Fig. 4.1, which depicts, in schematic form, a cross section of a sand mold with a solid piece of metal laying on it.

FIGURE 4.1 Schematic cross section of the mold.

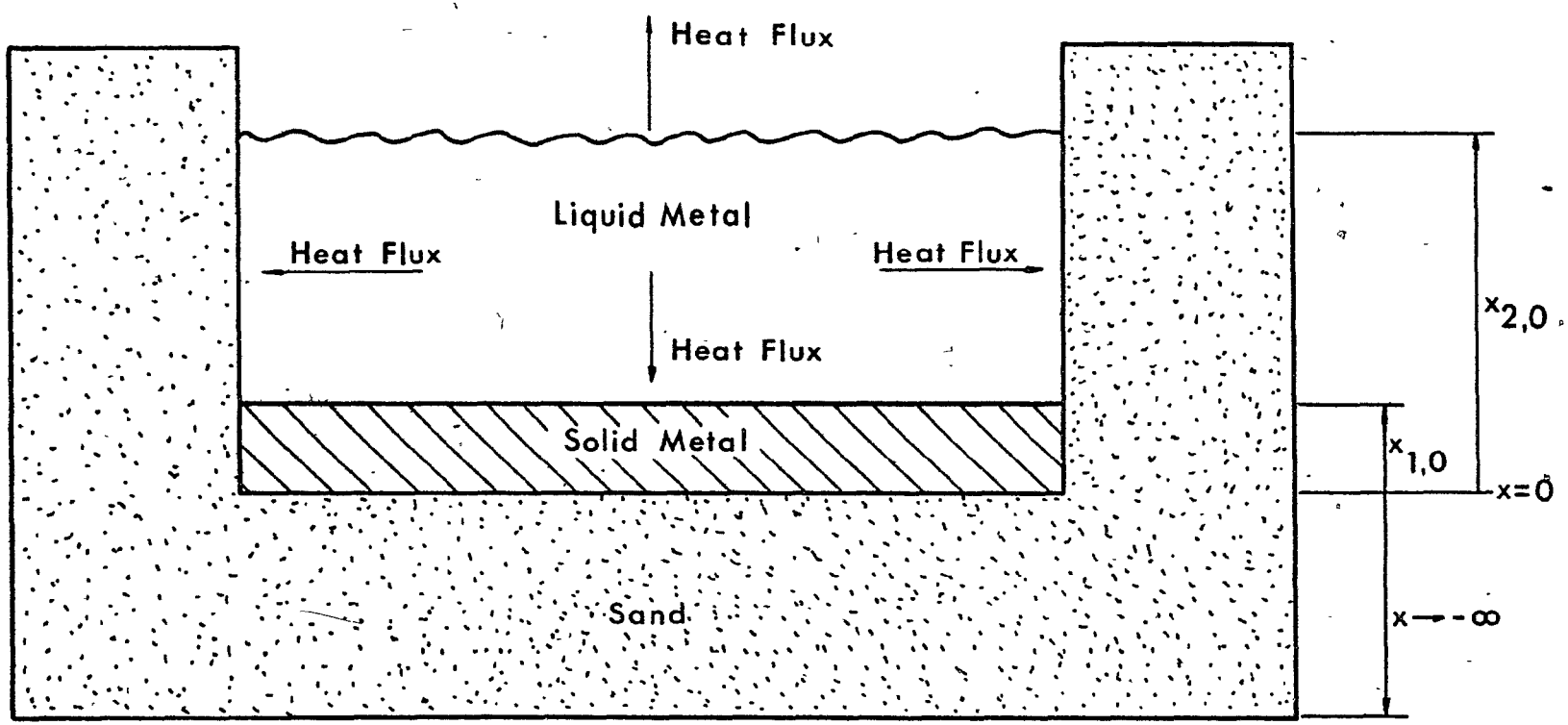
Heat Flux
Liquid Metal
Heat Flux
Heat Flux
Heat Flux
Solid Metal
Sand
$x_{2,0}$
$x_{1,0}$
x=0
x→-∞

The appropriate partial differential equations for the mold, solid, mushy and liquid regions and presented below:

a) mold

$$-\infty < x < 0 \qquad 0 < t \leq t_{final}$$

$$\alpha_{mold} \frac{\partial^2 T}{\partial x^2} = \frac{\partial T}{\partial t} \tag{4.3}$$

b) solid metal

$$0 \leq x \leq x_{solidus} \qquad 0 < t \leq t_{final}$$

$$\alpha_{solid} \frac{\partial^2 T}{\partial x^2} = \frac{\partial T}{\partial t} \tag{4.4}$$

c) mushy

$$x_{solidus} < x < x_{liquidus} \qquad 0 < t \leq t_{final}$$

$$\alpha_{mushy} \frac{\partial^2 T}{\partial x^2} = \frac{\partial T}{\partial t} \tag{4.5}$$

d) liquid metal

$$x_{liquidus} < x < x_{center\ line} \qquad 0 < t \leq t_{final}$$

$$\alpha_{liquid} \frac{\partial^2 T}{\partial x^2} = \frac{\partial T}{\partial t} \tag{4.6}$$

4.3 Initial and Boundary Conditions

These partial differential equations are to be solved using appropriate initial and boundary conditions. Before pouring liquid metal into the mold, the temperature of the mold is taken to be uniform and equal to T_o:

$$t = 0 \qquad -\infty \leq x \leq 0$$
$$T = T_o \tag{4.7}$$

The temperature of the solid piece of metal is taken to be uniform and equal to T_o:

$$t = 0 \qquad 0 \leq x \leq x_{1,0}$$
$$T = T_o \tag{4.8}$$

The bulk temperature of the liquid metal is taken to be uniform and equal to T_{bath}:

$$t = 0 \qquad x_{1,0} \leq x \leq x_{2,0}$$
$$T = T_{bath} \tag{4.9}$$

There is no mushy region at $t = 0$:

$$t = 0$$
$$x_{solidus} = x_{liquidus} \tag{4.10}$$

The mold is assumed to be semi-infinite in the negative x-domain with surface temperatures equal to T_o:

$$0 < t \leq t_{final} \qquad x = -\infty$$
$$T = T_o \tag{4.11}$$

The heat flux from the casting side to the interface is equal to the heat flux from the interface into the mold:

$$0 < t \leq t_{final} \qquad x = 0$$
$$-k_{mold} \frac{\partial T_{mold}}{\partial x} = -k_{casting} \frac{\partial T_{casting}}{\partial x} \tag{4.12}$$

Also, to allow for the thermal resistance of any air gaps between the sample and the sand:

$$0 < t \leq t_{final} \qquad x = 0$$
$$-k_{mold} \frac{\partial T_{mold}}{\partial x} = \frac{T^*_{casting} - T^*_{mold}}{R_T} \tag{4.13}$$

where: $T^*_{casting}$ = temperature of the casting surface in contact with the mold

T^*_{mold} = temperature of the mold surface in contact with the casting

R_T = thermal resistance due to air gap

The temperature at the interface between the solid and mushy region of the alloy is taken to be constant and equal to the solidus temperature:

$$0 < t \leq t_{final} \qquad x = x_{solidus}$$
$$T = T_{solidus} \tag{4.14}$$

The temperature at the interface between the liquid and the mushy region of the alloy is taken to be constant and equal to the liquidus temperature:

$$0 < t \leq t_{final} \qquad x = x_{liquidus}$$
$$T = T_{liquidus} \tag{4.15}$$

The amount of metal being solidified (or melted) is dependent on the difference between the heat fluxes from the bulk liquid metal to the solid/liquid interface and from this interface into the body of the solid metal:

$$0 < t \leq t_{final}$$

$$\dot{q}''_{conv} + HF\,\dot{m}'' = - k_{solid} \left.\frac{\partial T}{\partial x}\right|_{x = x_{solidus}} \tag{4.16}$$

where $\dot{q}''_{conv}$ = heat flux due to convection from liquid to the freezing zone

$\dot{m}''$ = amount of metal being solidified (or melted)

HF = latent heat of fusion

The heat flux, $\dot{q}''_{conv}$, depends on the heat transfer coefficient as well as on the superheat:

$$\dot{q}''_{conv} = h(T_{bath} - T_{liquidus}) \qquad (4.17)$$

where h = heat transfer coefficient

4.4 Assumptions

The explicit method used in this study to solve the heat transfer problem involved the following assumptions:

i) The metal was assumed to be an alloy because even unalloyed metals contain a certain amount of impurities resulting in a finite melting range.

ii) It was assumed to have an air gap between the metal and the mold which provided a resistance to the heat flow.

iii) Conduction through the side wall was ignored as was radiation from the liquid surface to the ambient because both would not influence the results during the pertinent early stages of the heat flow.

iv) The heat flow was taken to be unidirectional.

v) Latent heat was assumed to be absorbed in a linear manner between the solidus and liquidus temperatures of the alloy. This assumption was made to simplify the model. The latent heat was accounted for by assuming an artificially high specific heat over the range of the mushy zone. This was achieved by defining the heat capacity as in equation (4.18):

$$C_{p,m} = \frac{HF}{(T_L - T_S)} \qquad (4.18)$$

where $C_{p,m}$ = heat capacity of mushy zone

HF = latent heat of fusion

T_L = liquidus temperature

T_S = solidus temperature

4.5 Explicit Finite-Difference Technique

In order to apply the explicit method, the system being studied was divided into a series of finite volume elements. Then, nodal points were located at the centres of these elements (Fig. 4.2) and a heat balance was performed in them. The explicit technique requires that the temperature gradient between adjacent nodal points be assumed to be linear as well as the material within each node be assumed to have both uniform temperature and thermophysical properties. Nodal point number one was located at the mold/ambient interface, the other nodal points having increasing numbers toward the center line of the system. Nodal points number one, five and six are located in half nodes since they lie on boundary lines.

A heat balance was established over the finite elements as given in equation (4.19):

heat input - heat output = rate of heat accumulation (4.19)

This equation (4.19), applied to nodal point N, yields the following relation written in numerical notation:

FIGURE 4.2 Network of nodal points.

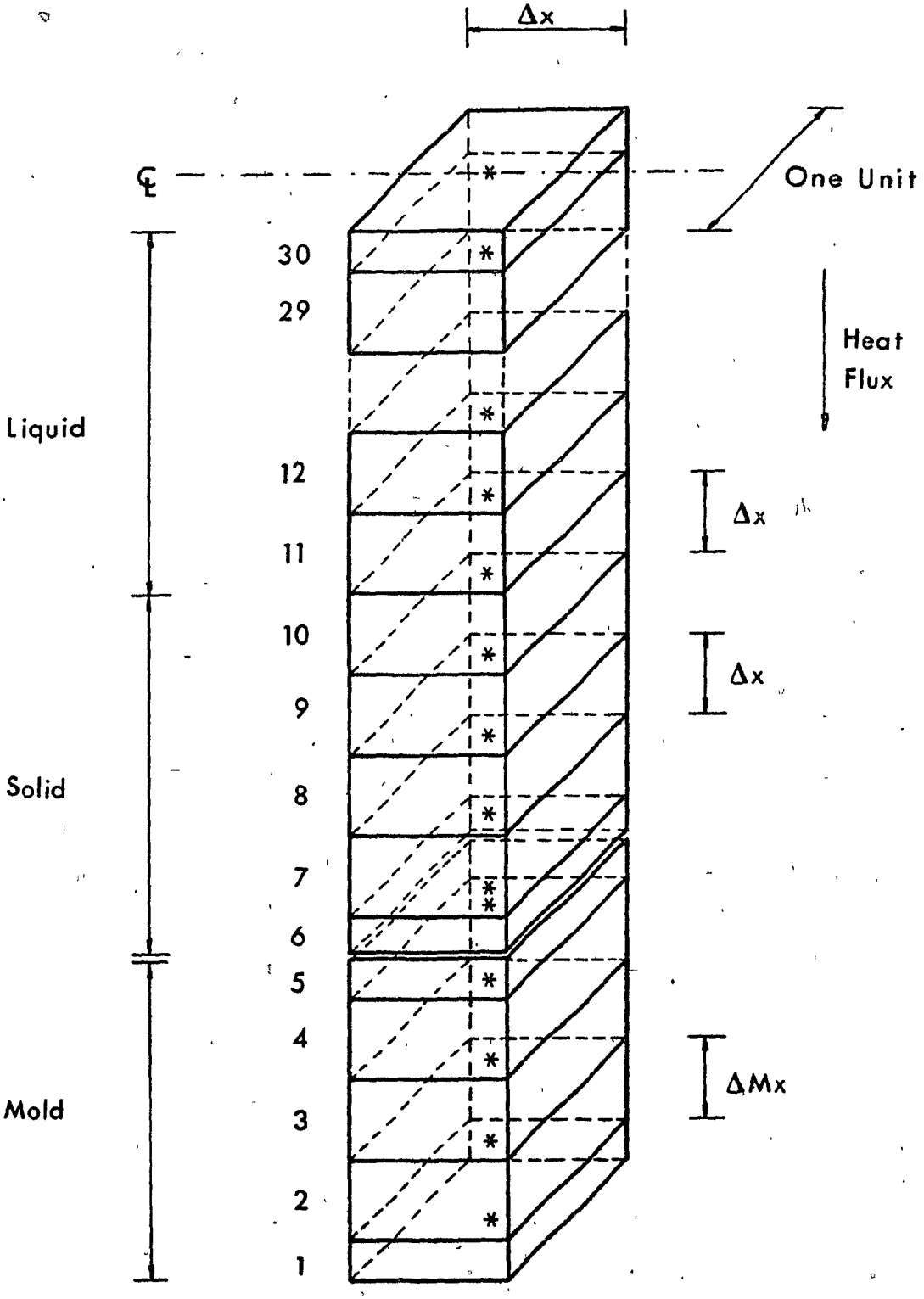
Δx
One Unit
Heat
Flux
Liquid
Solid
Mold
30
29
12
11
10
9
8
7
6
5
4
3
2
1
Δx
Δx
ΔMx

$$\frac{k_{N,N+1}(\Delta x \cdot 1)}{\Delta x}(T_{N+1} - T_N) - \frac{k_{N,N-1}(\Delta x \cdot 1)}{\Delta x}(T_N - T_{N-1}) = \frac{\rho C_p(\Delta x \cdot \Delta x \cdot 1)}{\Delta t}(T'_N - T_N) \quad \ldots\ldots(4.20)$$

for $1 < N < 5$ and $6 < N < 30$

Rearranging equation (4.20), it follows that:

$$T'_N = T_N\{1 - M_{N,N+1} - M_{N,N-1}\} + M_{N,N+1}T_{N+1} + M_{N,N-1}T_{N-1} \quad \ldots\ldots(4.21)$$

where T'_N = new temperature at time $t + \Delta t$ at nodal point N

T_N = temperature at time t at nodal point N

T_{N+1} = temperature at time t at nodal point N+1

T_{N-1} = temperature at time t at nodal point N-1

$$M_{N,N+1} = \frac{k_{N,N+1} \cdot \Delta t}{\rho C_p \Delta x^2} \quad (4.22)$$

$$M_{N,N-1} = \frac{k_{N,N-1} \cdot \Delta t}{\rho C_p \Delta x^2} \quad (4.23)$$

$k_{N,N+1}$ = equivalent thermal conductivity between nodal points N and N+1

$k_{N,N-1}$ = equivalent thermal conductivity between nodal points N and N-1

Δt = time increment

ρ = density of node N

C_p = heat capacity of node N

Δx = nodal point spacing

The equivalent thermal conductivity between nodal points N and N+1, for instance, is given by:

$$k_{N,N+1} = \frac{2 \cdot k_N \cdot k_{N+1}}{k_N + k_{N+1}} \tag{4.24}$$

for $1 \leq N < 5$ and $6 \leq N < 30$

Applying equation (4.19) to nodal point 1, yields the following equation:

$$\frac{k_2(\Delta x \cdot 1)}{\Delta x}(T_2 - T_1) - h_{AMB}(\Delta x \cdot 1)(T_1 - T_{AMB}) = \frac{\rho C_p(\frac{\Delta x}{2} \cdot \Delta x \cdot 1)}{\Delta t}(T_1' - T_1) \tag{4.25}$$

Transforming equation (4.25) into finite-difference form, yields:

$$T_1' = T_1\{1 - 2M - 2H\} + 2MT_2 + 2HT_{AMB} \tag{4.26}$$

where T_1' = new temperature at time t + Δt at nodal point 1

T_1 = temperature at time t at nodal point 1

T_2 = temperature at time t at nodal point 2

T_{AMB} = ambient temperature

$$M = \frac{k_{2,1}\,\Delta t}{\rho\, C_p\, \Delta x^2} \tag{4.27}$$

$$H = \frac{h_{AMB}\ \Delta t}{\rho\ C_p\ \Delta x} \qquad (4.28)$$

$k_{2,1}$ = equivalent thermal conductivity between nodal points 2 and 1. In this case, $k_{2,1} = k_{SAND}$

h_{AMB} = heat transfer coefficient for the ambient

Δx = ΔMx as shown in Fig. 4.2

Performing the heat balance given in equation (4.19) to nodal point number 30, yields the following equation:

$$-\frac{k_{30,29}(\Delta x \cdot 1)}{\Delta x}(T_{30} - T_{29}) - \frac{k_{30,29}(\Delta x \cdot 1)}{\Delta x}(T_{30} - T_{29}) = \frac{\rho\ C_p(\Delta x \cdot \Delta x \cdot \cancel{1})}{\Delta t}(T'_{30} - T_{30}) \qquad .....(4.29)$$

The first term in the above equation has a negative sign because the temperature difference in parentheses should be equal to $(T_{31} - T_{30})$, but as 30 is the last nodal point and it is the center line of the system, T_{31} is equal to T_{29}.

Putting equation (4.29) in finite difference form, it becomes:

$$T'_{30} = T_{30}\{1 - 2M\} + 2MT_{29} \qquad (4.30)$$

where T'_{30} = new temperature at time $t + \Delta t$ at nodal point 30

T_{30} = temperature at time t at nodal point 30

T_{29} = temperature at time t at nodal point 29

$$M = \frac{k_{30,29}\Delta t}{\rho\, C_p\, \Delta x^2} \tag{4.31}$$

$k_{30,29}$ = equivalent thermal conductivity between nodal points 30 and 29 and is given by:

$$k_{30,29} = \frac{2 \cdot k_{30} \cdot k_{29}}{k_{30} + k_{29}} \tag{4.32}$$

Applying the heat balance represented by equation (4.19) to nodal point 5 yields:

$$h_{INT}(\Delta x \cdot 1)(T_6 - T_5) - \frac{k_{5,4}(\Delta x \cdot 1)}{\Delta x}(T_5 - T_4) = \frac{\rho\, C_p(\frac{\Delta x}{2} \cdot \Delta x \cdot 1)}{\Delta t}(T_5' - T_5) \tag{4.33}$$

Transforming the above equation, gives:

$$T_5' = T_5\{1 - 2H_{INT} - 2M\} + 2H_{INT}T_6 + 2MT_4 \tag{4.34}$$

where T_5' = new temperature at time $t + \Delta t$ at nodal point 5

T_5 = temperature at time t at nodal point 5

T_6 = temperature at time t at nodal point 6

T_4 = temperature at time t at nodal point 4

$$H_{INT} = \frac{h_{INT}\,\Delta t}{\rho\, C_p\, \Delta x} \tag{4.35}$$

$$M = \frac{k_{5,4}\,\Delta t}{\rho\, C_p\, \Delta x^2} \tag{4.36}$$

h_{INT} = heat transfer coefficient for the metal/mold interface

Δx = ΔMx as shown in Fig. 4.2

$k_{5,4}$ = equivalent thermal conductivity between nodal points 5 and 4. In this case, $k_{5,4} = k_{SAND}$.

Applying equation (4.19) to nodal point 6, gives:

$$\frac{k_{7,6}(\Delta x \,.\, 1)}{\Delta x}(T_7 - T_6) - h_{INT}(\Delta x \,.\, 1)(T_6 - T_5) = \frac{\rho\, C_p (\frac{\Delta x}{2} \,.\, \Delta x \,.\, 1)}{\Delta t}(T_6' - T_6) \tag{4.37}$$

The above equation transforms into:

$$T_6' = T_6\{1 - 2M - 2H_{INT}\} + 2MT_7 + 2H_{INT}T_5 \tag{4.38}$$

where T_6' = new temperature at time t + Δt at nodal point 6

T_6 = temperature at time t at nodal point 6

T_7 = temperature at time t at nodal point 7

T_5 = temperature at time t at nodal point 5

$$M = \frac{k_{7,6}\,\Delta t}{\rho\, C_p\, \Delta x^2} \tag{4.39}$$

$$H_{INT} = \frac{h_{INT}\,\Delta t}{\rho\, C_p\, \Delta x} \tag{4.40}$$

$k_{7,6}$ = equivalent thermal conductivity between nodal points 7 and 6, and is given by:

$$k_{7,6} = \frac{2 \cdot k_7 \cdot k_6}{k_7 + k_6} \tag{4.41}$$

The modulus M, as presented in equation (4.21), can have two values $M_{N,N+1}$ and $M_{N,N-1}$. The first corresponds to the heat flux entering nodal point N from nodal point N+1. The second corresponds to the heat flux leaving nodal point N and going to nodal point N-1. The numerical values of these moduli are dependent on the phases present and are applied to nodal points $6 < N \leq 30$.

For the solid region of the alloy, the modulus M is given by:

$$M_s = \frac{k_s \, \Delta t}{\rho \, C_{p,s} \, \Delta x^2} \tag{4.42}$$

where k_s = thermal conductivity of solid alloy

$C_{p;s}$ = heat capacity of solid region

For the mushy region, the value of M is:

$$M_m = \frac{k_m \, \Delta t}{\rho \, C_{p,m} \, \Delta x^2} \tag{4.43}$$

where k_m = thermal conductivity of mushy region

$C_{p,m}$ = heat capacity of mushy region

As pointed out in Section 4.4, $C_{p,m}$ is assumed to be artificially high in order to take into account the latent heat of fusion of the alloy. Equation (4.18) defines the $C_{p,m}$ value.

For the liquid region, the modulus M is given by:

$$M_l = \frac{k_l \, \Delta t}{\rho \, C_{p,l} \, \Delta x^2} \tag{4.44}$$

where k_l = thermal conductivity of the liquid alloy

$C_{p,l}$ = heat capacity of the liquid alloy

The possibility of two adjacent nodal points being in regions of different phases was taken into account by using the proper values of the modulus M. When nodal point N is in the solid region and the adjacent nodal point is in the mushy region, the modulus M is given by:

$$M_{s,m} = \frac{k_{s,m} \, \Delta t}{\rho \, C_{p,s} \, \Delta x^2} \tag{4.45}$$

where

$$k_{s,m} = \frac{2 \cdot k_s \cdot k_m}{k_s + k_m} \tag{4.46}$$

k_s = thermal conductivity of solid alloy

k_m = thermal conductivity of mushy region

$C_{p,s}$ = heat capacity of solid alloy

When nodal point N is in the mushy region and the adjacent nodal point is in the solid region, the value of M is:

$$M_{m,s} = \frac{k_{s,m}\ \Delta t}{\rho\ C_{p,m}\ \Delta x^2} \tag{4.47}$$

where $C_{p,m}$ = heat capacity of mushy region

and $k_{s,m}$ was given in the equation (4.46).

When nodal point N is in the liquid region and the adjacent nodal point is in the mushy region, the modulus M is given by:

$$M_{l,m} = \frac{k_{l,m}\ \Delta t}{\rho\ C_{p,l}\ \Delta x^2} \tag{4.48}$$

where $$k_{l,m} = \frac{2\ .\ k_l\ .\ k_m}{k_l + k_m} \tag{4.49}$$

k_l = thermal conductivity of liquid alloy

k_m = thermal conductivity of mushy region

$C_{p,l}$ = heat capacity of liquid alloy

When nodal point N is in the mushy region and the adjacent nodal point is in the liquid region, the modulus M is expressed as:

$$M_{m,l} = \frac{k_{l,m}\ \Delta t}{\rho\ C_{p,m}\ \Delta x^2} \tag{4.50}$$

where $C_{p,m}$ = heat capacity of mushy region

and $k_{l,m}$ is given in equation (4.49).

The presence of a thermal resistance between nodal points 6 and 5 acts to transform the dimensionless number M (equation (4.21)) into H_{INT} (equation (4.34), and equation (4.38)). For modelling purposes

it is assumed that the thermal resistance is of negligible thickness and heat capacity. The value of C_p in equation (4.35) is equal to the heat capacity of the mold material while the value of C_p in equation (4.40), as well as in equation (4.39), can be equal to $C_{p,l}$, $C_{p,m}$ or $C_{p,s}$, symbols which have already been defined.

4.6 Stability

The accuracy of the solution of the explicit method is determined by the values of Δt and Δx, because these two variables control the value of the modulus M. Decreasing the value of M improves the accuracy of the solution by converging the finite-difference method.[24,25] Basically, to obtain stability, the coefficient of T_N (temperature at time t at nodal point N) must be non-negative. As the values of M varied depending on the phase where the nodal point N was located, the values chosen for Δt and Δx to impart accuracy to the results were: 0.001 second for the time increment, and 0.05 cm and 1.9 cm for the nodal point spacing in the casting side and in the mold side, respectively.

As determined by other authors[25,26], increasing the number of nodal points increases the accuracy of the model, while Δt has a relatively small effect on the solution.

4.7 Computer Model

A program, written in the FORTRAN computing language and executed on an IBM 370/158 digital computer, was used to solve the finite difference equations presented in Section 4.5. It began by setting the temperature distribution and the modulus M with their initial values.

Then, temperature profiles were computed in a stepwise procedure for successive Δt time steps. Obviously, for the calculation of the next temperature distribution, the phase existing in each nodal point was checked to allow for the use of the proper data. Such a computer program, calculating the temperature distribution throughout the system (mold and casting), allowed the determination of whether or not the solid will be remelted, for each data set. The program used an IBM FORTRAN (G1) compiler and it is listed in Appendix A along with all the symbols involved.

The thermophysical properties for the Pb-Sn alloy and for the pure lead, presented in Table 4.1, are reported by Chiesa and Guthrie[27], the only exception being the thermal conductivity of the mushy zone which was estimated to be between that for the liquid and the solid. The heat capacity and the thermal conductivity of sand are given elsewhere[28] as 0.2 cal/g^{o}C and 0.002 cal/cm^{o}C sec, respectively, while its density is reported by Paschkis[29] as being 1.6 g/cm^{3}. The heat transfer coefficients for the ambient and for the metal/mold interface were chosen in reasonable agreement with reported[28] values and were taken as 0.0015 cal/cm^{2} ^{o}C sec and 0.01 cal/cm^{2} ^{o}C sec, respectively.

When the metal was assumed to be pure lead, the liquidus temperature was selected to be 327^{o}C (600 K) while the solidus temperature was taken as 326.9^{o}C (599.9 K).

4.8 Experiments for Temperature Measurement

Experiments for temperature measurement were carried out to check the accuracy of the heat transfer model. Two chromel-alumel

TABLE 4.1

Thermophysical Properties used in Heat Transfer Calculations

Property	Phase	Sand	Pb-19% Sn	Pb
density (g/cm^3)	-	1.6	11.3	11.3
latent heat (cal/g)	solid	-	5.54	5.6
heat capacity (cal/g ^oC)	liquid	-	0.0387	0.0387
	solid	0.2	0.03	0.03
thermal conductivity (cal/cm ^oC sec)	liquid	-	0.039	0.039
	solid	0.002	0.083	0.083
	mushy	-	0.061	-

thermocouples were placed in each of the three samples embedded in the mold, as shown in exaggerated form in Fig. 4.3. Two other type K (chromel-alumel) thermocouples were also placed in the bath in front of the first and the third samples, as seen in Fig. 4.4. Each of the eight thermocouples was checked for accuracy by immersing it in boiling water. Only thermocouples which gave a reading within ± 2°C of the expected value were used in the experiments. The thermocouples were connected to a micro-processor (seen in Fig. 4.3 and in Fig. 4.4) which served as an interface between them and the IBM/370 computer. The micro-processor registered a temperature reading each tenth of a second for a duration of 50 seconds.

FIGURE 4.3 Positions of thermocouples inside the samples.

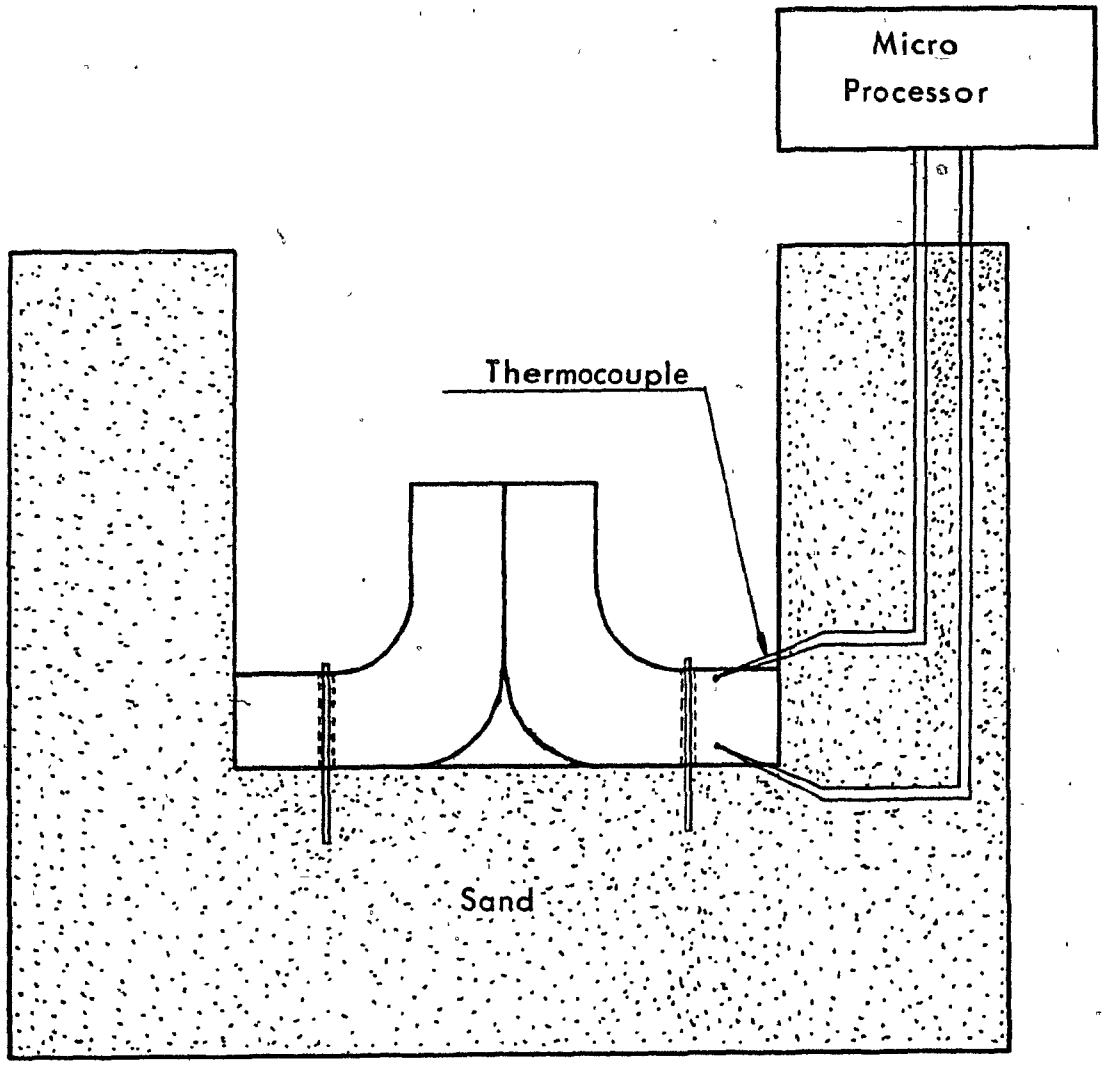
Micro
Processor
Thermocouple
Sand

FIGURE 4.4 Positions of thermocouples in the bath.

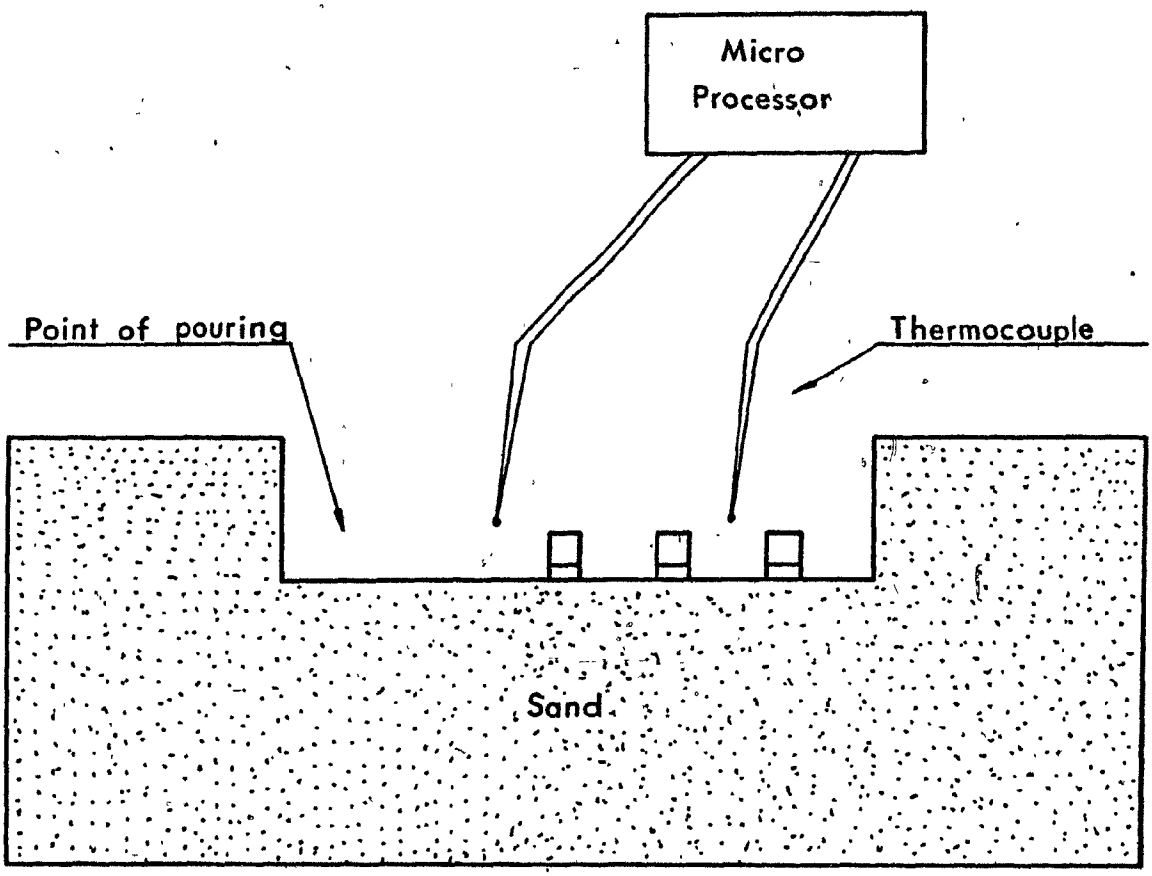
Micro
Processor
Point of pouring
Thermocouple
Sand

Experiments using oxidized samples and 100°C of superheat were performed with Pb (experiment number F14, Tables 3.7 and 3.10) and a Pb-19% Sn alloy (experiment number F15, Tables 3.7 and 3.10). The results from these experiments were compared with those from the model and are presented in the next section.

4.9 Results

Before presenting the results obtained it should be pointed out how the bath temperature, at the time when the liquid metal contacts the solid metal, was estimated. The only way found to determine these temperatures for the three different positions in the runner, was by the use of percentages of the superheat. Difficulties arise because while the liquid metal is flowing in the mold, a solidified layer begins to grow from the mold wall toward the center of the casting, thus changing the pertinent values for the heat transfer and thereby affecting the amount of heat lost in the runner during the flow of molten metal. The thickness of this solid layer changes with time, being dependent on many other variables such as superheat, mold properties, etc., and this makes it very difficult to calculate its numerical value.

The experimental results for the thermocouples in front of the first and third samples (Fig. 4.4) are presented in Fig. 4.5 and 4.6 for Pb and in Fig. 4.7 and 4.8 for the Pb-19% Sn alloy. The numerical values involved are shown in Table 4.2 in which position 1 means that the thermocouple was in front of the sample at position 1, and the same applies to the thermocouple at position 3. The percentages of the superheat were obtained by subtracting the liquidus temperatures,

FIGURE 4.5 Relationship between bath temperature in front of position 1 and time. Material = Pb. Superheat = 100°C.

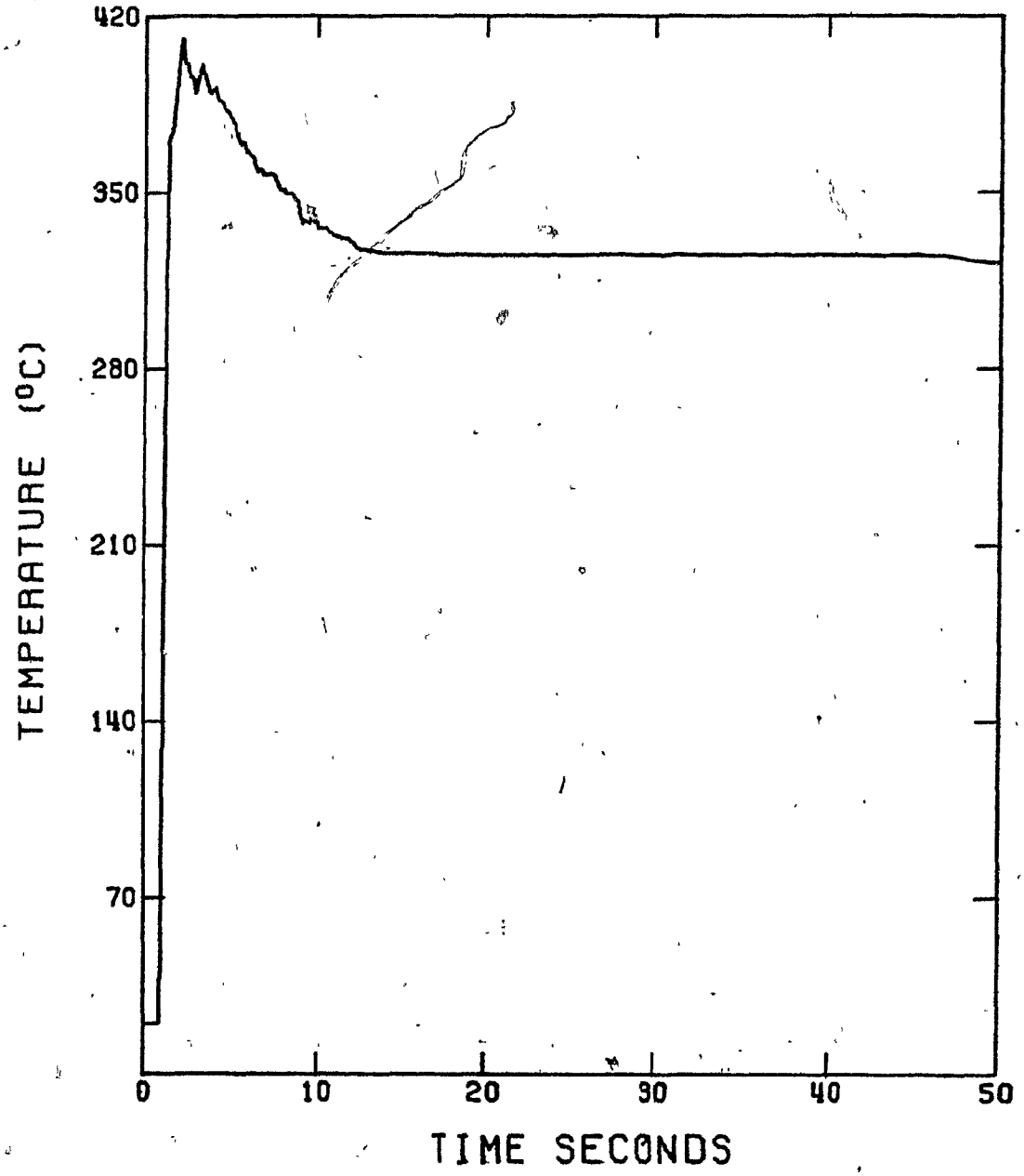
420
350
280
210
140
70
TEMPERATURE (°C)
0
10
20
30
40
50
TIME SECONDS

FIGURE 4.6 Relationship between bath temperature in front of position 3 and time. Material = Pb. Superheat = 100°C.

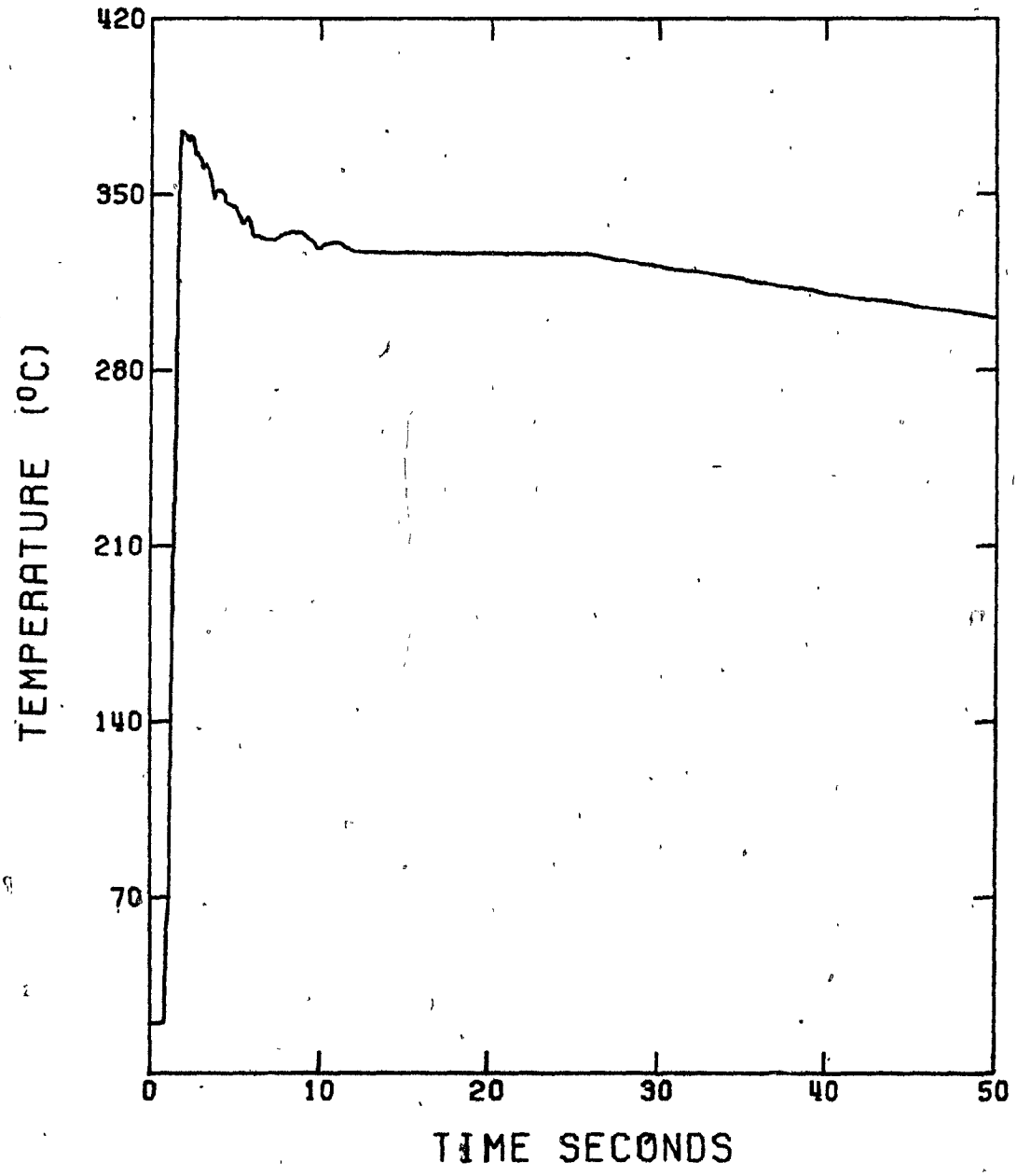
420
350
280
210
140
70
TEMPERATURE (°C)
0
10
20
30
40
50
TIME SECONDS

FIGURE 4.7 Relationship between bath temperature in front of position 1 and time. Material = Pb-19% Sn. Superheat = 100°C.

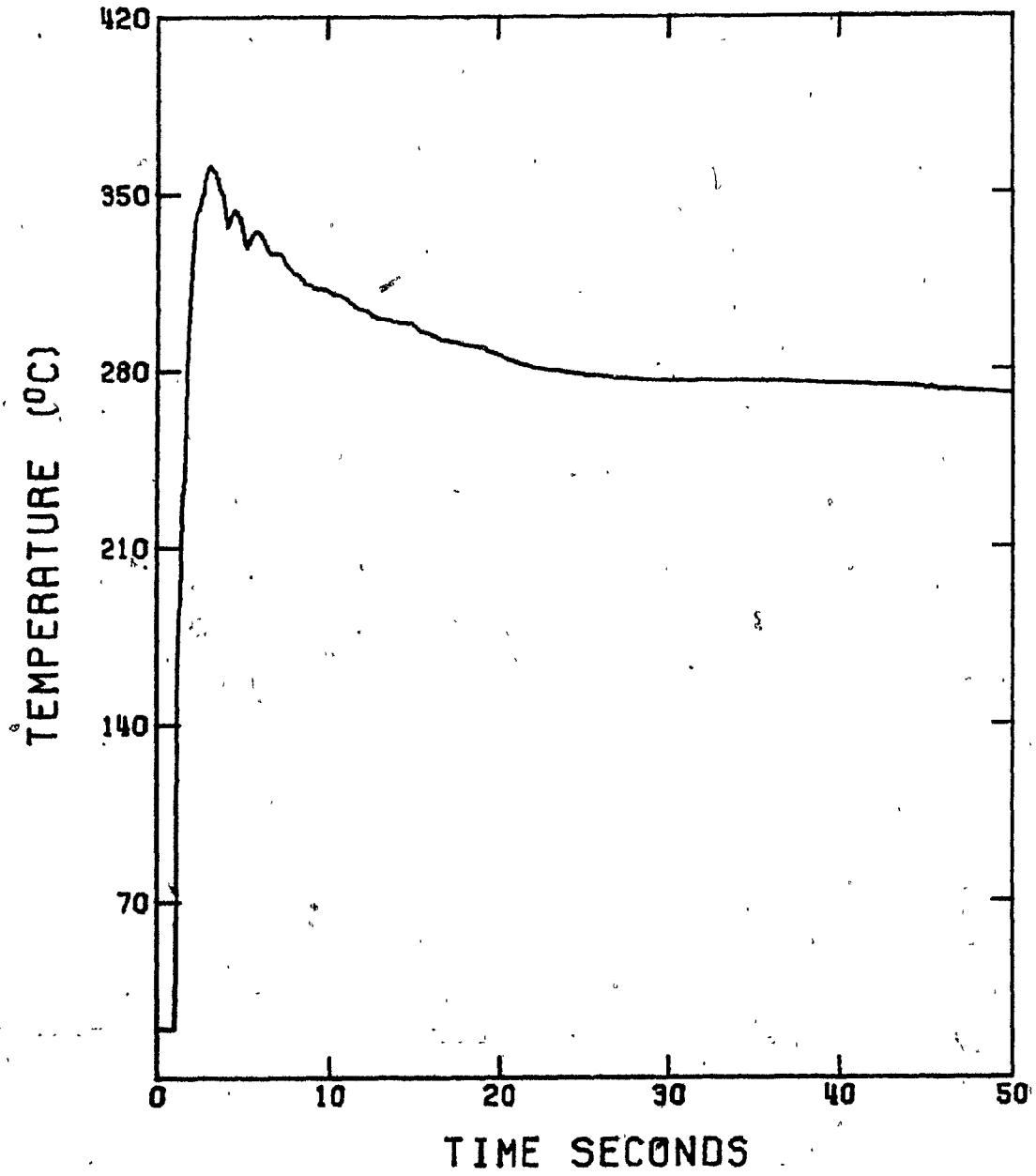
420
350
280
210
140
70
TEMPERATURE (°C)
0
10
20
30
40
50
TIME SECONDS

FIGURE 4.8 Relationship between bath temperature in front of position 3 and time. Material = Pb-19% Sn. Superheat = 100°C.

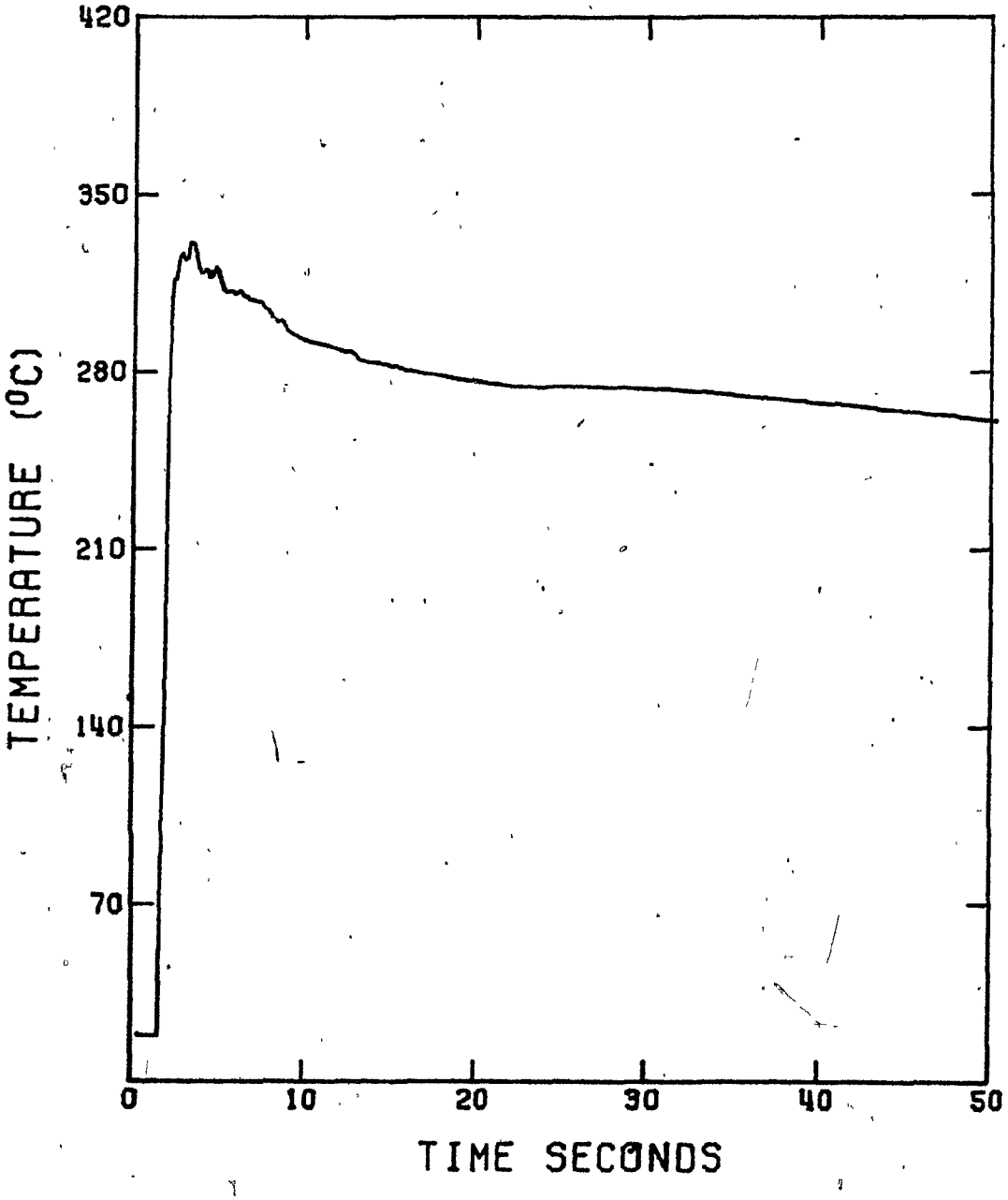
420
350
280
210
140
70
TEMPERATURE (°C)
0
10
20
30
40
50
TIME SECONDS

327°C (600 K) for Pb and 280°C (553 K) for the Pb-19% Sn alloy, from the temperature readings obtained in the respective positions. Since the initial superheats were of the order of 100°C, those values as percentages were found to be 82% for position 1 and 48% for position 3. The percentage for position 2 was estimated to be between those for position 1 and position 3, therefore 65% was the value used.

TABLE 4.2

Experimental Values of Temperature Measurements

Experiment Number	Material	Superheat (°C)	Position	Temperature Readings (°C)	Percentage of Superheat
F14	Pb	100	1	410 (683 K)	83
			3	376 (649 K)	49
F15	Pb-19% Sn	100	1	361 (634 K)	81
			3	327 (600 K)	47

4.9.1 Comparison Between Experimental and Theoretical Results

The experimental and theoretical results are presented in Figures 4.9 to 4.14. The theoretical results are for nodal point number 10 (Fig. 4.2); experimental ones are for the thermocouple inserted at the top of the horizontal part of the sample (Fig. 4.3). Figure 4.9 represents the results obtained for position 1 (Fig. 3.5) in the runner when using pure lead with 100°C superheat. As can be seen, the model predicts the remelting of the sample.

FIGURE 4.9 Comparison of the experimental and predicted temperature at nodal point 10. Material = Pb. Superheat = 100°C. Position 1.

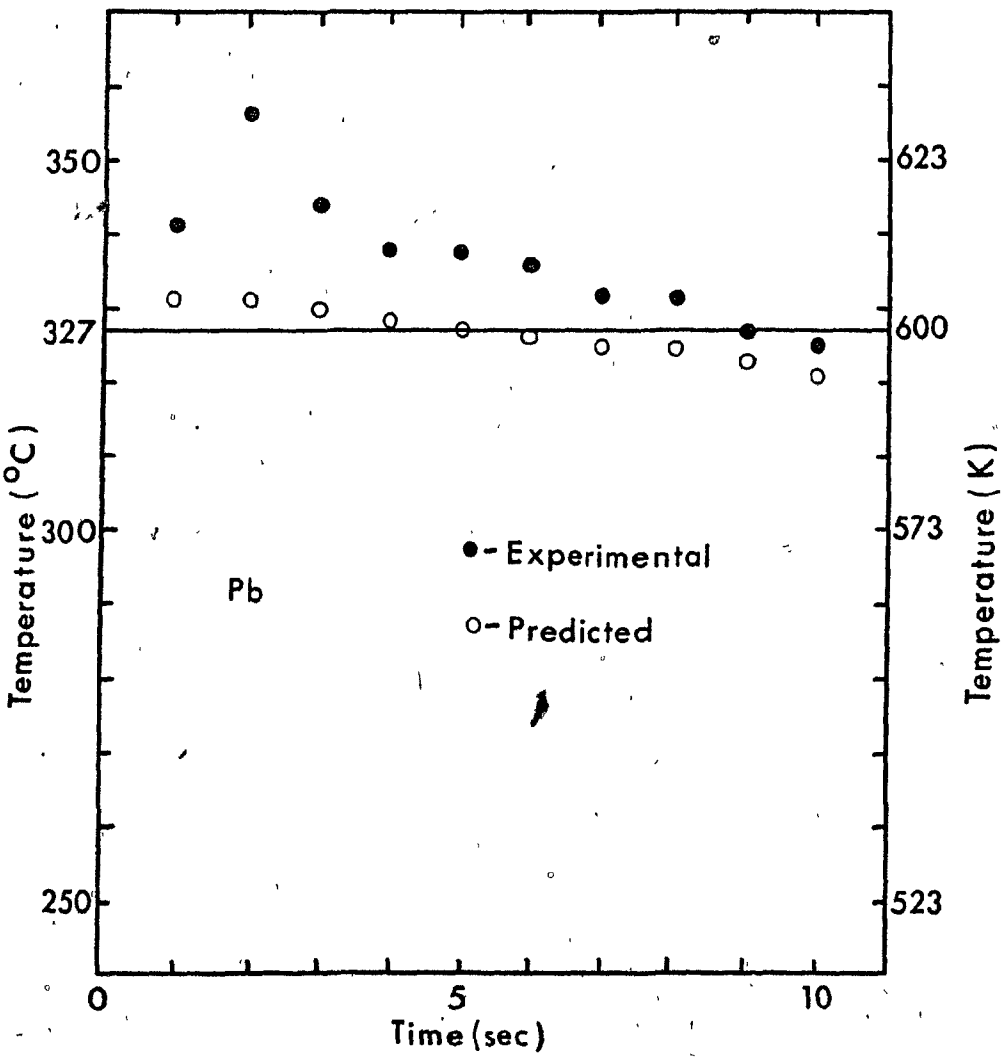
350
327
300
250
623
600
573
523
0
5
10
Time (sec)
Temperature (°C)
Temperature (K)
Pb
●- Experimental
○- Predicted

Figure 4.10 represents the results for position 1 (Fig. 3.5) in the channel when using the Pb-19% Sn alloy with 100°C of superheat. The model predicts reasonably well the temperature reached by that nodal point. Figures 4.11 and 4.12 represent the results for position 2 (Fig. 3.5) in the channel when using lead and the Pb-19% Sn alloy, respectively, and both having 100°C of superheat. Again the model is in reasonable agreement with the experimental results. Figures 4.13 and 4.14 show the results for position 3 (Fig. 3.5) in the runner when using lead and the Pb-19% Sn alloy, respectively, and again both having 100°C of superheat. The theoretical results are again in approximate agreement with the experimental ones.

4.9.2 Predictions of the Model

Since the predicted temperatures for nodal point 10 (Fig. 4.2) located just inside the solid sample were in good agreement with the values obtained in experiments by means of thermocouples (Fig. 4.3), it was decided to check whether temperature predictions of the model coincided with remelting of the solid sample as determined by subsequent microstructural analysis. The temperature-time curves are shown in Figures 4.15-4.17, for experiments F3, F10 and F12 (Tables 3.7 and 3.10), respectively. By comparing Figures 4.15-4.17 to the results presented in Table 3.10 it is seen that whenever the sample was remelted the model predicts a maximum temperature which was above the liquidus temperature and that whenever the sample was not remelted, the model predicts a maximum temperature which was below the liquidus temperature.

FIGURE 4.10 Comparison of the experimental and predicted temperature at nodal point 10. Material = Pb-19% Sn. Superheat = 100°C. Position 1.

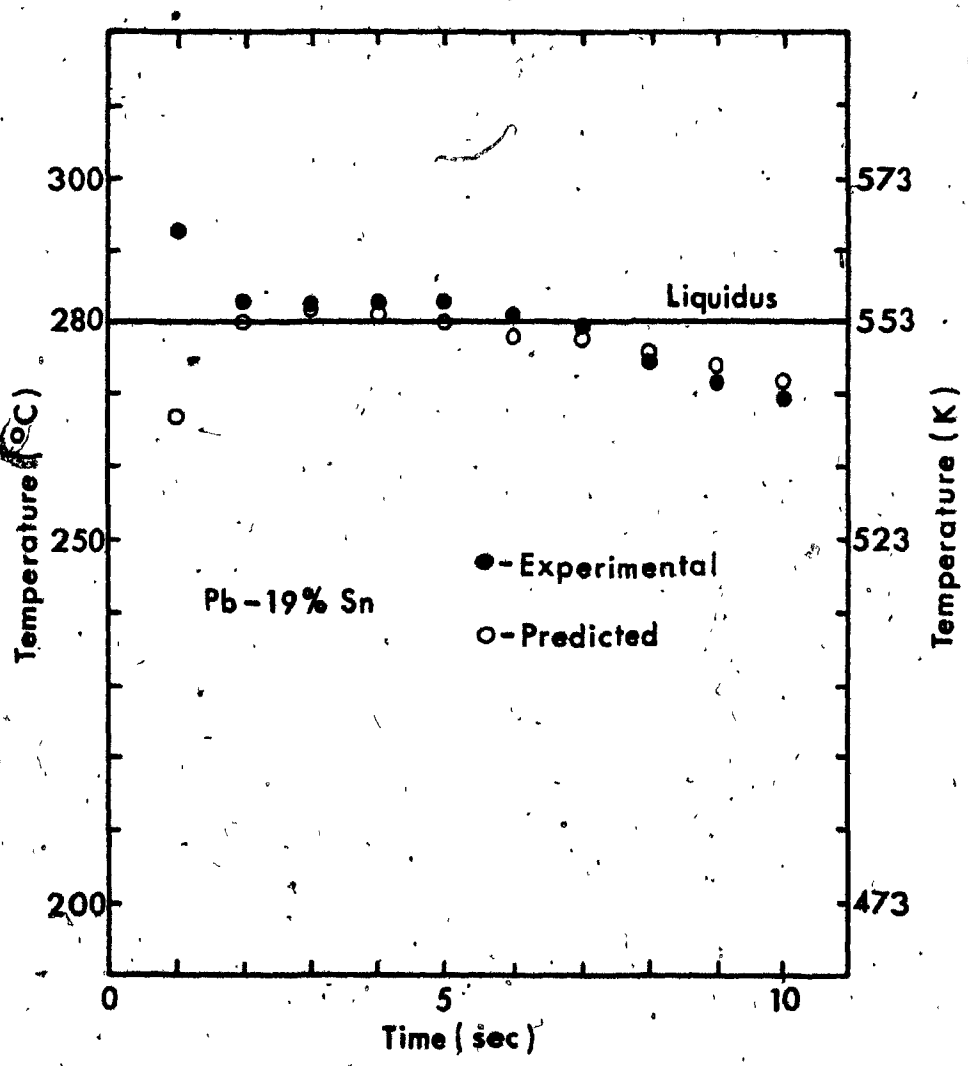
300
280
250
200
573
553
523
473
Liquidus
Pb – 19% Sn
●– Experimental
○– Predicted
Temperature (°C)
Temperature (K)
0
5
10
Time (sec)

FIGURE 4.11 Comparison of the experimental and predicted temperature at nodal point 10. Material = Pb. Superheat = 100°C. Position 2.

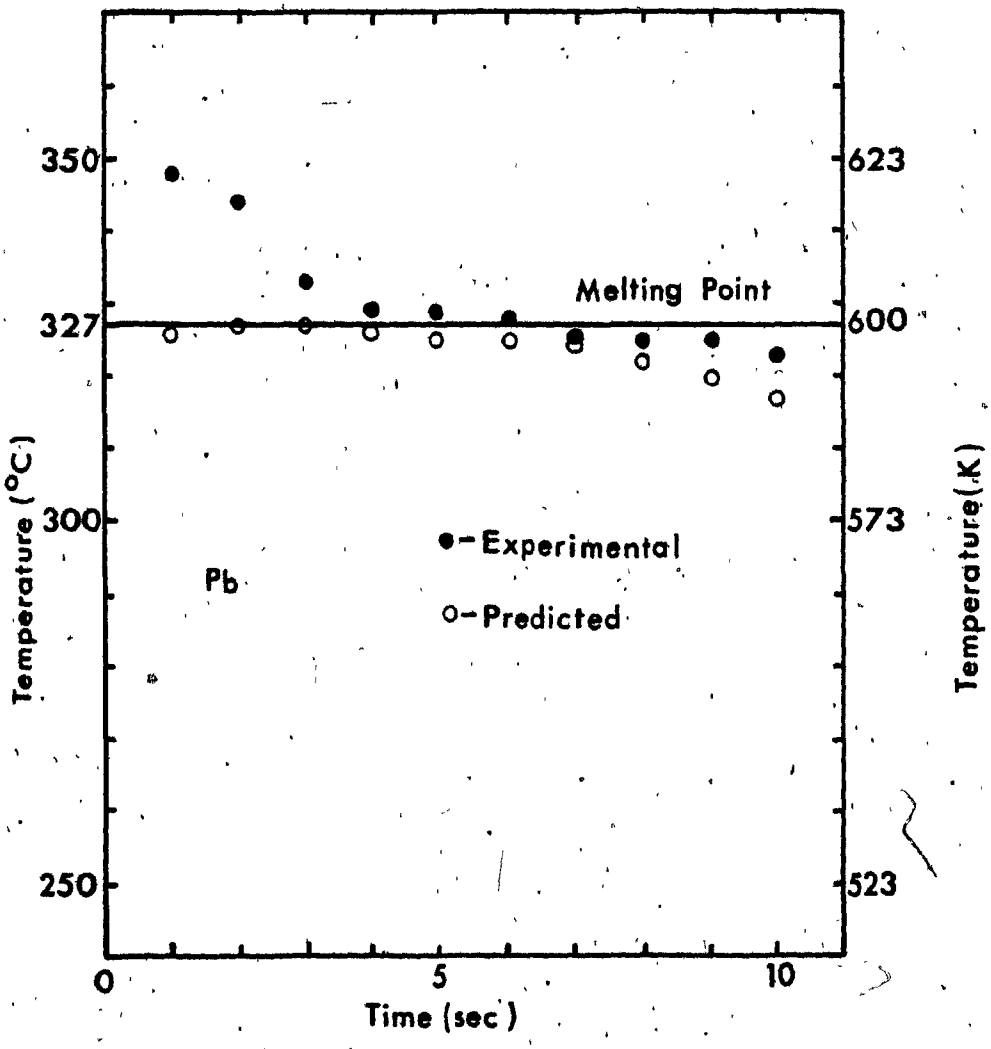
350
327
300
250
623
600
573
523
Melting Point
Temperature (°C)
Temperature (K)
Pb
●-Experimental
○-Predicted
0
5
10
Time (sec)

FIGURE 4.12 Comparison of the experimental and predicted temperature at nodal point 10. Material = Pb-19% Sn. Superheat = 100°C. Position 2.

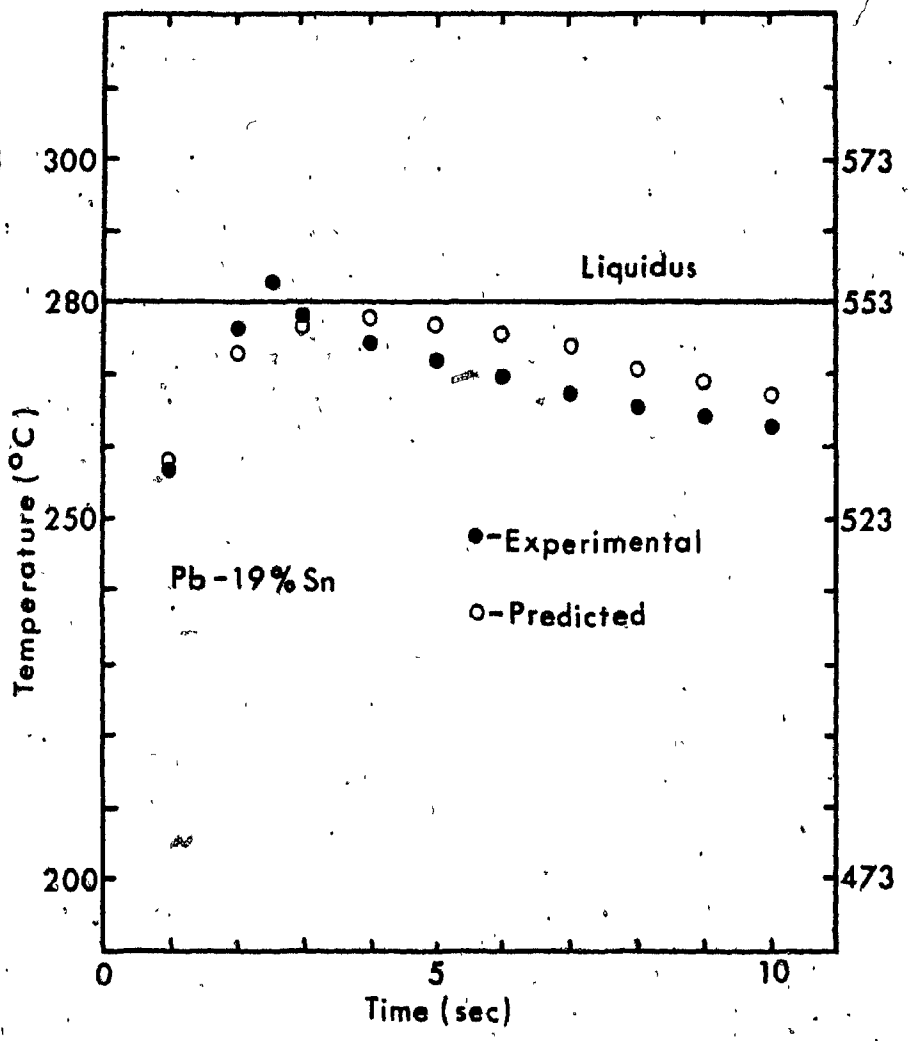
300
280
250
200
573
553
523
473
Liquidus
Pb - 19% Sn
●-Experimental
○-Predicted
Temperature (°C)
Temperature (K)
0
5
10
Time (sec)

FIGURE 4.13 Comparison of the experimental and predicted temperature at nodal point 10. Material = Pb. Superheat = 100°C. Position 3.

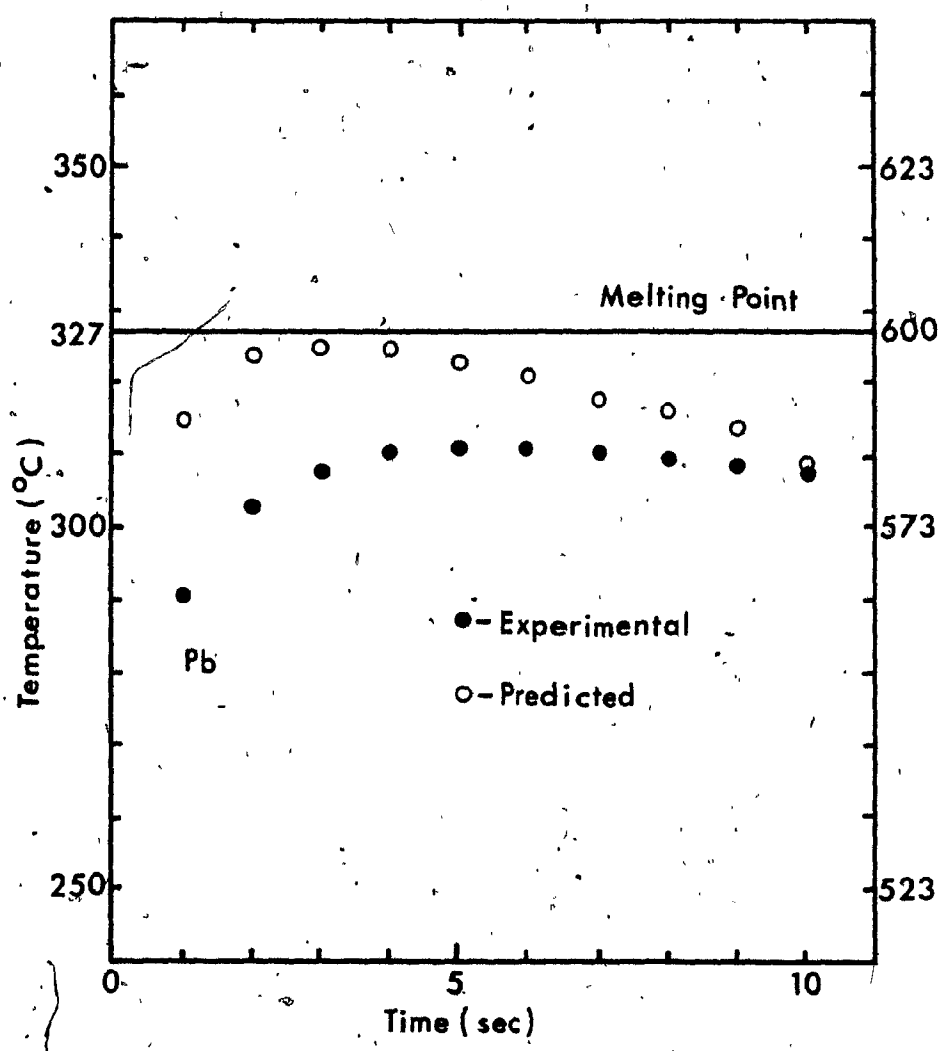
350
327
300
250
623
600
573
523
Melting Point
Temperature (°C)
Temperature (K)
Pb
●– Experimental
○– Predicted
0
5
10
Time (sec)

FIGURE 4.14 Comparison of the experimental and predicted temperature at nodal point 10. Material = Pb-19% Sn. Superheat = 100°C. Position 3.

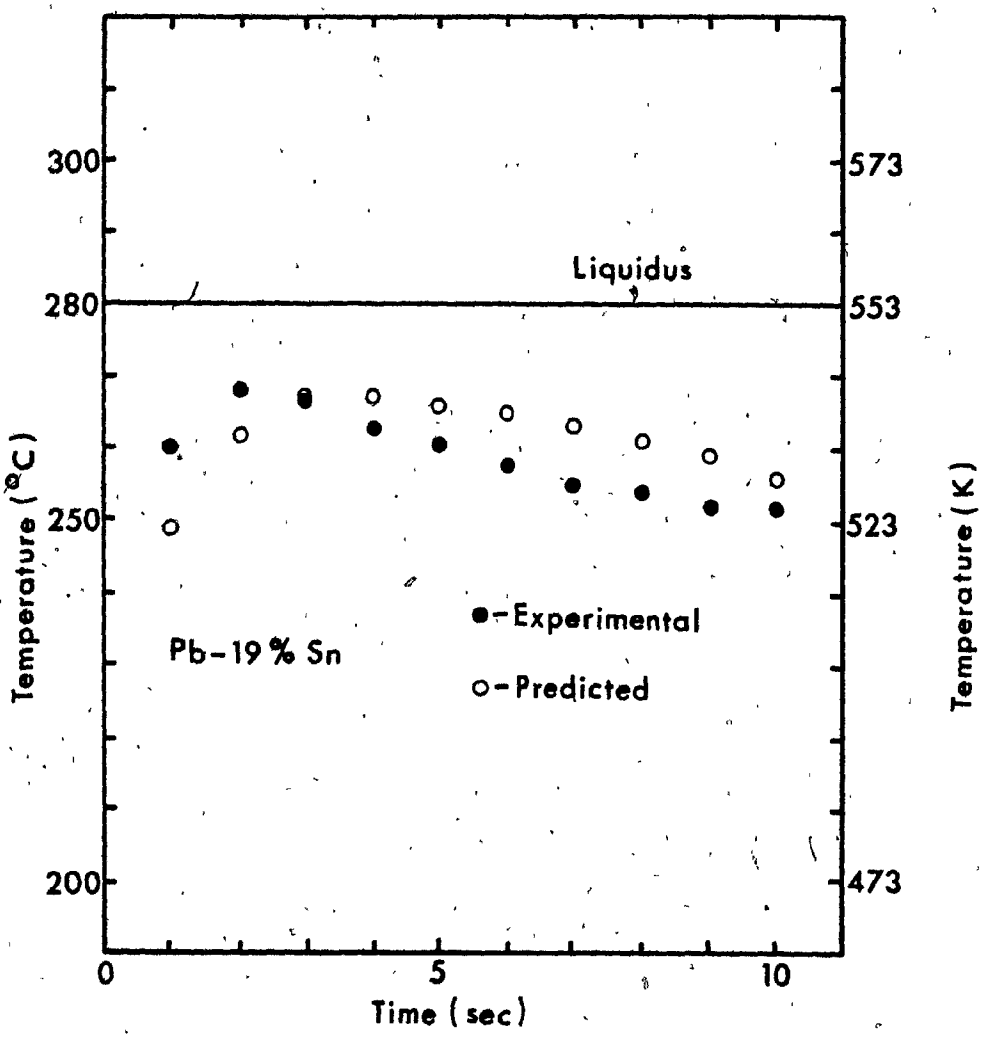
300
280
250
200
573
553
523
473
Liquidus
Temperature (°C)
Temperature (K)
Pb-19 % Sn
●-Experimental
○-Predicted
0
5
10
Time (sec)

FIGURE 4.15 Predicted temperatures at nodal point 10 at different positions in the mold. Material = Pb. Superheat = 60°C.

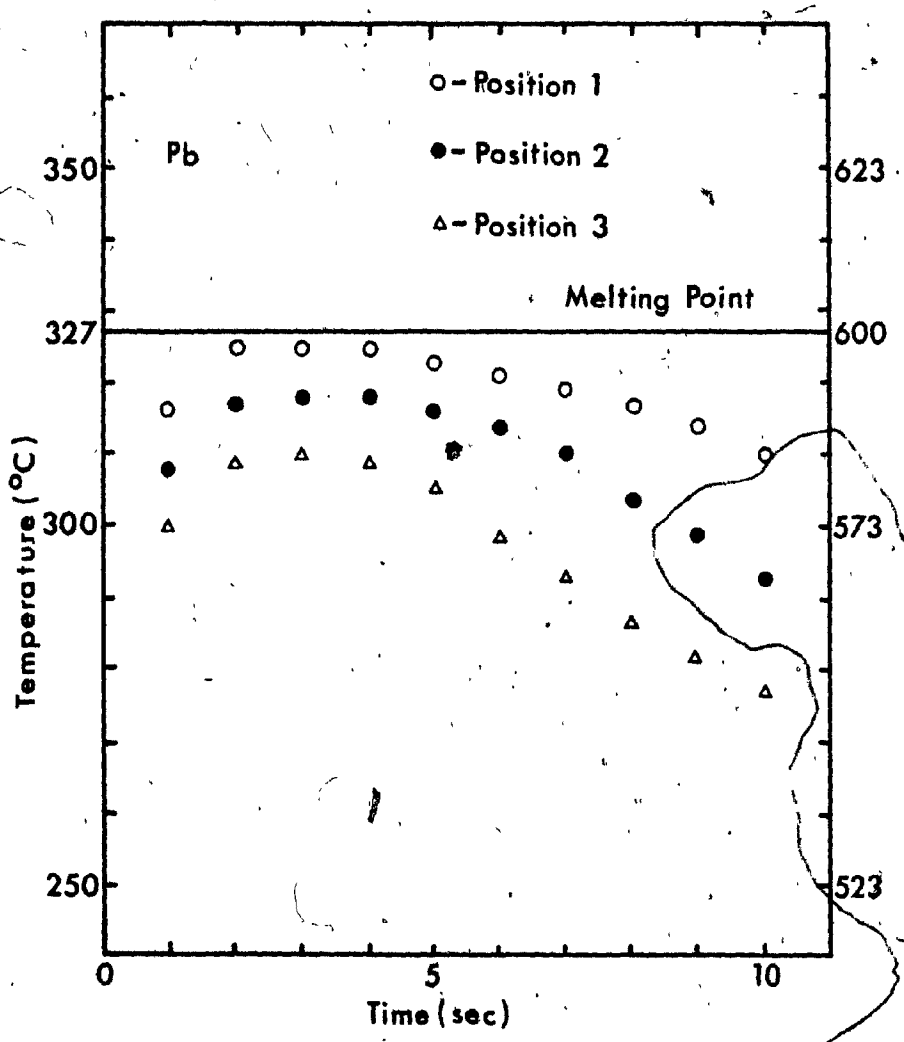
Pb
○ – Position 1
● – Position 2
△ – Position 3
Melting Point
350
327
300
250
623
600
573
523
Temperature (°C)
Temperature (K)
0
5
10
Time (sec)

FIGURE 4.16 Predicted temperatures at nodal point 10 at different positions in the mold. Material = Pb-19% Sn. Superheat = 60°C.

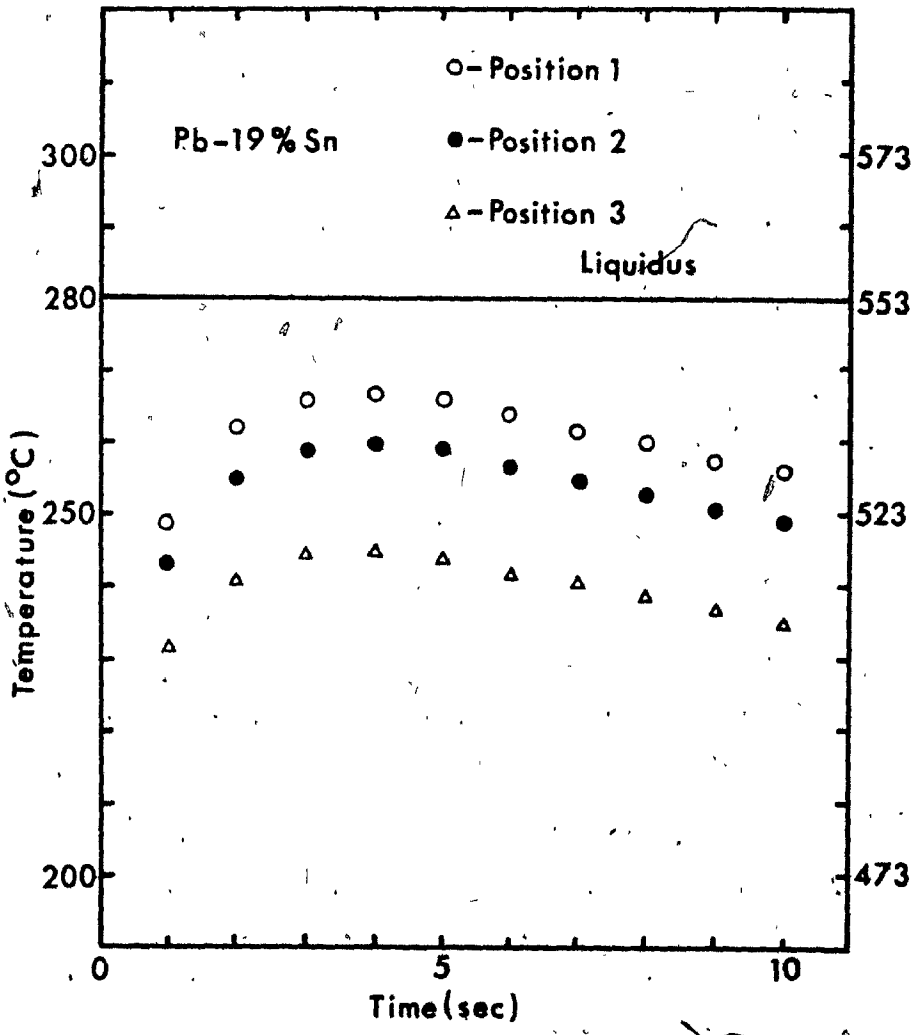
Pb-19% Sn
○ - Position 1
● - Position 2
△ - Position 3
Liquidus
300
280
250
200
573
553
523
473
0
5
10
Time (sec)
Temperature (°C)
Temperature (K)

FIGURE 4.17 Predicted temperatures at nodal point 10 at different positions in the mold. Material = Pb. Superheat = 20°C.

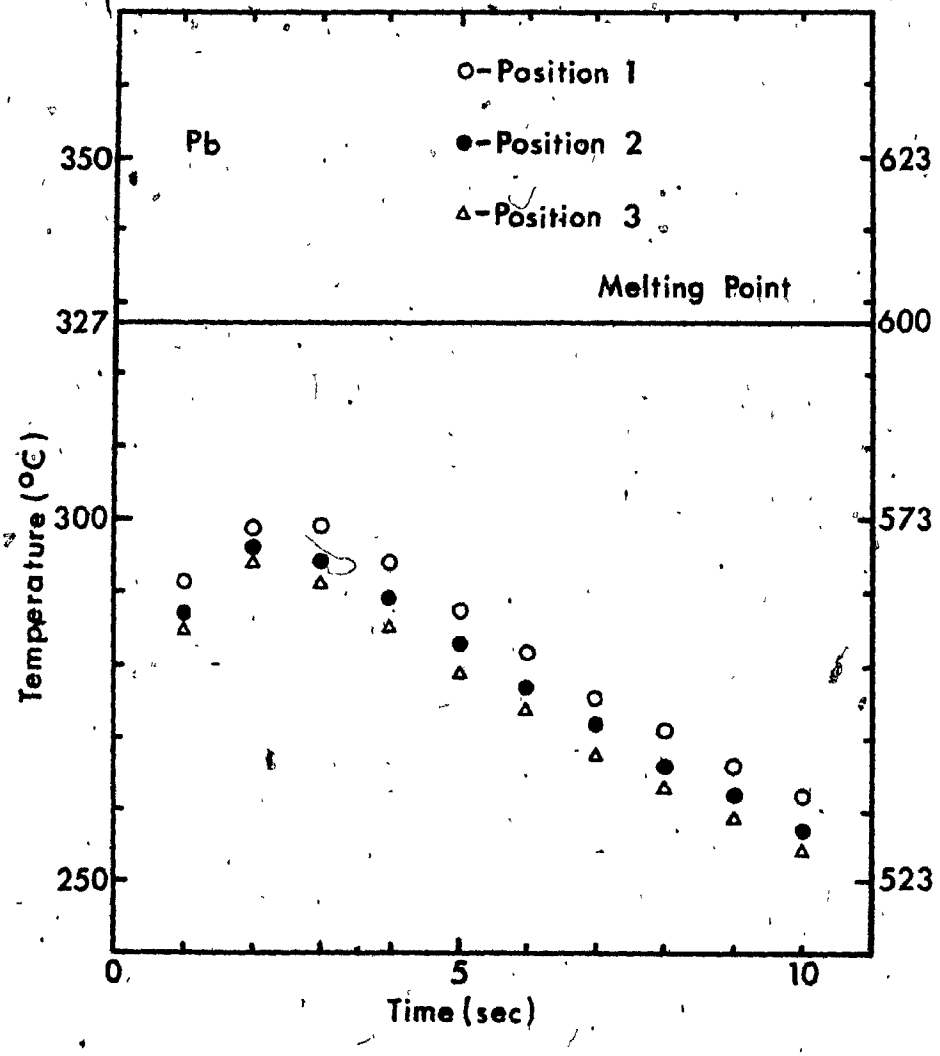
Pb
○-Position 1
●-Position 2
△-Position 3
Melting Point
350
327
300
250
623
600
573
523
0
5
10
Time (sec)
Temperature (°C)
Temperature (K)

4.9.3 Effect of Solid Temperature and Superheat on Cold Shut Formation

In real castings when liquid metal meets solidified metal, the temperature of the solid metal is not usually equal to ambient temperature as considered thus far in the present model and in the experiments. The next step in using the model was to determine, for each position in the runner, the effect of the temperature of the solid on the superheat necessary to avoid cold shuts. The critical conditions obtained for lead in position 1 (Fig. 4.18), position 2 (Fig. 4.19), and position 3 (Fig. 4.20) in the runner show that, as expected, the higher the solid temperature, the lower the superheat necessary to remelt the sample (and so avoid cold shuts). The curves shown in Figures 4.18-4.20 show the limiting conditions for cold shut formation. Points above the curves provide castings free from cold shuts, while values taken below the curves facilitate the formation of cold shuts. It is interesting to notice that the relationship between the critical superheat and the solid temperature is almost linear at solid temperatures less than or equal to 300°C (573 K). For higher temperatures of the solid, the slope of the curve increases considerably.

The same analysis was made on the Pb-19% Sn alloy, and the results are presented in Figures 4.21-4.23 for positions 1-3, respectively.

4.9.4 Effect of Position in the Mold on Cold Shut Formation

As the position in the runner also has a strong effect on the remelting process because the liquid metal loses superheat downstream, the relationship between the critical superheat and the distance downstream in the runner was analyzed. Figures 4.24 and 4.25 were drawn

presenting the curves for various solid temperatures. They show for Pb and Pb-19% Sn alloy the critical superheat, at a certain distance in the mold and at a certain solid temperature, which is necessary to remelt the solid. For instance, Fig. 4.24 shows that, at 20 cm from the point of pouring and with the solid at 250°C (523 K), the minimum superheat required to remelt the solid Pb is 50°C.

Although the theoretical predictions did not take into account convection in the liquid and/or an oxide layer at nodal point 10, the computer program is sufficiently flexible to allow for their use. The simple approach used is shown to be in reasonable agreement with experimental results.

FIGURE 4.18 Relationship between critical superheat to form cold shuts and temperature of solid sample. Material = Pb. Position 1.

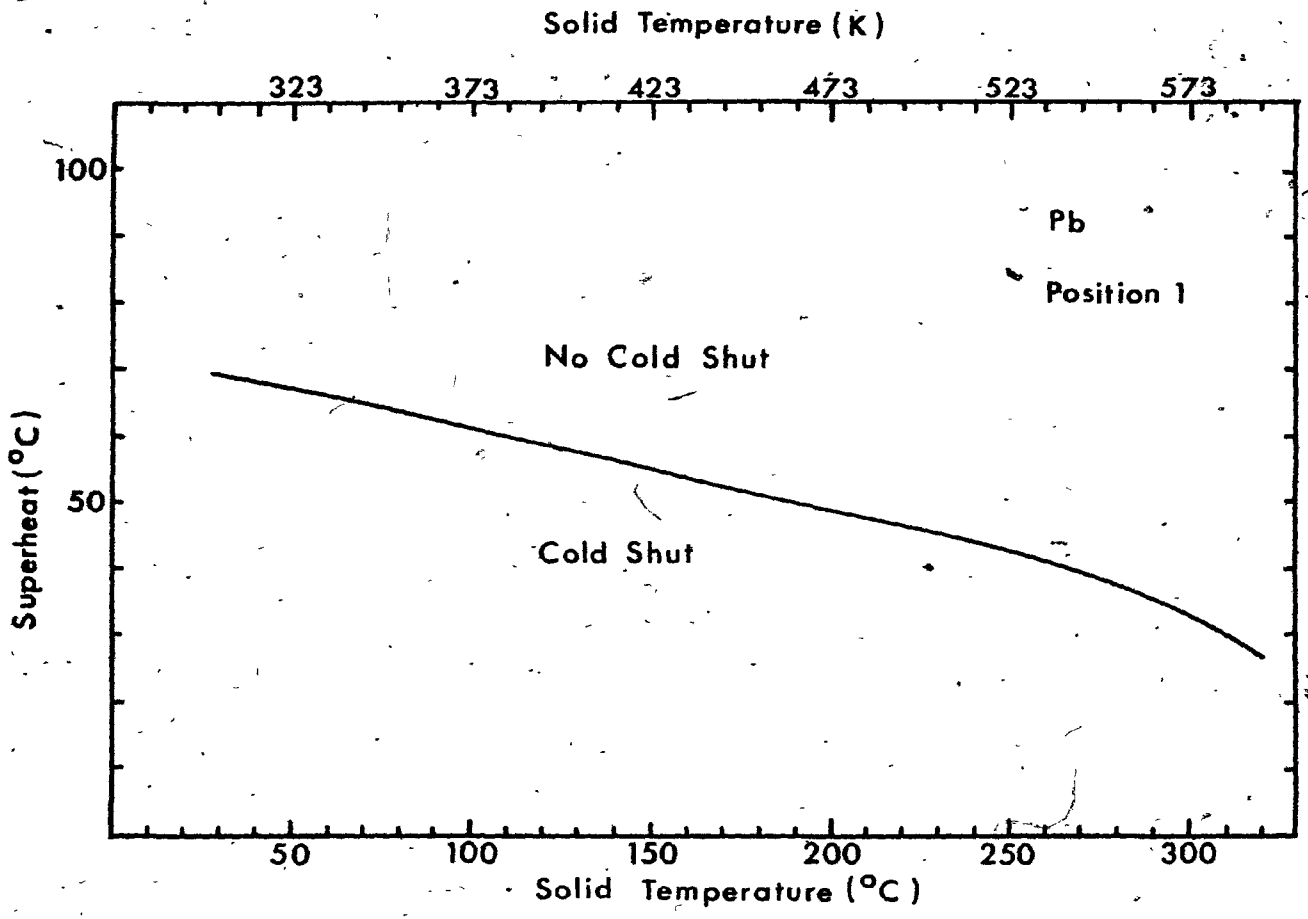
Solid Temperature (K)
323
373
423
473
523
573
100
50
Superheat (°C)
Pb
Position 1
No Cold Shut
Cold Shut
50
100
150
200
250
300
Solid Temperature (°C)

FIGURE 4.19 Relationship between critical superheat to form cold shuts and temperature of solid sample. Material = Pb. Position 2.

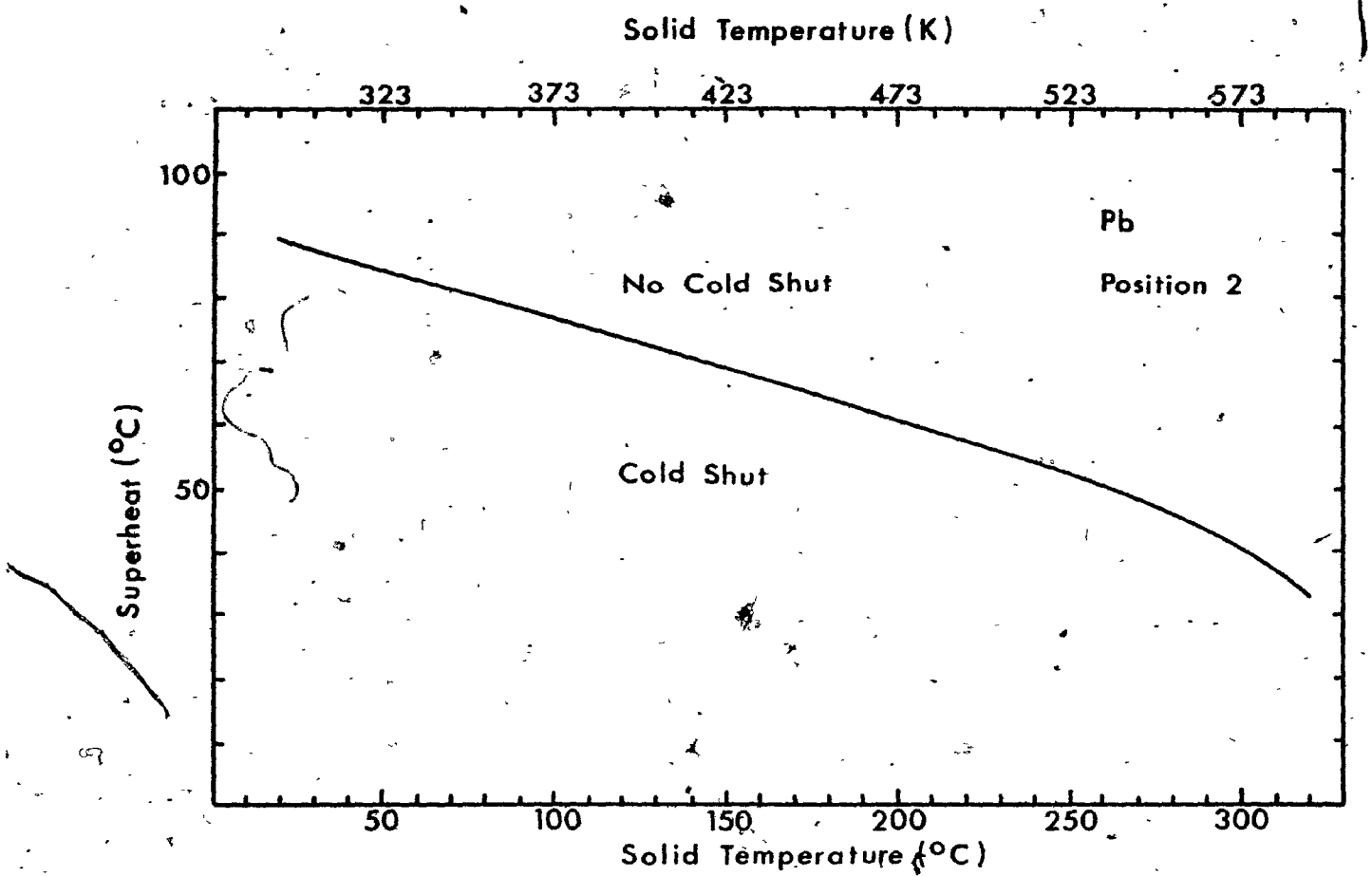
Solid Temperature (K)
323
373
423
473
523
573
100
50
Superheat (°C)
Pb
No Cold Shut
Position 2
Cold Shut
50
100
150
200
250
300
Solid Temperature (°C)

FIGURE 4.20 Relationship between critical superheat to form cold shuts and temperature of solid sample. Material = Pb. Position 3.

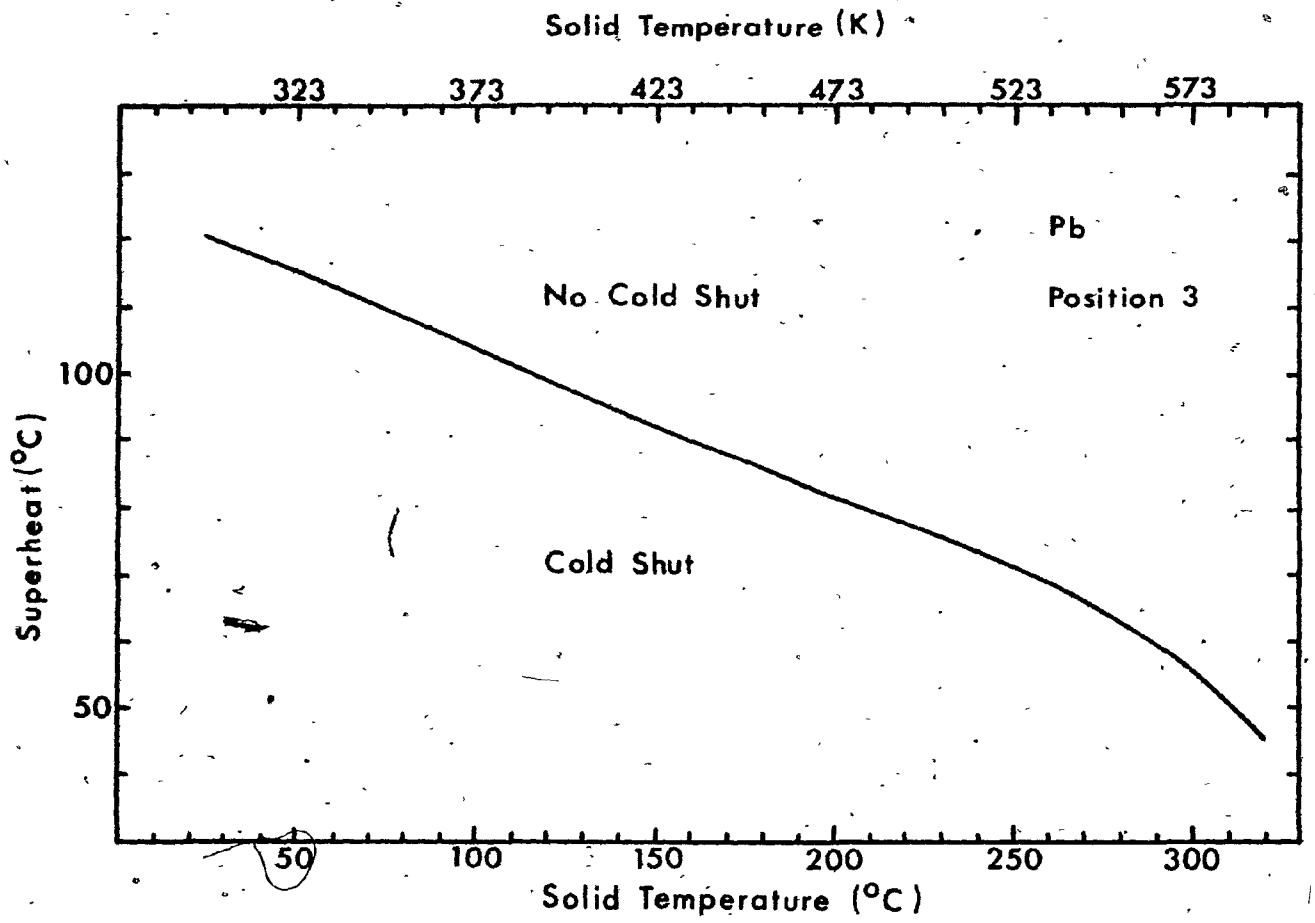
Solid Temperature (K)
323
373
423
473
523
573
Pb
No Cold Shut
Position 3
100
50
Superheat (°C)
Cold Shut
50
100
150
200
250
300
Solid Temperature (°C)

FIGURE 4.21 Relationship between critical superheat to form cold shuts and temperature of solid sample. Material = Pb-19% Sn. Position 1.

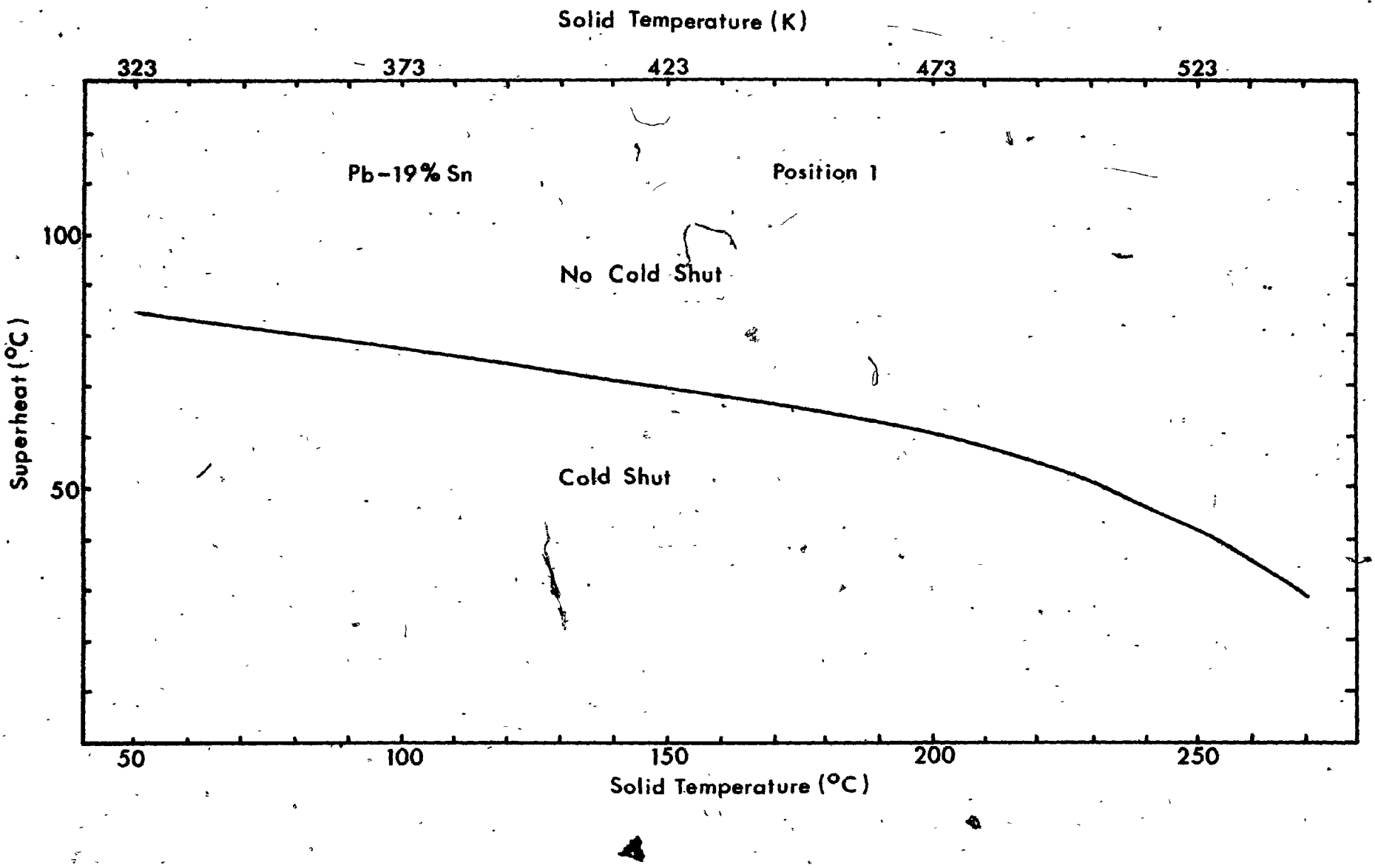
Solid Temperature (K)
323
373
423
473
523
Pb-19% Sn
Position 1
100
No Cold Shut
Superheat (°C)
50
Cold Shut
50
100
150
200
250
Solid Temperature (°C)

FIGURE 4.22 Relationship between critical superheat to form cold shuts and temperature of solid sample. Material = Pb-19% Sn. Position 2.

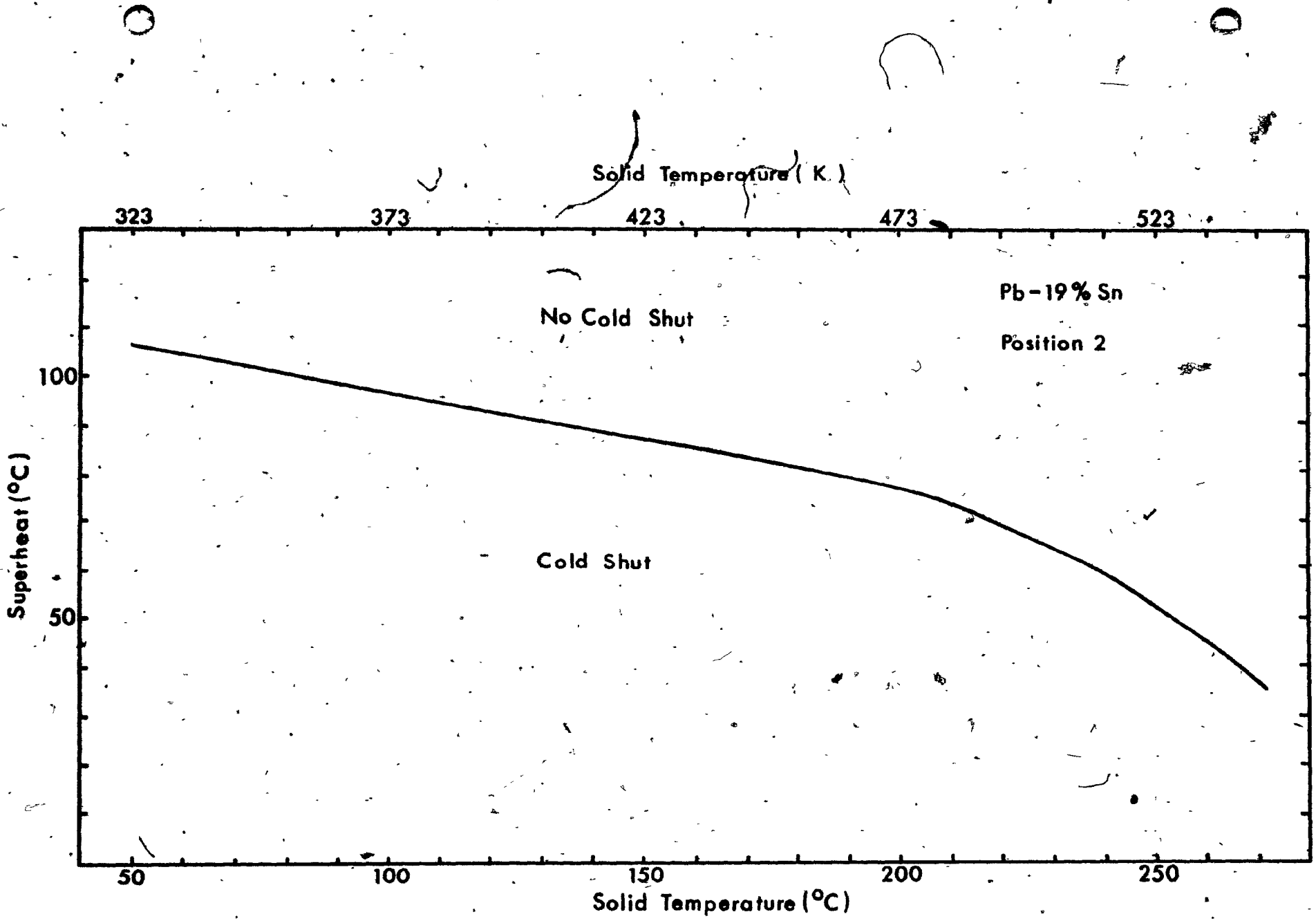
Solid Temperature (K)
323
373
423
473
523
Pb - 19 % Sn
Position 2
No Cold Shut
Cold Shut
100
50
Superheat (°C)
50
100
150
200
250
Solid Temperature (°C)

FIGURE 4.23 Relationship between critical superheat to form cold shuts and temperature of solid sample. Material = Pb-19% Sn. Position 3.

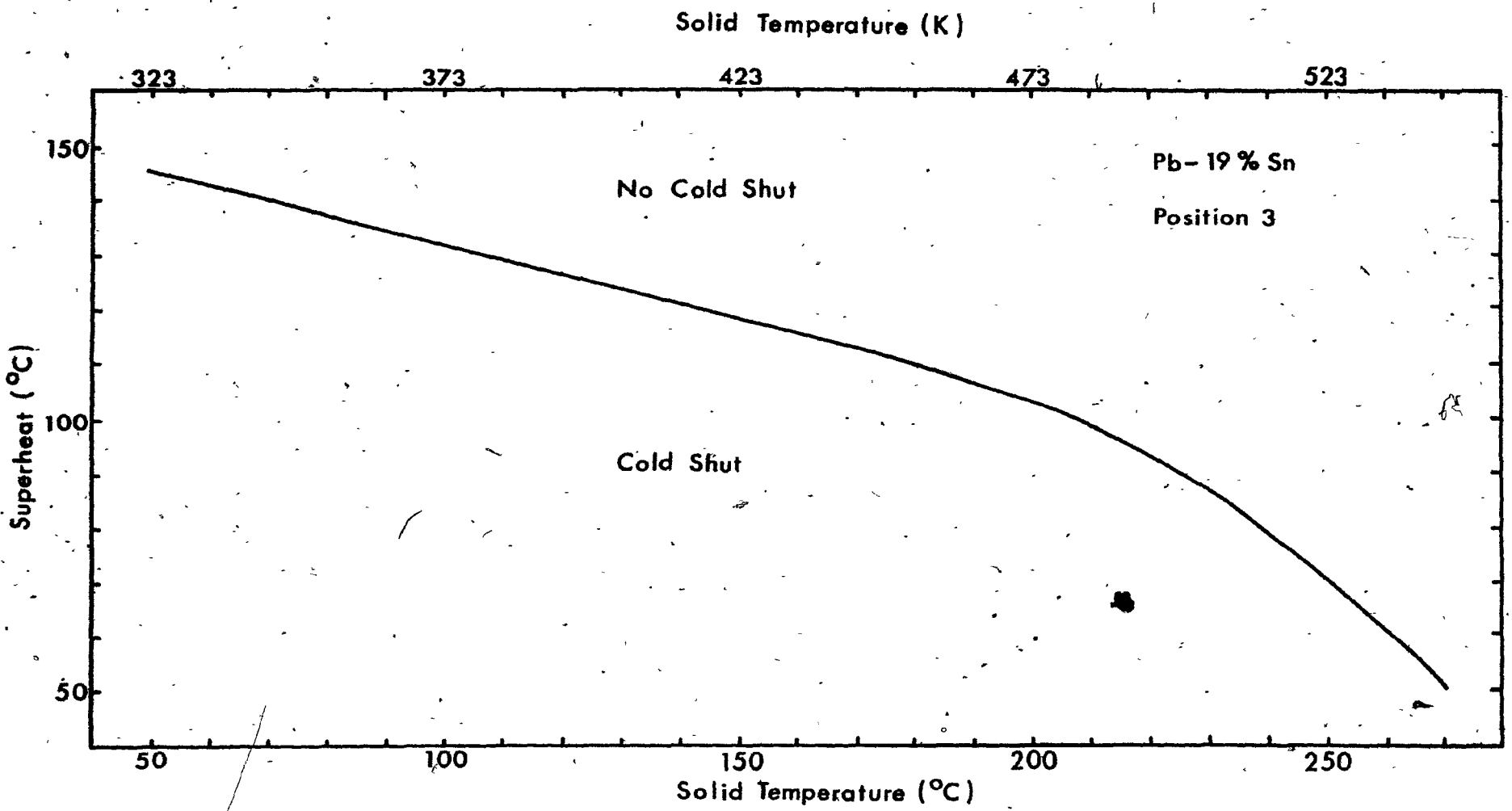
Solid Temperature (K)
323
373
423
473
523
150
100
50
Superheat (°C)
No Cold Shut
Cold Shut
Pb– 19 % Sn
Position 3
50
100
150
200
250
Solid Temperature (°C)

FIGURE 4.24 Relationship between critical superheat to form cold shuts and position in the mold. Material = Pb.

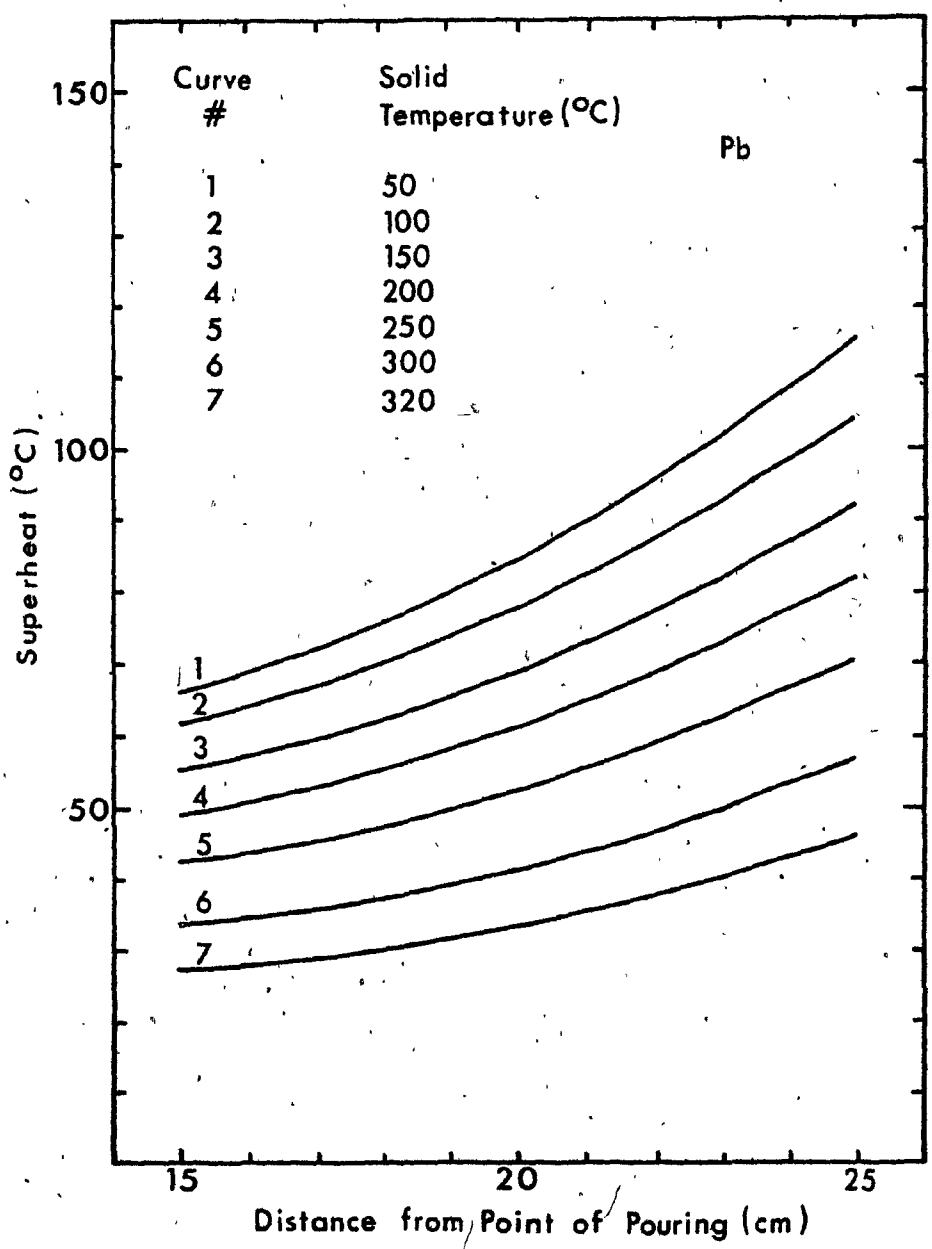
Curve #
Solid Temperature (°C)
Pb
1 50
2 100
3 150
4 200
5 250
6 300
7 320
150
100
50
Superheat (°C)
15
20
25
Distance from Point of Pouring (cm)

FIGURE 4.25 Relationship between critical superheat to form cold shuts and position in the mold. Material = Pb-19% Sn.

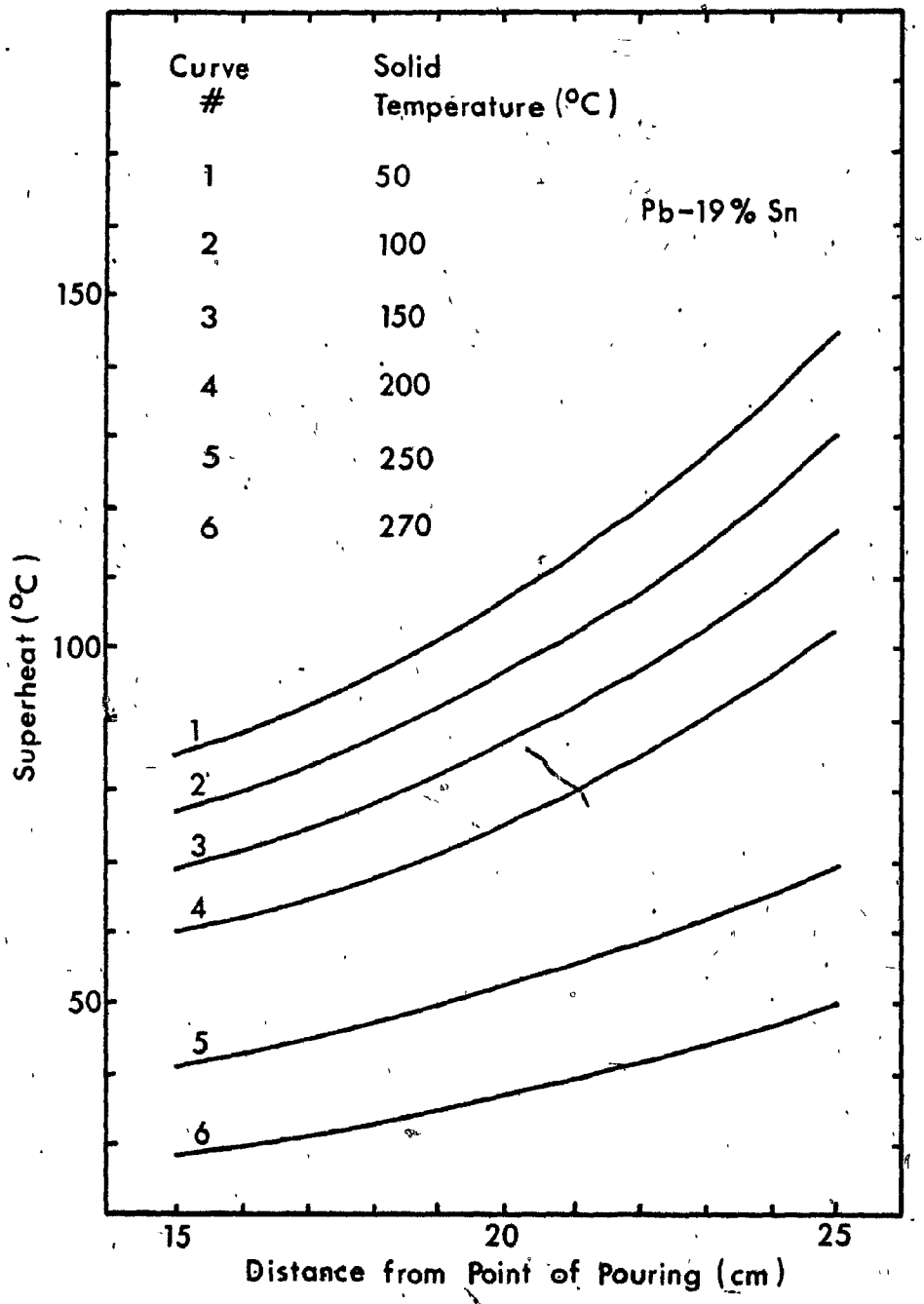
Curve #
Solid Temperature (°C)
1 50
2 100
3 150
4 200
5 250
6 270
Pb-19% Sn
Superheat (°C)
150
100
50
1
2
3
4
5
6
15
20
25
Distance from Point of Pouring (cm)

CHAPTER 5. DISCUSSION

As it was found that the major aim of the few works encountered in the literature was to determine methods to avoid cold shuts, this study was undertaken in an attempt to determine the mechanism of formation of such casting defects.

During the course of the experiments it was found to be very difficult to produce a suitable vertical cold shut. This kind of special defect seems to be formed only under a very specific set of conditions which are unlikely to occur in practice. In addition, not knowing in advance the exact place where the cold shut would be formed made the production of an appropriate defect even more difficult. The use of solid inserts overcame the difficulties and it allowed for temperature measurements.

5.1 Mechanism of Cold Shut Formation

From the experiments carried out in this study, it was found that cold shuts originate whenever a liquid metal meets a solid metal, and in addition only when the liquid does not have sufficient thermal energy to remelt the solid. This is shown schematically in Figure 5.1. The liquid flowing over the solid forms, instantaneously, a solid shell (Fig. 5.1a). At $t_1 > 0$, heat flowing from the liquid toward the solid, through the shell, partially remelts this shell (Fig. 5.1b). At $t_2 > t_1$, if the heat transported through the shell is not sufficient to remelt both the shell and the solid, then cold shuts are formed, as shown in Fig. 5.1c. If the thermal energy is sufficient to completely remelt the shell and the solid, then the formation of cold shuts is avoided (Fig. 5.1d). This explanation is in agreement with that which was found

FIGURE 5.1 Schematic diagram of cold shut formation.

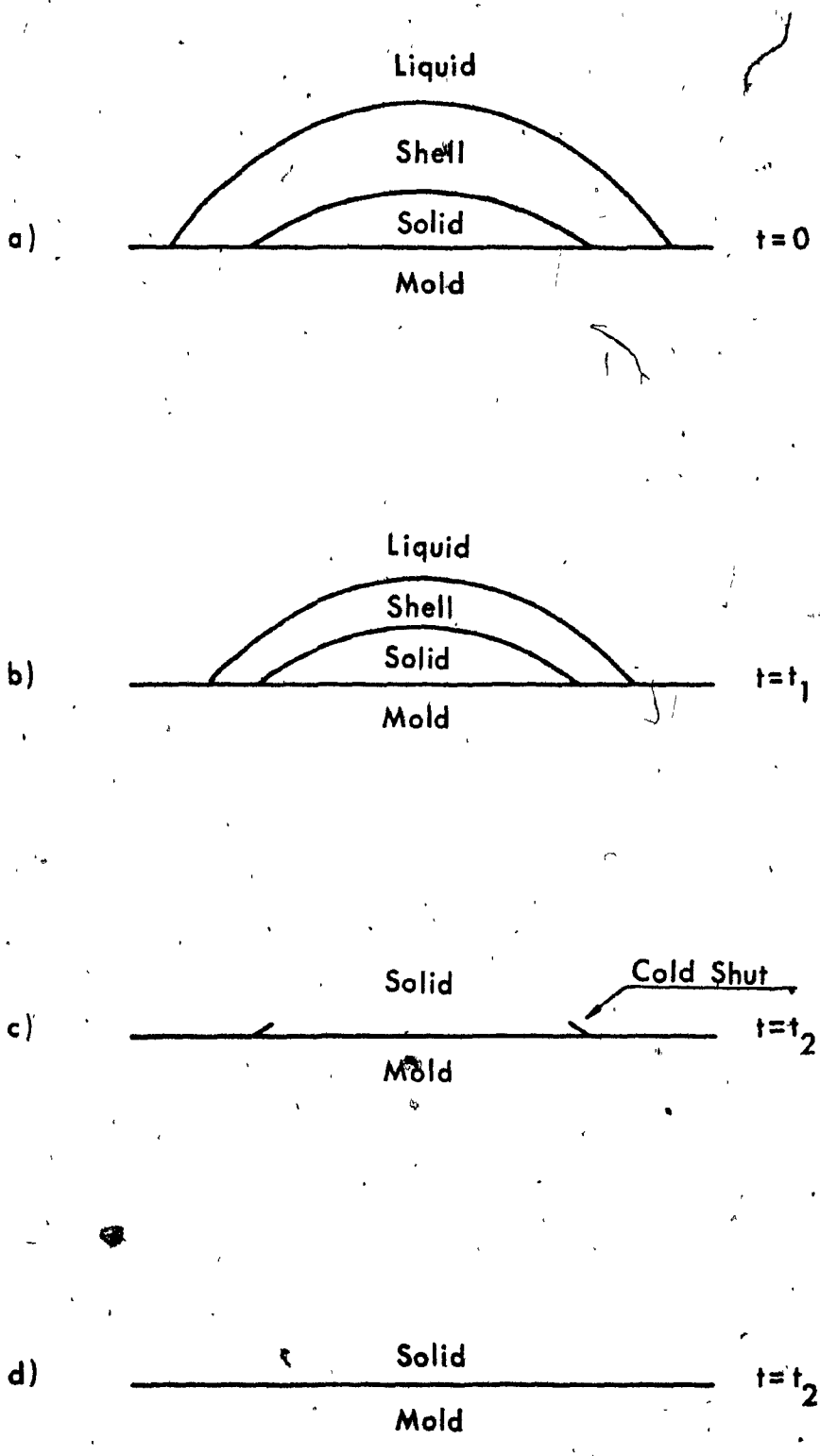
Liquid
Shell
Solid
a)
Mold
t = 0
Liquid
Shell
Solid
b)
Mold
t = t1
Solid
Cold Shut
c)
Mold
t = t2
d)
Solid
Mold
t = t2

by Gorbachev and Zhukov[8] (Chapter 1, Section 1.2.1) in studying the elimination of soft structures in white iron. The solidified eddy, in their case, corresponds to the solid insert used in this study.

5.2 Effect of Superheat and Alloy Composition on Cold Shut Formation

As already mentioned, since there is a solid portion in the mold, cold shut formation depends on the amount of heat which will be extracted from the liquid by conduction through the solid. Therefore, the remelting of the solidified layer is strongly dependent on the superheat at which the liquid meets the solid. Lillieqvist[10] has shown this (Fig. 1.12) and Figure 5.2 shows that, for pure lead, the Pb-19% Sn alloy, and the Pb-61.9% Sn alloy, there is a certain superheat above which the formation of cold shuts is avoided. The data used in Figure 5.2 were obtained from Table 3.10 (oxidized samples only) and the superheats were calculated as being 82% for position 1, 65% for position 2, and 48% of the initial superheat for position 3 in the channel. Figure 5.2 also shows that, unlike for the effective superheat, the composition of the alloy (as reported by Kvasha et al.[9]) does not have a noticeable influence on the remelting process, although the alloy composition influences the final aspect of the cold shuts, as will be seen later. In Figure 5.2 the dotted lines represent the unknown limit critical values for the formation of cold shuts and, for the alloys studied, it was found that the minimum effective superheat necessary to avoid the formation of cold shuts is somewhere between 50°C and 60°C. It should be pointed out here that these values were obtained when remelting a solid sample of metal at the ambient temperature. In practice the

FIGURE 5.2 Relationship between effective superheat, alloy composition and occurrence of cold shuts.

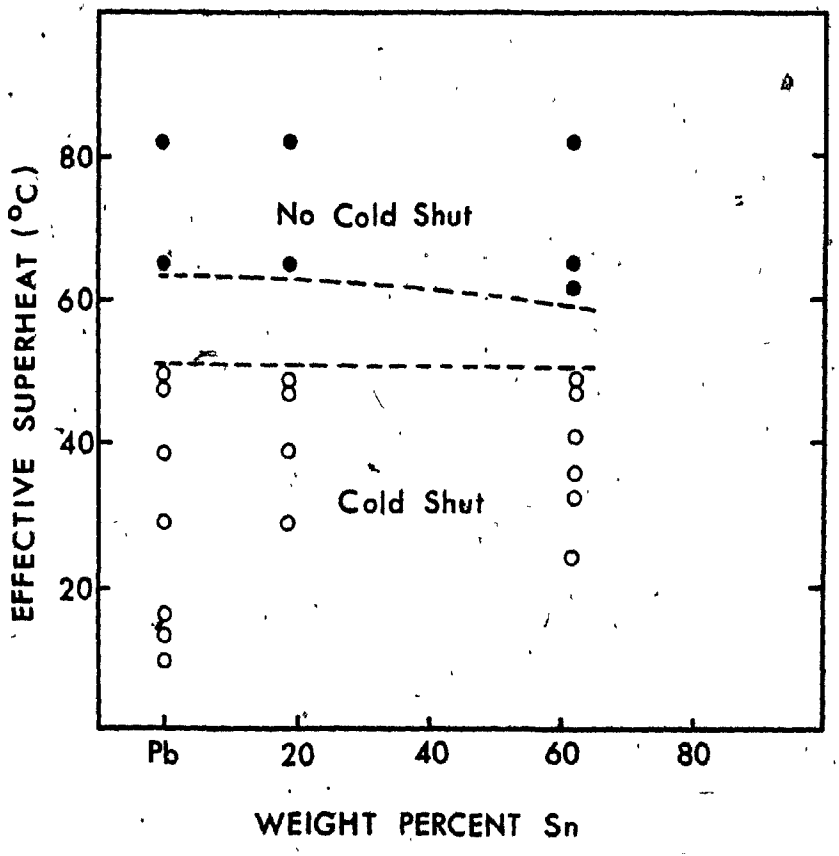
EFFECTIVE SUPERHEAT (°C)
80
60
40
20
No Cold Shut
Cold Shut
Pb
20
40
60
80
WEIGHT PERCENT Sn

effective superheat necessary to avoid the formation of the defect should be much lower than that presented in Figure 5.2.

The alloy composition influences the aspect of the cold shuts by affecting the mode of solidification. This is done in the following way: To completely remelt the solid insert it was found that, for the unalloyed lead and for the Pb-61.9% Sn alloy (eutectic composition) - which have a congruent melting point - it was necessary to heat the solid piece of metal above the melting point, as shown in Figure 4.11, Figure 4.13, and Figure 4.15. In both cases, the solid/liquid interface is planar, as outlined in Figure 5.3. On the other hand, for the Pb-19% Sn alloy, which has the larger freezing range (Fig. 3.7), the solid insert, when heated to within the mushy zone (Figs. 4.12, 4.14 and 4.16), is partially remelted. This results in the cold shuts presented in Figures 3.22 and 3.23, which are neither as visible nor as continuous as those presented in Figures 3.18 (unalloyed lead), 3.20 and 3.21 (the last two both for the Pb-61.9% Sn alloy). The partial remelting of the solid surface is possible due to the mushy zone, being a mixture of solid and liquid portions of metal. In this case, as is well known, the solid/liquid interface is no longer planar, becoming dendritic, as shown in Figure 5.4.

5.3 Effect of Superheat and Head of Metal on Misrun

A misrun is an exaggerated form of shut and it refers to castings in which the molten metal does not penetrate all parts of the mold. Misruns are mainly due to a lack of fluidity in the metal, and this usually occurs because the metal is poured at too low a temperature.

FIGURE 5.3 Schematic diagram for the remelting of an unalloyed metal.

FIGURE 5.4 Schematic diagram for the remelting of a large freezing range alloy.

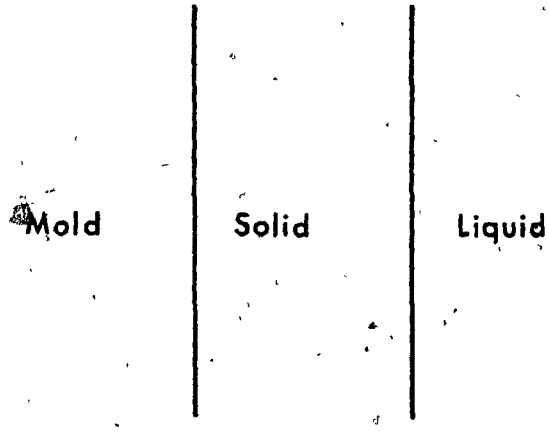
Mold
Solid
Liquid

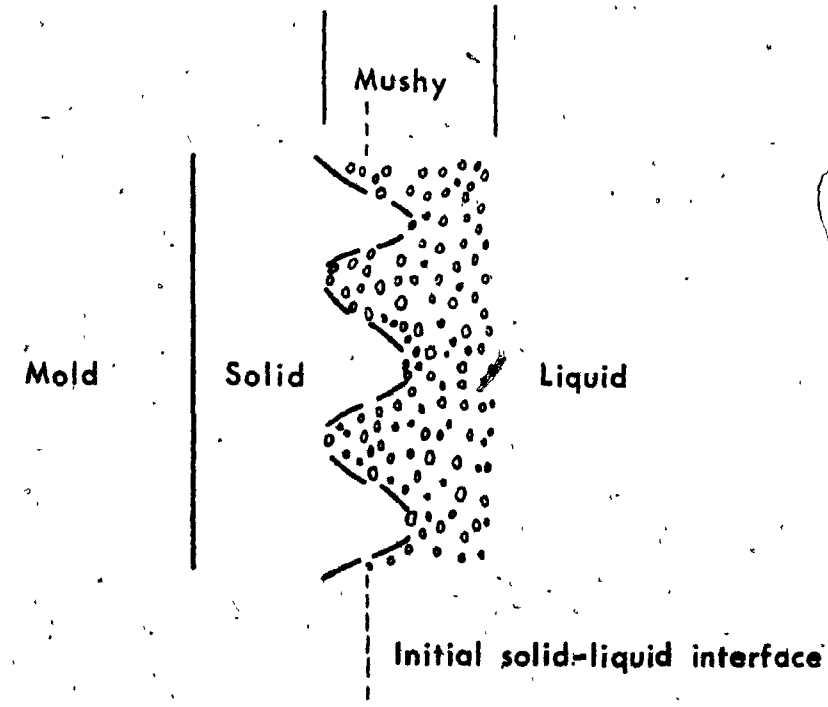
Mushy
Mold
Solid
Liquid
Initial solid-liquid interface

It was found in this study that the head of metal also has a relative influence on the occurrence of misruns. A careful analysis of Tables 3.5 and 3.6 shows that, at a superheat of 20°C, the weight of molten lead in the ladle must be greater than, say, 2200 grams to avoid a misrun (no collision of the two liquid streams). Plotting the data from those two tables yields the results shown in Figure 5.5. Although the number of experiments was not sufficient to allow for a final conclusion, it can be seen that the amount of lead (head of metal) and the superheat are the two factors which allow one to specify when a misrun will occur. Assuming that the dotted line lies on critical values of both variables (head of metal and superheat), then experimental values taken above the line will provide a casting where the two streams will collide, while values taken below the line will result in the liquid streams not meeting.

5.4 Effect of Position in the Mold on Cold Shut Formation

The influence of the position in the mold on cold shut formation, shown in Figures 4.26 and 4.27, can be explained on the basis of superheat. In fact, these positions mean effective superheat, since the molten metal loses heat as it flows in the mold. In other words, the distance from the point of pouring inside the runner is inversely proportional to the effective superheat - which was found to be percentages of the initial superheat for different positions in the mold - at which the liquid metal reaches that position, as is presented in Figure 5.6.

FIGURE 5.5 Relationship between the head of metal, the superheat and the occurrence of misruns.

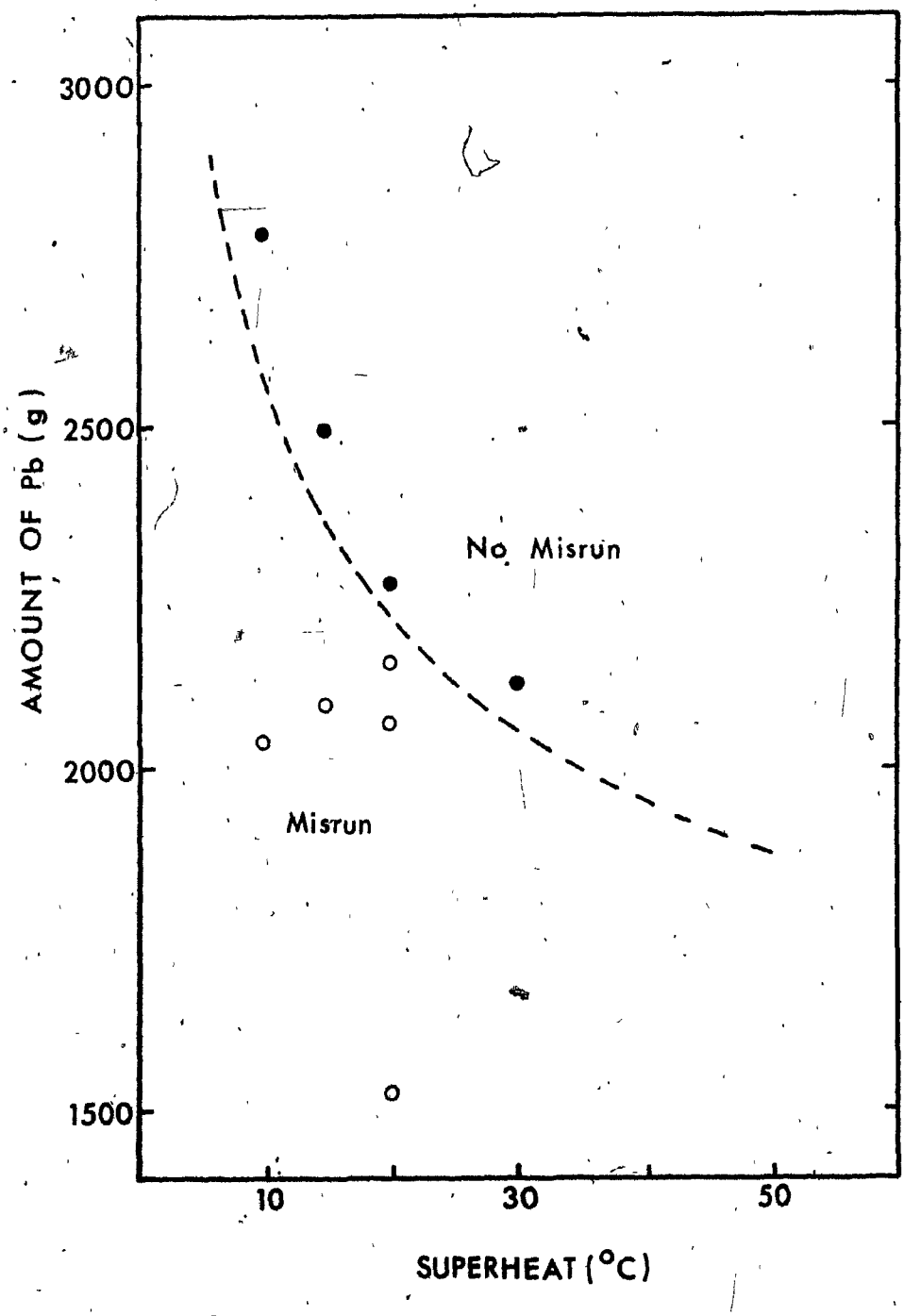
3000
2500
2000
1500
AMOUNT OF Pb (g)
No Misrun
Misrun
10
30
50
SUPERHEAT (°C)

FIGURE 5.6 Relationship between position in the mold and the superheat at which the liquid reaches the position (which is expressed as percentage of the initial superheat).

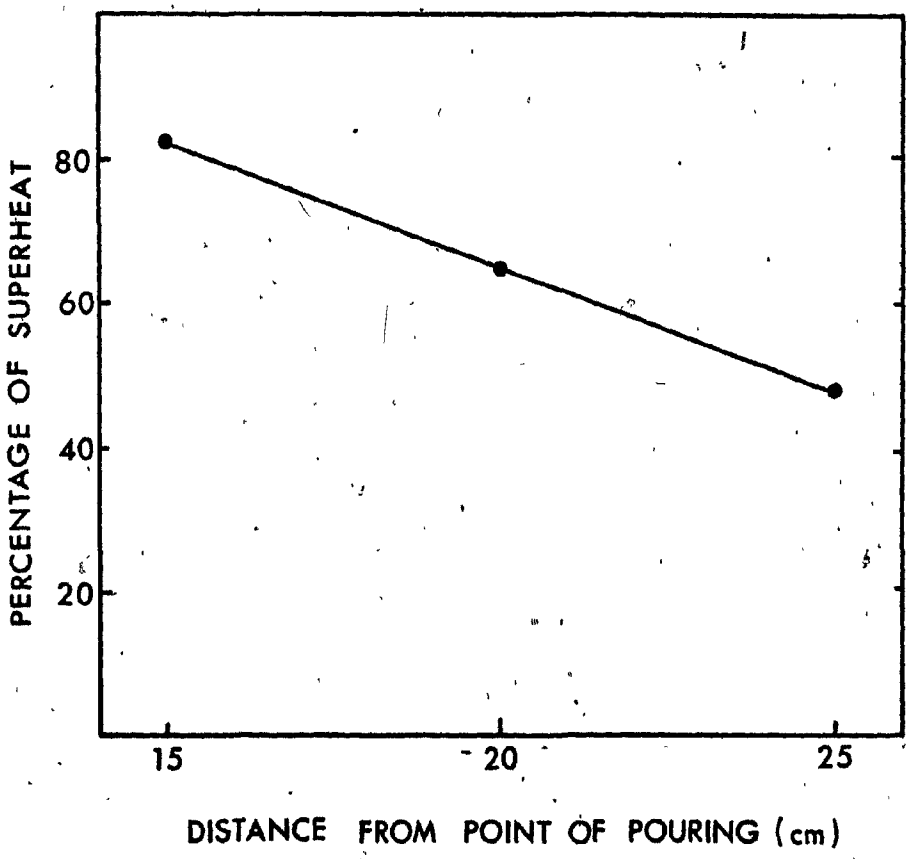
PERCENTAGE OF SUPERHEAT
80
60
40
20
15
20
25
DISTANCE FROM POINT OF POURING (cm)

5.5 Effect of Pouring Rate on Cold Shut Formation

Figures 3.10 and 3.11, resulting from experiments number B2 and B5 (Table 3.3) respectively, show that, for similar values of pouring rates (276 g/sec and 290 g/sec), 70°C is not a sufficiently high superheat to avoid the formation of a cold shut. Decreasing the pouring rate to 58 g/sec and increasing the superheat to 100°C (experiment number B9, Table 3.3) caused the formation of very deep cold shuts (Fig. 3.12). This means that the increase in superheat did not compensate for the decrease in the pouring rate, and that the formation of cold shuts is affected by both the superheat and the pouring rate.

As already stated, the remelting of the solid formed is strongly dependent on the amount of heat carried by the liquid metal. Actually, the effect of pouring rate on cold shut formation represents the influence of the effective superheat on the defect formation. In other words, low pouring rates signify that the superheat at which the molten metal meets the solid already formed is also low, as the liquid metal loses heat while flowing in the mold. On the other hand, for higher pouring rates, the heat losses are much lower than those for lower pouring rates, and then the effective superheat is substantially higher.

CHAPTER 6. CONCLUSIONS AND SUGGESTIONS FOR FURTHER WORK

6.1 Conclusions

Some conclusions which can be drawn from the present work are given below.

1. Cold shuts are formed only when one of the streams of metal is already solid at the time when the two streams collide, and even then only when the liquid does not have sufficient energy to completely remelt the solid.
2. The meeting of two streams of liquid metal has a high probability of forming cold shuts because the collision splashes molten metal which solidifies when it comes in contact with the mold. This solid can be the origin of a cold shut.
3. An oxide film on the surface of the solid stream will favour the formation of the defect since this film makes it more difficult to remelt the solid.
4. Cold shut formation is strongly dependent on the effective superheat, and this can be controlled by a combination of the pouring rate with the superheat at pouring.
5. The appearance of the cold shut is affected by the mode of solidification (alloy composition).
6. The farther the liquid metal is from the point of pouring, the higher is the probability for cold shut formation.
7. Water is an adequate fluid for simulating the collision of two streams of molten metal inside a channel.
8. It was verified through experiments on an idealised system that the occurrence of cold shuts could be predicted from

first principles using the heat transfer model presented in the text.

6.2 Suggestions for Further Work

From the results obtained in this study, it is thought that the following investigations would lead to a better understanding of cold shut formation.

1. The use of other alloys should be tried to verify the results obtained in this work for lead and lead-tin alloys.
2. The use of heated inserts in future experiments would supply more precise data to check the heat transfer model developed here.
3. The heat transfer model could be expanded to two dimensions for more accurate remelting predictions.
4. An investigation of the relationship between pouring rate, superheat and the occurrence of cold shuts would be valuable and shed more light on the formation of this type of defect.

APPENDIX A

Programming

LIST OF SYMBOLS FOR THE PROGRAMME

XTL	liquidus temperature
XTS	solidus temperature
VT	pouring temperature
XTP	temperature of solid metal
MT	total time
N1	key for the use of convection
F	factor for convection
CML	thermal conductivity of liquid metal
CMS	thermal conductivity of solid metal
CMM	thermal conductivity of mushy zone
CMO	thermal conductivity of mold
HCML	heat capacity of liquid metal
HCMS	heat capacity of solid metal
HCMO	heat capacity of mold
RO	density of metal
ROMO	density of mold
HF	latent heat of fusion for the metal
HI	heat transfer coefficient at metal/mold interface
HAMB	heat transfer coefficient for the ambient
AT	ambient temperature
XTM	initial temperature of the mold
DT	iteration time
DX	nodal point spacing in the metal side

DMX	nodal point spacing in the mold side
W(i)	temperature of nodal point i at time t
T(i)	temperature of nodal point i at time t + Δt

SOURCE LISTING

OF

PROGRAM SAND 1

Developed by

Luiz Augusto Siqueira Bittencourt

McGill University 1979

```
      DIMENSION T(35),W(35),B(60)
      READ(9,*)  XTL,XTS,VT,XTP,MT,N1,F,CML,CMS,CMM,CMO,
     *HCML,HCMS,HCMO,RO,ROMO,HF,HI,HAMB,AT,XTM,DT,DX,DMX
      DO 5 I=1,5
      T(I)=XTM
    5 W(I)=XTM
      COXI=CMS
      ROXI=RO
      XC=0.0
      HCMM=HF/(XTL-XTS)
      CML1=CML*F
      XS=RO*HCMS*DX
      XL=RO*HCML*DX
      XM=RO*HCMM*DX
      XMML=CML*DT/(XL*DX)
      X1=XMML
      XMML1=XMML*F
      XMO=CMO*ROMO*HCMO
      XML=CML*RO*HCML
      XML1=XML*F
      XMS=CMS*RO*HCMS
      XMM=CMM*RO*HCMM
      XOXI=ROXI*HCMS*DX
      HCL=(1.+SQRT(XMO/XML))*HI
      HCS=(1.+SQRT(XMO/XMS))*HI
      HCM=(1.+SQRT(XMO/XMM))*HI
      HML=(1.+SQRT(XML/XMO))*HI
      HMS=(1.+SQRT(XMS/XMO))*HI
      HMM=(1.+SQRT(XMM/XMO))*HI
      HLINT=HI*DT/XL
      HSINT=HI*DT/XS
      HMINT=HI*DT/XM
      XMO1=ROMO*HCMO*DMX
      HLMO=HI*DT/(ROMO*HCMO*DMX)
      HSMO=HLMO
      HMMO=HLMO
      HAMB=HAMB*DT/(ROMO*HCMO*DMX)
      XMMO=CMO*DT/(XMO1*DMX)
      CLM=2.*CML*CMM/(CML+CMM)
      CLM1=2.*CML1*CMM/(CML1+CMM)
      CSM=2.*CMS*CMM/(CMS+CMM)
      XLM=CLM*DT/(XM*DX)
      X2=XLM
      XLM1=CLM1*DT/(XM*DX)
      CSL=2.*CMS*CML/(CMS+CML)
      CSL1=2.*CMS*CML1/(CMS+CML1)
      COXIS=2.*COXI*CMS/(COXI+CMS)
```

```
      COXIL=2.*COXI*CML/(COXI+CML)
      COXIL1=2.*COXI*CML1/(COXI+CML1)
      COXIM=2.*COXI*CMM/(COXI+CMM)
      XOXIL=COXIL*DT/(XOXI*DX)
      X5=XOXIL
      XOXIL1=COXIL1*DT/(XOXI*DX)
      XOXIS=COXIS*DT/(XOXI*DX)
      XOXIM=COXIM*DT/(XOXI*DX)
      XSL=CSL*DT/(XS*DX)
      X3=XSL
      XSL1=CSL1*DT/(XS*DX)
      XSM=CSM*DT/(XS*DX)
      XMMS=CMS*DT/(XS*DX)
      XMLM=CLM*DT/(XL*DX)
      X4=XMLM
      XMLM1=CLM1*DT/(XL*DX)
      XMMM=CMM*DT/(XM*DX)
      XLS=CSL*DT/(XL*DX)
      X6=XLS
      XLS1=CSL1*DT/(XL*DX)
      XMSM=CSM*DT/(XM*DX)
      HX=HLMO
      DO 7 I=6,10
      T(I)=XTP
      W(I)=XTP
    7 CONTINUE
      SH=VT-XTL
      HF=HF+HCML*SH
      DO 10 I=11,30
      T(I)=VT
      W(I)=VT
   10 CONTINUE
      B(1)=XMML
      B(2)=XMML1
      B(3)=HLINT
      B(4)=HSINT
      B(5)=HMINT
      B(6)=HLMO
      B(7)=HAMB
      B(8)=XMMO
      B(9)=XLM
      B(10)=XLM1
      B(11)=XOXIL
      B(12)=XOXIL1
      B(13)=XOXIS
      B(14)=XOXIM
      B(15)=XSL
```

```
      B(16)=XSL1
      B(17)=XSM
      B(18)=XMMS
      B(19)=XMLM
      B(20)=XMLM1
      B(21)=XMMM
      B(22)=XLS
      B(23)=XLS1
      B(24)=XMSM
      B(25)=HX
      B(26)=2.*(XMML+HLINT)
      B(27)=2.*(XMML1+HLINT)
      B(28)=2.*XMML
      B(29)=2.*XMML1
      B(30)=2.*(HX+XMMO)
      B(31)=2.*XMMO
      B(32)=2.*(XMMO+HAMB)
      B(33)=2.*(XLM+HMINT)
      B(34)=2.*(XLM1+HMINT)
      B(35)=2.*(XMMM+HMINT)
      B(36)=2.*(XSL+HSINT)
      B(37)=2.*(XSL1+HSINT)
      B(38)=2.*(XSM+HSINT)
      B(39)=2.*(XMMS+HSINT)
      B(40)=XMML+XMLM
      B(41)=XMML1+XMLM1
      B(42)=XLM+XMMM
      B(43)=XLM1+XMMM
      B(44)=2.*XMMM
      B(45)=XMML+XLS
      B(46)=XMML1+XLS
      B(47)=XLM+XMSM
      B(48)=XLM1+XMSM
      B(49)=XMMM+XMSM
      B(50)=XSL+XMMS
      B(51)=XSL1+XMMS
      B(52)=XSM+XMMS
      B(53)=2.*XMMS
      B(54)=XOXIL+XOXIS
      B(55)=XOXIL1+XOXIS
      B(56)=XOXIM+XOXIS
      B(57)=2.*XOXIS
      WRITE(6,6) (B(I),I=1,57)
    6 FORMAT(25(10X,F15.7/)//32(10X,F15.7/)//)
      DO 1500 JK=1,MT
      DO 1000 JN=1,1000
      IF(T(6).LE.XTL) GO TO 60
```

```
C       TEMPERATURE IN THE CASTING
   15 T(6)=(1-2*XMML-2*HLINT)*W(6)+2*XMML*W(7)+2*HLINT*T(5)
   16 T(7)=(1-2*XMML)*W(7)+XMML*(W(8)+T(6))
   17 T(8)=(1-2*XMML)*W(8)+XMML*(W(9)+T(7))
   18 T(9)=(1-2*XMML)*W(9)+XMML*(W(10)+T(8))
   19 T(10)=(1-2*XMML)*W(10)+XMML*(W(11)+T(9))
C       TEMPERATURE IN THE MOULD
   44 CONTINUE
      T(5)=(1.-2.*HX-2.*XMMO)*W(5)+2.*HX*T(6)+2.*XMMO*W(4)
      J=6
      DO 40 I=2,4
      K=J-I
      N=K+1
      M=K-1
   40 T(K)=(1.-2.*XMMO)*W(K)+XMMO*(T(N)+W(M))
      T(1)=(1.-2.*XMMO-2.*HAMB)*W(1)+2.*XMMO*T(2)+2.*HAMB*AT
      DO 50 I=1,30
      W(I)=T(I)
   50 CONTINUE
      XC=XC+DT
      GO TO 1000
   60 CONTINUE
      IF(T(6).LT.XTS) GO TO 70
      IF(T(7).LE.XTL)GO TO 75
C       T6=M     T7=L
      T(6)=(1.-2*XLM-2*HMINT)*W(6)+2*XLM*W(7)+2*HMINT*T(5)
      GO TO 80
C       T6=M     T7=M
   75 T(6)=(1-2*XMMM-2*HMINT)*W(6)+2*XMMM*W(7)+2*HMINT*T(5)
      GO TO 80
   70 IF(T(7).LE.XTL) GO TO 90
C       T6=S     T7=L
      T(6)=(1-2*XSL-2*HSINT)*W(6)+2*XSL*W(7)+2*HSINT*T(5)
      GO TO 80
   90 IF(T(7).LT.XTS) GO TO 100
C       T6=S     T7=M
      T(6)=(1-2*XSM-2*HSINT)*W(6)+2*XSM*W(7)+2*HSINT*T(5)
      GO TO 80
C       T6=S     T7=S
  100 T(6)=(1-2*XMMS-2*HSINT)*W(6)+2*XMMS*W(7)+2*HSINT*T(5)
   80 IF(T(6).LT.XTS)GO TO 150
      IF(T(7).LE.XTL) GO TO 160
C       T6=M     T7=L     T8=L
      T(7)=(1-XMML-XMLM)*W(7)+XMML*W(8)+XMLM*T(6)
      GO TO 300
  160 IF(T(8).LE.XTL) GO TO 170
C       T6=M     T7=M     T8=L
```

```
      T(7)=(1-XLM-XMMM)*W(7)+XLM*W(8)+XMMM*T(6)
      GO TO 300
C     T6=M     T7=M     T8=M
  170 T(7)=(1-2*XMMM)*W(7)+XMMM*(W(8)+T(6))
      GO TO 300
  150 IF(T(7).LE.XTL) GO TO 180
C     T6=S     T7=L     T8=L
      T(7)=(1-XMML-XLS)*W(7)+XMML*W(8)+XLS*T(6)
      GO TO 300
  180 IF(T(7).LT.XTS) GO TO 190
      IF(T(8).LE.XTL) GO TO 200
C     T6=S     T7=M     T8=L
      T(7)=(1-XLM-XMSM)*W(7)+XLM*W(8)+XMSM*T(6)
      GO TO 300
C     T6=S     T7=M     T8=M
  200 T(7)=(1-XMMM-XMSM)*W(7)+XMMM*W(8)+XMSM*T(6)
      GO TO 300
  190 IF(T(8).LE.XTL) GO TO 210
C     T6=S     T7=S     T8=L
      T(7)=(1-XSL-XMMS)*W(7)+XSL*W(8)+XMMS*T(6)
      GO TO 300
  210 IF(T(8).LT.XTS) GO TO 220
C     T6=S     T7=S     T8=M
      T(7)=(1-XSM-XMMS)*W(7)+XSM*W(8)+XMMS*T(6)
      GO TO 300
C     T6=S     T7=S     T8=S
  220 T(7)=(1-2*XMMS)*W(7)+XMMS*(W(8)+T(6))
  300 IF(T(7).GT.XTL) GO TO 17
      IF(T(7).LT.XTS) GO TO 400
      IF(T(8).LE.XTL) GO TO 320
C     T7=M     T8=L     T9=L
      T(8)=(1-XMML-XMLM)*W(8)+XMML*W(9)+XMLM*T(7)
      GO TO 500
  320 IF(T(9).LE.XTL) GO TO 330
C     T7=M     T8=M     T9=L
      T(8)=(1-XLM-XMMM)*W(8)+XLM*W(9)+XMMM*T(7)
      GO TO 500
C     T7=M     T8=M     T9=M
  330 T(8)=(1-2*XMMM)*W(8)+XMMM*(W(9)+T(7))
      GO TO 500
  400 IF(T(8).LE.XTL) GO TO 410
C     T7=S     T8=L     T9=L
      T(8)=(1-XMML-XLS)*W(8)+XMML*W(9)+XLS*T(7)
      GO TO 500
  410 IF(T(8).LT.XTS) GO TO 430
      IF(T(9).LE.XTL) GO TO 420
C     T7=S     T8=M     T9=L
```

```
      T(8)=(1-XLM-XMSM)*W(8)+XLM*W(9)+XMSM*T(7)
      GO TO 500
C     T7=S      T8=M      T9=M
  420 T(8)=(1-XMMM-XMSM)*W(8)+XMMM*W(9)+XMSM*T(7)
      GO TO 500
  430 IF(T(9).LE.XTL) GO TO 440
C     T7=S      T8=S      T9=L
      T(8)=(1-XSL-XMMS)*W(8)+XSL*W(9)+XMMS*T(7)
      GO TO 500
  440 IF(T(9).LT.XTS) GO TO 450
C     T7=S      T8=S      T9=M
      T(8)=(1-XSM-XMMS)*W(8)+XSM*W(9)+XMMS*T(7)
      GO TO 500
C     T7=S      T8=S      T9=S
  450 T(8)=(1-2*XMMS)*W(8)+XMMS*(W(9)+T(7))
  500 IF(T(8).GT.XTL) GO TO 18
      IF(T(8).LT.XTS) GO TO 600
      IF(T(9).LE.XTL) GO TO 520
C     T8=M      T9=L      T10=L
      T(9)=(1-XMML-XMLM)*W(9)+XMML*W(10)+XMLM*T(8)
      GO TO 700
  520 IF(T(10).LE.XTL) GO TO 530
C     T8=M      T9=M      T10=L
      T(9)=(1-XLM-XMMM)*W(9)+XLM*W(10)+XMMM*T(8)
      GO TO 700
C     T8=M      T9=M      T10=M
  530 T(9)=(1-2*XMMM)*W(9)+XMMM*(W(10)+T(8))
      GO TO 700
  600 IF(T(9).LE.XTL) GO TO 610
C     T8=S      T9=L      T10=L
      T(9)=(1-XMML-XLS)*W(9)+XMML*W(10)+XLS*T(8)
      GO TO 700
  610 IF(T(9).LT.XTS) GO TO 630
      IF(T(10).LE.XTL) GO TO 620
C     T8=S      T9=M      T10=L
      T(9)=(1-XLM-XMSM)*W(9)+XLM*W(10)+XMSM*T(8)
      GO TO 700
C     T8=S      T9=M      T10=M
  620 T(9)=(1-XMMM-XMSM)*W(9)+XMMM*W(10)+XMSM*T(8)
      GO TO 700
  630 IF(T(10).LE.XTL) GO TO 640
C     T8=S      T9=S      T10=L
      T(9)=(1-XSL-XMMS)*W(9)+XSL*W(10)+XMMS*T(8)
      GO TO 700
  640 IF(T(10).LT.XTS) GO TO 650
C     T8=S      T9=S      T10=M
      T(9)=(1-XSM-XMMS)*W(9)+XSM*W(10)+XMMS*T(8)
```

```
      GO TO 700
C     T8=S      T9=S      T10=S
  650 T(9)=(1-2*XMMS)*W(9)+XMMS*(W(10)+T(8))
  700 IF(N1.EQ.0) GO TO 705
      IF(JK.EQ.1.AND.JN.LE.N1) GO TO 710
  705 XMML=X1
      XLM=X2
      XOXIL=X5
      GO TO 720
  710 CONTINUE
      XMML=XMML1
      XLM=XLM1
      XOXIL=XOXIL1
  720 CONTINUE
      IF(T(9).GT.XTL) GO TO 19
      IF(T(9).LT.XTS) GO TO 800
      IF(T(10).LE.XTL) GO TO 820
C     T9=M      T10=L      T11=L
      T(10)=(1-XMML-XMLM)*W(10)+XMML*W(11)+XMLM*T(9)
      GO TO 850
  820 IF(T(11).LE.XTL) GO TO 830
C     T9=M      T10=M      T11=L
      T(10)=(1-XLM-XMMM)*W(10)+XLM*W(11)+XMMM*T(9)
      GO TO 850
C     T9=M      T10=M      T11=M
  830 T(10)=(1-2*XMMM)*W(10)+XMMM*(W(11)+T(9))
      GO TO 850
  800 IF(T(10).LE.XTL) GO TO 810
C     T9=S      T10=L      T11=L
      T(10)=(1-XMML-XLS)*W(10)+XMML*W(11)+XLS*T(9)
      GO TO 850
  810 IF(T(10).LT.XTS) GO TO 835
      IF(T(11).LT.XTL) GO TO 825
C     T9=S      T10=M      T11=L
      T(10)=(1-XLM-XMSM)*W(10)+XLM*W(11)+XMSM*T(9)
      GO TO 850
C     T9=S      T10=M      T11=M
  825 T(10)=(1-XMMM-XMSM)*W(10)+XMMM*W(11)+XMSM*T(9)
      GO TO 850
  835 IF(T(11).LE.XTL) GO TO 840
C     T9=S      T10=OXI    T11=L
      T(10)=(1-XOXIL-XOXIS)*W(10)+XOXIL*W(11)+XOXIS*T(9)
      GO TO 850
  840 IF(T(11).LT.XTS) GO TO 845
C     T9=S      T10=OXI    T11=M
      T(10)=(1-XOXIM-XOXIS)*W(10)+XOXIM*W(11)+XOXIS*T(9)
      GO TO 850
```

```
C      T9=S      T10=OXI      T11=S
  845 T(10)=(1-2*XOXIS)*W(10)+XOXIS*(W(11)+T(9))
  850 CONTINUE
      DO 2000 NM=11,30
      K1=NM-1
      K2=NM+1
      IF(T(K1).LE.XTL) GO TO 2001
      DO 2050 NK=11,30
      K3=NK-1
      K4=NK+1
      IF(NK.EQ.30) W(K4)=T(K3)
      T(NK)=(1-2*XMML)*W(NK)+XMML*(W(K4)+T(K3))
 2050 CONTINUE
      GO TO 3000
 2001 IF(NM.EQ.30) W(K2)=T(K1)
      IF(NM.GT.11) GO TO 2002
      IF(JN.GT.N1) GO TO 2002
      IF(JK.GT.1) GO TO 2002
      IF(N1.EQ.0) GO TO 2002
      IF(JK.EQ.1.AND.JN.LE.N1) GO TO 2004
      GO TO 2002
 2004 CONTINUE
      XMML=XMML1
      XLM=XLM1
      XSL=XSL1
      GO TO 2003
 2002 XMML=X1
      XLM=X2
      XSL=X3
 2003 CONTINUE
      IF(T(K1).LT.XTS) GO TO 2100
      IF(T(NM).LE.XTL) GO TO 2200
C     TK1=M      TNM=L      TK2=L
      T(NM)=(1-XMML-XMLM)*W(NM)+XMML*W(K2)+XMLM*T(K1)
      GO TO 2000
 2200 IF(T(K2).LE.XTL) GO TO 2220
C     TK1=M      TNM=M      TK2=L
      T(NM)=(1-XLM-XMMM)*W(NM)+XLM*W(K2)+XMMM*T(K1)
      GO TO 2000
C     TK1=M      TNM=M      TK2=M
 2220 T(NM)=(1-2*XMMM)*W(NM)+XMMM*(W(K2)+T(K1))
      GO TO 2000
 2100 IF(T(NM).LE.XTL) GO TO 2120
C     TK1=S      TNM=L      TK2=L
      T(NM)=(1-XMML-XLS)*W(NM)+XMML*W(K2)+XLS*T(K1)
      GO TO 2000
 2120 IF(T(NM).LT.XTS) GO TO 2130
```

```
      IF(T(K2).LT.XTL) GO TO 2140
C     TK1=S     TNM=M     TK2=L
      T(NM)=(1-XLM-XMSM)*W(NM)+XLM*W(K2)+XMSM*T(K1)
      GO TO 2000
C     TK1=S     TNM=M     TK2=M
 2140 T(NM)=(1-XMMM-XMSM)*W(NM)+XMMM*W(K2)+XMSM*T(K1)
      GO TO 2000
 2130 IF(T(K2).LE.XTL) GO TO 2150
C     TK1=S     TNM=S     TK2=L
      T(NM)=(1-XSL-XMMS)*W(NM)+XSL*W(K2)+XMMS*T(K1)
      GO TO 2000
 2150 IF(T(K2).LT.XTS) GO TO 2160
C     TK1=S     TNM=S     TK2=M
      T(NM)=(1-XSM-XMMS)*W(NM)+XSM*W(K2)+XMMS*T(K1)
      GO TO 2000
C     TK1=S     TNM=S     TK2=S
 2160 T(NM)=(1-2*XMMS)*W(NM)+XMMS*(W(K2)+T(K1))
 2000 CONTINUE
      XMML=X1
      XLM=X2
      XSL=X3
      XOXIL=X5
 3000 CONTINUE
  900 GO TO 44
 1000 CONTINUE
      WRITE(6,55) XC,(T(I),I=1,30)
   55 FORMAT(2X,F10.4//10(3X,F5.0)/10(3X,F5.0)/
     *10(3X,F5.0)//)
 1500 CONTINUE
  950 CALL EXIT
      END
```

REFERENCES

1. Analysis of Casting Defects, AFS, 1974.

2. Logan, T.: "Casting from the user's standpoint", AFS Transactions, Vol.65, 1957, 97-99.

3. Heiner, R.W., Loper, C.R. and Rosenthal, P.C.: Principles of metal casting, McGraw-Hill Book Company, 1967.

4. Davies, G.J.: Solidification and casting, Applied Science, 1973.

5. Beeley, P.R.: Foundry Technology, John Wiley and Sons, 1972.

6. Taylor, H.F., Flemings, M.C. and Wulff, J.: Foundry engineering, John Wiley and Sons, 1959.

7. Metals Handbook, Vol.5, part B, Melting and Casting, 8th edition, ASM.

8. Gorbachev, I.A. and Zhukov, A.A.: "Elimination of soft structures in the white iron layer on castings", Russian Castings Production, n. 7, July 1975, 277-278.

9. Kvasha, F.S., Lakedemonskii, A.V., Vasile'v, V.A. and Saikin, V.T.: "The mechanism of lap formation on the surface of iron castings", Russian Castings Production, n. 10, October 1968, 443-444.

10. Lillieqvist, G.A.: "Influence of temperature on fluidity and surface appearance of steel castings", AFS Transactions, Vol.58, 1950, 261-269.

11. Higgins, R.A.: Engineering Metallurgy, Part II, Metallurgical Process Technology, Hodder and Stoughton, 1974.

12. Ragone, D.V., Adams, C.M. and Taylor, H.F.: "A new method for determining the effect of solidification range on fluidity", AFS Transactions, Vol.64, 1956, 653-657.

13. Niesse, J.E., Flemings, M.C. and Taylor, H.F.: "Application of theory in understanding fluidity of metals", AFS Transactions, Vol.67, 1959, 685-697.

14. Niesse, J.E., Flemings, M.C. and Taylor, H.F.: "Fluidity of a series of magnesium alloys", AFS Transactions, Vol.65, 1957, 207-211.

15. Flemings, M.C., Niiyama, E. and Taylor, H.F.: "Fluidity of Aluminum Alloys", AFS Transactions, Vol.69, 1961, 625-635.

16. Wood, D.H. and Mara, G.L.: "Eliminating cold shut defects in deep, single-pass, electron beam welds in uranium", Welding Journal, Vol.56, n. 7, March 1977, 88-92.

17. Arata, Y., Terai, K. and Matsuda, S.: "Study on characteristics of weld defect and its prevention in electron beam welding (Report III) - characteristics of cold shut", JWRI Transactions, Vol.3, n. 2, 1974, 81-88.

18. Anon.: "Eliminating surface defects on zinc die castings", Die Casting Engineer, Vol.21, n. 1, Jan.-Feb. 1977, 24-28.

19. Winship, J.: "Diecasting sharpens its edge", American Machinist, Vol.118, n. 24, November 25, 1974, 77-88.

20. Semones, D.E. and Safranek, W.H.: "New method for electroplating wear-resistant nickel-phosphorus coatings in steel die cavities", Die Casting Engineer, Vol.17, n. 6, Nov.-Dec. 1973, 12-18.

21. Szekely, J. and Themelis, N.J.: Rate Phenomena in Process Metallurgy, Wiley-Interscience, 1971.

22. Bird, R.B., Steward, W.E. and Lightfoot, E.N.: Transport Phenomena, John Wiley & Sons, 1960.

23. Metals Handbook, Vol.8, Metallography, Structures and Phase Diagrams, 8th Edition, ASM.

24. Carnahan, B., Luther, H.A. and Wilkes, J.O.: Applied Numerical Methods, John Wiley & Sons, 1969.

25. Argyropoulos, S.A.: M.Eng. Thesis, McGill University, Dept. of Mining and Metallurgical Eng., Montreal, 1977.

26. Mucciardi, F.A.: M.Eng. Thesis, McGill University, Dept. of Mining and Metallurgical Eng., Montreal, 1977.

27. Chiesa, F.M. and Guthrie, R.I.L.: "Natural convective heat transfer rates during the solidification and melting of metals and alloy systems", Journal of Heat Transfer, August 1974, 377-384.

28. Geiger, G.H. and Poirier, D.R.: Transport Phenomena in Metallurgy, Addison-Wesley Publishing Company, 1973.

29. Paschkis, V.: "Influence of dry sand conductivity on rate of freezing of steel slabs", AFS Transactions, Vol.58, 1950, 147-152.

30. Iida, S. et al.: Tables of Physical Constants (Butsuri Jyosuhyo), Asakura, Tokyo, 1969 (Japanese).